The Astbury Centre for
Structural Molecular Biology

UNIVERSITY OF LEEDS

ANNUAL REPORT 2017

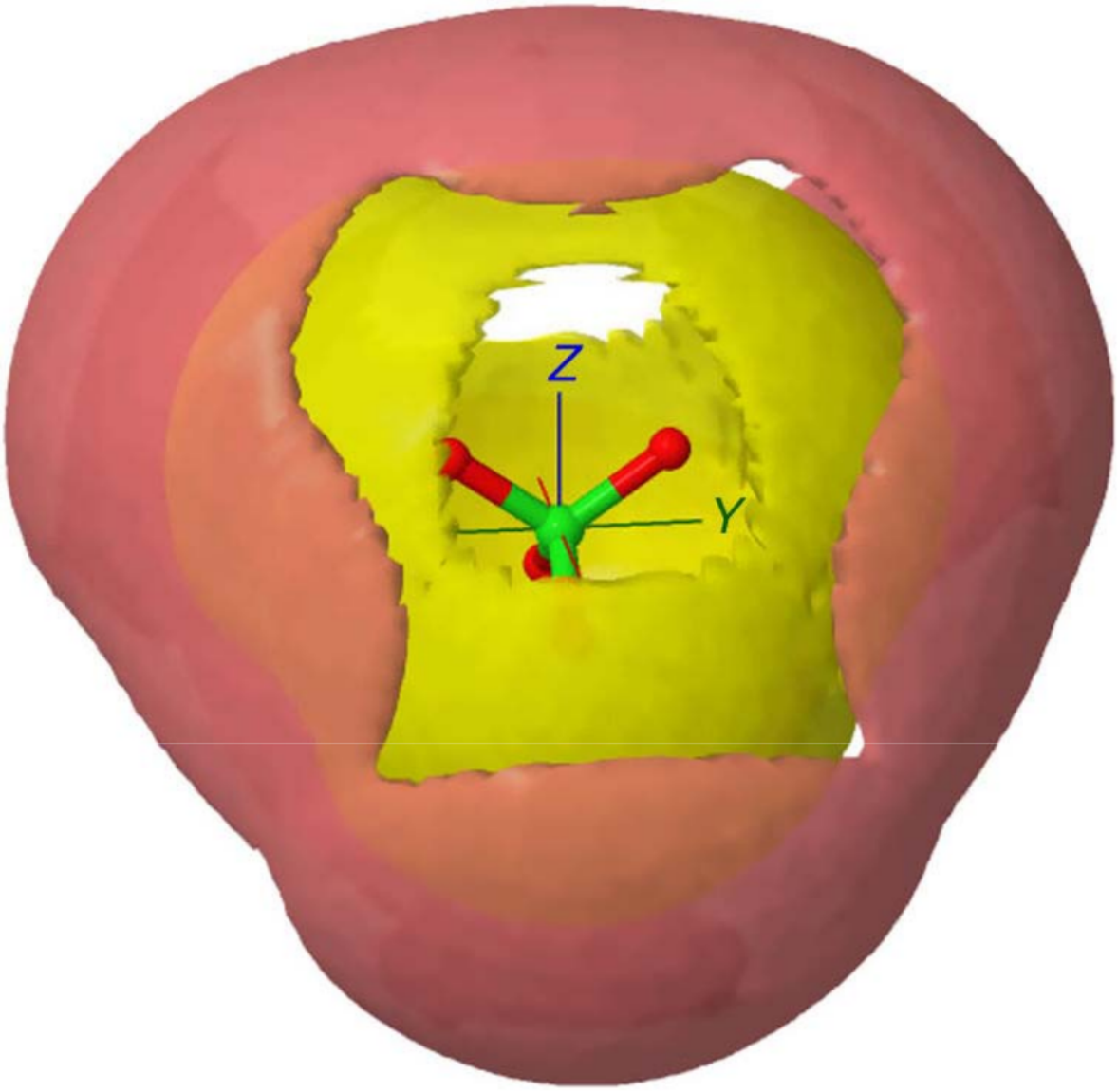

Front cover illustration

Spatial density function of Mg (red) and water (yellow) around a perchlorate ion in an aqueous $Mg(ClO_4)_2$ solution . The structure of this mimetic of water on Mars was determined using neutron diffraction in combination with hydrogen isotope labelling and empirical structure refinement. This investigation was a collaboration between the Dougan (Leeds) and Soper (ISIS Facility, Rutherford Appleton Laboratory) groups and published in *Nat. Commun* in 2017. More details can be found on p15 of this report.

Mission Statement

The Astbury Centre for Structural Molecular Biology will promote interdisciplinary research of the highest standard on the structure and function of biological molecules, biomolecular assemblies and complexes using physico-chemical, molecular biological and computational approaches.

Introduction

Welcome to the Annual Report of the Astbury Centre for Structural Molecular Biology 2017. It has been yet another busy and successful year and this letter highlights a few of our many successes. The Astbury Report highlights both the collegiality, vibrancy and interdisciplinarity of our centre and the research discoveries we have made. The strength of our community and our collaborations, as well as the contributions we have made to others through our engagement in public-facing events is something we are immensely proud of. I would like to thank every member of the Centre for their hard work over the year: our support staff, technicians, facility managers, students, post-docs, fellows, academic staff and, of course, Lucy Gray for wonderful organisation and her excellent administrative support. Our success comes from our strong multidisciplinary science, as well as our collegiality and teamwork. Thank you all!

During 2017 the Centre continued in its quest to "Understand Life in Molecular Detail" through multiple different activities, including seminars, publications, public lectures and other events. We continued to enjoy an excellent seminar series (organised by Joe Cockburn), hosting 9 lectures during the year with speakers from the UK, France and Germany. A fantastic eleventh Annual Astbury Lecture was given by Prof Tom Muir, (Princeton University) on the 7th July, entitled "Synthetic Protein Chemistry: from the test tube to the cell". This annual event was followed by our tradition of a highly competitive sports day and barbecue hosted by the Astbury Society (see http://www.astbury.leeds.ac.uk/about/society.php). On 14th and 15th September, 147 members attended the Centre's Biennial Research Retreat held at Shrigley Hall Hotel, Pott Shrigley, Macclesfield. Students, post-docs and PIs shared their recent exciting scientific discoveries, through talks, posters and the ever-popular "Flash Poster" presentations. Poster prizes were awarded to Matt Iadanza (first prize), Jessica Ebo and Brendan Farrell (runners up) for the best posters at the retreat.

We are delighted to announce that the University of Leeds via the Astbury Centre has become a formal partner with the Rosalind Franklin Institute that will be based at the Harwell campus, Oxford. More news regarding developments and activities will be reported next year.

The Astbury BioStructure Laboratory was officially opened on 31st January by the Director of the Wellcome Triust, Dr Jeremy Farrar. He unveiled the facility that hosts a 950 MHz nuclear magnetic resonance spectrometer and two 300 kV electron microscopes. This £17m equipment investment in our Centre funded by the University and Wellcome Trust will enable world-leading biological research here in Leeds. It is already bearing fruit, as shown by the EM and NMR data in the reports that follow is this year's Annual Report. We anticipate that our facilities will be sought after by researchers in both academia and industry in the UK, Europe and beyond. We look forward to sharing our expertise with them.

The Astbury Centre continued to contribute to public engagement events with a significant presence at the 'Be Curious' event in March, the 'Pint of Science' event in May, 'Light Night Leeds' event in October and the 'One Day At Leeds' event in November. We are currently looking forward to the second Astbury Conversation that will be held at the University of Leeds on 16th & 17th April 2018 (see http://www.astburyconversation.leeds.ac.uk).

This year we launched the first VC Jordan/PR Radford Prize, which was awarded to Bob Schiffrin for the best PhD student thesis in the Astbury Centre. This annual prize is a result of generous donation from alumnus Craig Jordan who travelled from the USA to attend the Annual Lecture and present Bob with the prize (see http://www.astbury.leeds.ac.uk/prize).

The Centre welcomed Frank Sobott and Antreas Kalli to the membership in 2017. As a result of generous funding from Leeds alumnus, Peter Cheney, we welcomed visits from Kelly Chibale (University of Cape Town, South Africa), Steve Polyak (University of Washington, Seattle, USA), Preben Morth (University of Oslo, Norway) and Travis Beddoe (La Trobe University, Victoria, Australia) who each came for sabatticals of different length to form collaborations with our

members (see http://www.astbury.leeds.ac.uk/people/fellows.php). This included hosting Cheney fellow Professor Herbert Waldmann at a chemical biology research retreat in Grasmere that was attended by 20 Astbury colleagues and visitors from the Max Planck Institute for Molecular Physiology and Lead Discovery Center (Dortmund, Germany). We were also delighted to welcome our new PhD students and postdocs to our Centre this year, bringing our total number of researchers to >400, including 68 academic staff, 339 PhD students, 96 postdoctoral researchers and 7 Research Fellows.

Astbury Centre members published their research in a wide range of journals in 2017 including Nature Communications, Nature Microbiology and Angewande Chemie-International. A full list can be found at the end of this report. In terms of grant income, Astbury members also enjoyed many successes in 2017 with £22M of new project and programme grants bringing the Astbury grant portfolio to a striking £61.5M share of £98M of grants. This impressive figure is testament to the hard work and success of our members and some of the larger awards in 2017 included grants over £1M, awarded to Sheena Radford (Wellcome Trust Investigator Award), Richard Bayliss (Cancer Research UK) and Lorna Dougan (EPSRC). These are of course accompanied by the many successful grants obtained by Astbury members and we are much indebted to the funding agencies that support our science, including BBSRC, EPSRC, MRC, the Wellcome Trust, charities, ERC, EU and Industry. We also acknowledge, with thanks, the support of the University of Leeds; the Faculties of Biological Sciences, Maths and Physical Sciences and Medicine and Health, and the Schools of Chemistry, Molecular and Cellular Biology, Biomedical Sciences and Physics and Astronomy for their support of the Centre and our research.

There was continued success in 2017 for members of the Astbury Centre in terms of peer recognition. Anastasia Zhuravleva was invited to speak at the 62nd Annual Meeting of the Biophysical Society in the Future of Biophysics Burroughs Wellcome Fund Symposium. This symposium highlighted the work of four young investigators doing cutting-edge research at the interface of the physical and life sciences and Anastasia was chosen as one of the very best young scientists in the field. Sheena Radford was elected Fellow of the Biophysical Society. Daniel Hurdiss (Ranson group) won The Microbiology Society's 2017 "Sir Howard Dalton Young Microbiologist of the Year" competition and won the prize for best oral presentation at the DNA tumour virus meeting of the International Papillomavirus Society. PhD student Joan Mayol Llinas (Nelson group) won the poster prize at the "Synthetic Tools for the Exploration of 3D Pharmaceutical Space" meeting of the Dial-a-Molecule EPSRC Grand Challenge network. PhD student Rani Moons (Sobott group) won the Bordoli Prize of the British Mass Spectrometry Society for the best young person's poster presentation. Hester Beard (Bon group) won the runner-up prize for her poster presentation at the RSC Chemical Biology and Bio-organic Postgraduate Symposium 2017 in Glasgow. Well done all.

The Astbury Society, led by the presidents Jessica Ebo and Emily Turri, played a spectacular role in Astbury activities in 2017. Events included the famous Christmas quiz night and a hugely successful fifth May Ball. With continued fund raising through cake bakes and coffee mornings, the Society continues to support the "Leeds Children's Charity" with donations reaching an impressive £3887.06 to date. See http://www.astbury.leeds.ac.uk/about/society.php for photos of these events.

I hope that you enjoy reading this Annual Report. Thank you to David Brockwell and Lucy Gray for editing this report, everyone who contributed to it, and all who participated in the Astbury Centre's activities in 2017. I look forward to continuing our successes in the year ahead.

Sheena E. Radford, FMedSci, FRS
Director, Astbury Centre for Structural Molecular Biology,
Leeds, February 2017

Please note that this report (as well as those from previous years) is also available as a PDF document which can be downloaded from our website (www.astbury.leeds.ac.uk).

CONTENTS

Contributions indexed by Astbury Centre Principal Investigator

Investigation of the photosynthetic protein Light-Harvesting Complex II: protection against photo-damage and artificial light harvesting

Ashley Hancock and Peter Adams

Introduction

Light-Harvesting Complex II (LHCII) is a membrane protein with embedded chromophores (chlorophylls and carotenoids) that absorb solar photons and transfer energy as electronic excited states towards Photosystem I and II. When environmental conditions lead to relatively high light intensities, LHCII can adopt a photoprotective state in which excitation energy is safely dissipated as heat, a process known as Non-Photochemical Quenching (NPQ) of chlorophyll fluorescence. *In vivo*, NPQ is triggered by a combination of factors including low pH and the action of specific enzymes leading to a dramatic shortening of LHCII fluorescence lifetime. *In vitro*, purified LHCII suspended in detergent or reconstituted in liposomes can reversibly adopt a quenched NPQ-like state. Previous spectroscopy of these *in vitro* models revealed changes in exciton dynamics and protein-pigment conformation that accompany quenching. However, the LHCII-LHCII interactions are poorly characterized.

Results and Discussion

We have performed correlated fluorescence lifetime imaging microscopy (FLIM) and atomic force microscopy (AFM) of LHCII complexes bound to mica and manipulated their environment to show varying degrees of quenching. AFM showed that LHCII self-assembles onto mica substrates forming 2D-domains of 100s nanometres in width. FLIM showed that LHCII trimers in these aggregates are in a quenched state, with a much lower fluorescence lifetime (<0.3 ns) compared to free trimers in solution (2 to 4 ns). In contrast, LHCII-LHCII interactions were disrupted by the presence of thylakoid lipids or common phospholipids and led to an intermediate length fluorescent lifetime (approx. 0.8 ns). To our knowledge, this is the first *in vitro* correlation of nanoscale membrane imaging to the state of LHCII quenching of a minimal number of complexes. The results suggest that lipids could play a key role in modulating the extent of LHCII-LHCII interactions within the thylakoid membrane and so alter the propensity for the complex to activate NPQ.

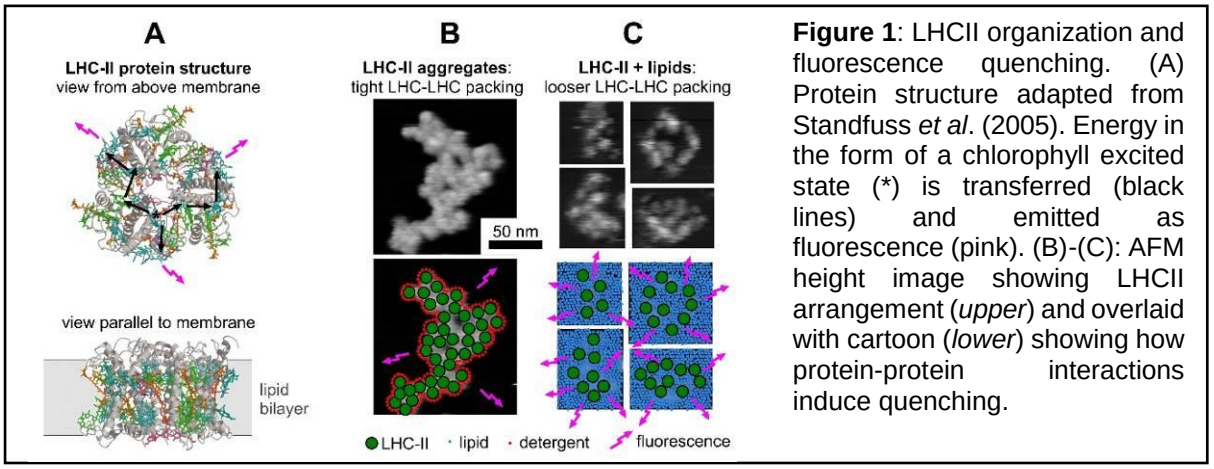

Figure 1: LHCII organization and fluorescence quenching. (A) Protein structure adapted from Standfuss *et al*. (2005). Energy in the form of a chlorophyll excited state (*) is transferred (black lines) and emitted as fluorescence (pink). (B)-(C): AFM height image showing LHCII arrangement (*upper*) and overlaid with cartoon (*lower*) showing how protein-protein interactions induce quenching.

In ongoing work, we are developing protein-lipid vesicles (proteoliposomes) comprised of thylakoid lipids and a variety of concentrations of LHCII. Preliminary data shows that quenching increases with LHCII/lipid ratio as shown by cuvette-based fluorescence spectroscopy and fluorescence microscopy. Furthermore, we are able to introduce non-native chromophores into the lipid bilayer which show evidence of Förster resonance energy transfer (FRET) to the LHCII. This could be a method to increase the effective absorption cross-section of LHCII, which would allow a greater portion of the solar spectrum to be utilized.

Funding
This work was funded by the BBSRC (fellowship grant # BB/M013723/1).

Collaborators
External: Cvetelin Vasilev, C. Neil Hunter, and Matthew Johnson (University of Sheffield)

Targeting the cancer supercontroller Myc through inhibition of Aurora-A

Selena Burgess, Mark Richards, Eoin Leen, Patrick McIntyre and Richard Bayliss

Introduction

Aurora-A is a Ser/Thr protein kinase that coordinates cell cycle events, such as mitotic entry, with the reorganization of the microtubule network in mitotic spindle assembly and ciliary resorption. The catalytic activity of Aurora-A is stimulated upon interaction with the microtubule-associated protein TPX2, which recruits Aurora-A to microtubules and promotes kinase autophosphorylation. Crystal structures of Aurora-A show how this activation process converts the kinase from an inactive to an active conformation, and how this can be manipulated using synthetic proteins such as the shark single domain antibody VNAR-D01 (Bayliss et al. 2017a).

More recently, Aurora-A was found to moonlight as a regulator of Myc family oncoproteins, through kinase-dependent and kinase-independent mechanisms. Myc proteins are transcription factors that markedly alter gene expression through both activation and repression. The three human Myc proteins, c-Myc, N-Myc and L-Myc have regions of sequence homology, called Myc boxes (MB0 – MBIV), that mediate interactions with critical partner proteins. We previously determined the crystal structure of Aurora-A bound to a region of N-Myc C-terminal to MB1. The binding sites of N-Myc and TPX2 overlap, which has prompted us to investigate the cell-cycle dependence of these interactions.

Results

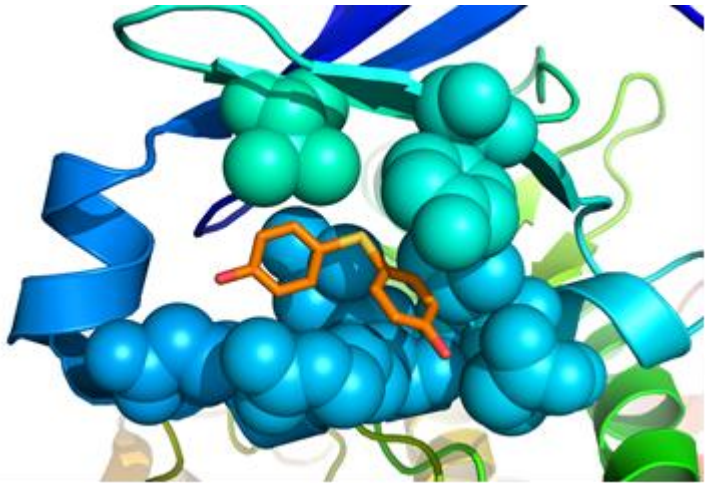

Figure 1: Crystal structure of a fragment hit bound to the Y-pocket of Aurora-A. Aurora-A kinase is shown in cartoon representation, with residues that line the Y-pocket shown as atomic spheres. The fragment hit is shown as sticks, coloured (carbon, orange; sulphur, yellow; oxygen, red).

TPX2 binds to three hydrophobic pockets on the surface of Aurora-A, termed the Y, F and W pockets. The interaction can be disrupted by mutations in any of the three hydrophobic motifs of TPX2 that recognise these pockets (McIntyre et al., 2017). To assess the druggability of these pockets, and to identify starting points for inhibitor development, we carried out a fragment-based screen *in crystallo* using the Xchem laboratory at Diamond Light Source in Harwell (in collaboration with Frank von Delft). 1103 crystals of Aurora-A were soaked with individual chemical fragments, small organic molecules of ~ 300Da, and full datasets were collected on 944 of them to a resolution of ~ 2 Å. The data were analysed using PanDDA (Pan-Dataset Density Analysis) software, developed at DLS. 59 hits were identified, of which 46 bound to the sites of TPX2 interaction (35 in the Y-pocket, 20 in the F-pocket and 1 in the W-pocket). 22 of these compounds were selected for follow-up studies and the crystal structures were refined and deposited in the PDB. Binding affinities of these compounds for Aurora-A were determined using isothermal titration calorimetry, and the most potent series had dissociation constants of 15 μM and 170 μM, respectively. The activity of Aurora-A in the

presence of fragments was determined using a number of different kinase assays through our collaborators at LifeArc. Fragments were then classified as inhibitors or activators of kinase activity. This is consistent with our previous work on proteins such as TPX2 and VNAR-D01 that activate or inhibit Aurora-A through binding to the same pockets as the fragments. Further development of these inhibitors is ongoing in collaboration with Adam Nelson (University of Leeds). This study demonstrates the potential of high-throughput crystallography facilities such as XChem to aid chemical probe discovery.

There is renewed interest in Aurora-A as a cancer drug target because it may provide a route to blocking the activity of Myc proteins (Bayliss 2017b). Our previous work focussed on the stabilisation of N-Myc protein by Aurora-A. In the past year we made progress towards understanding how Aurora-A regulates the transcriptional activity of N-Myc, through collaborative work with Martin Eilers (Büchel 2017). Aurora-A interacts with N-Myc and represses its transcriptional activity specifically in the S-phase of the cell cycle. This coincides with a marked reduction in the binding of N-Myc to a subset of factors that are critical for transcriptional activity, such as TFIIIC. We showed that Aurora-A competes with these other factors for binding N-Myc *in vitro*, providing a mechanism for the inhibition of Myc activity by Aurora-A.

Publications

Bayliss R., Burgess S.G., McIntyre P.J. (2017) Switching Aurora-A kinase on and off at an allosteric site. *FEBS J*. **284**:2947-2954.

Bayliss R., Burgess S.G., Leen E., Richards M.W. (2017) A moving target: structure and disorder in pursuit of Myc inhibitors. *Biochem. Soc. Trans*. **45**:709-717.

McIntyre P.J., Collins P.M., Vrzal L., Birchall K., Arnold L.H., Mpamhanga C., Coombs P.J., Burgess S.G., Richards M.W., Winter A., Veverka V., Delft F.V., Merritt A., Bayliss R. (2017) Characterization of Three Druggable Hot-Spots in the Aurora-A/TPX2 Interaction Using Biochemical, Biophysical, and Fragment-Based Approaches. *ACS Chem Biol*. **12**:2906-2914.

Büchel G., Carstensen A., Mak K.Y., Roeschert I., Leen E., Sumara O., Hofstetter J., Herold S., Kalb J., Baluapuri A., Poon E., Kwok C., Chesler L., Maric H.M., Rickman D.S., Wolf E., Bayliss R., Walz S., Eilers M. (2017). Association with Aurora-A Controls N-MYC-Dependent Promoter Escape and Pause Release of RNA Polymerase II during the Cell Cycle. *Cell Rep.* **21**:3483-3497.

Funding

This work was funded by Cancer Research UK, ERC, MRC and LifeArc.

Collaborators

External: M. Eilers (University of Würzburg, Germany), L. Chesler (ICR, London, UK), V. Veverka (IOCB, Prague, Czech Republic), F.V. Delft (DLS, Didcot, UK), A. Merrit (LifeArc, Stevenage, UK)

Repurposing ESCRT-III machinery for fabrication of eukaryote-like artificial cells

Andrew Booth and Paul Beales

Introduction

The bottom-up design and fabrication of artificial cells is a challenge of significant current focus in Synthetic Biology. Inspired by natural cells, these are compartmentalised chemical systems, usually utilising repurposed biomolecular components and reconstituting native biological machineries for new purposes. Synthetic vesicles composed of lipids or amphiphilic polymers have been a primary approach to the design of the chassis of an artificial cell. However these structures usually comprise a single compartment, akin to a prokaryote, and hence lack the advantages associated with the highly compartmentalised architectures of a eukaryote that facilitate multiple incompatible chemical processes to occur in parallel through spatially separated physical confinement. To address this challenge, our approach is to repurpose the natural membrane remodelling machinery of ESCRT-III, which is involved in the generation of multivesicular bodies in native cells, for controllable generation of new intraluminal compartments within giant lipid vesicles towards the feasible fabrication of next generation artificial cells with the desired internal complexity. ESCRT-III components are known to self-assemble in a spiral complex on the membrane surface that is responsible for membrane invagination and scission at the neck of the resultant vesicular buds (Figure 1). In order to gain this control in a practical system, we need a more in-depth understanding of ESCRT-III biophysics and we are reengineering this complex to simplify the number of distinct components required for predictable, reproducible *in vitro* function.

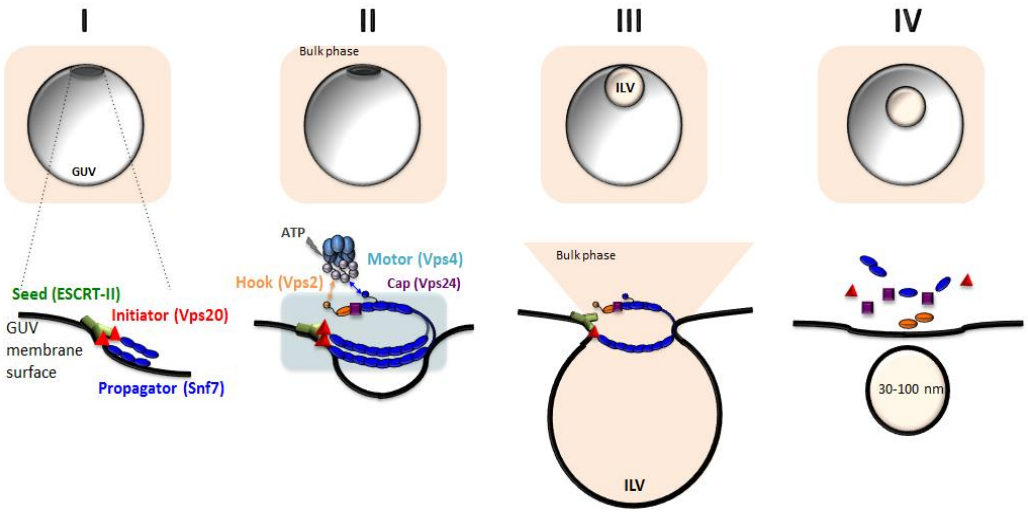

Figure 1: Cartoon of a proposed mechanism for ESCRT-III assembly and membrane remodelling to form ILVs inside a GUV.

Results

We have successfully reconstituted intraluminal vesicle (ILV) formation in an *in vitro* giant unilamellar vesicle (GUV) model system. As a first step to harnessing this process in controlled artificial cell fabrication, we need to understand which experimental parameters dictate the size and number of ILVs that form in each GUV. Our initial hypothesis was that this regulation would arise from controlling the concentration and stoichiometric ration of the different protein components that can crudely be assigned to individual functions of nucleation, growth, termination and ATP-dependent activation of the complex in prevalent models in the molecular biology literature.

To our surprise, this approach was not as predictable as would have been expected. Within a broad range of concentrations above a threshold required for function, only weak control of ILV size and number was attainable. This strongly suggests that ESCRT-III biophysics is more

complicated than current theories account for. Furthermore, we observed a greater variation in ILV size and number in an individual experiment than was evident in the average variability across the parameter space we explored. Most provocative was the realisaton that distinct “species” of GUV could be identified (Figure 2): (i) no ILVs; (ii) a large number of <2 μm ILVs; (iii) a few very large >3 μm ILVs; (iv) buds stalled at the outer membrane. GUVs did not tend to be observed containing populations of small and large ILVs, just one or the other: i.e., the heterogeneity in size and number of ILVs in a sample was primarily a heterogeneity between different GUVs rather than within individual GUVs. This strongly suggests that heterogeneities in GUV properties within a sample dominate the outcomes of ESCRT-III function more so than the concentration or stoichiometry of this complex.

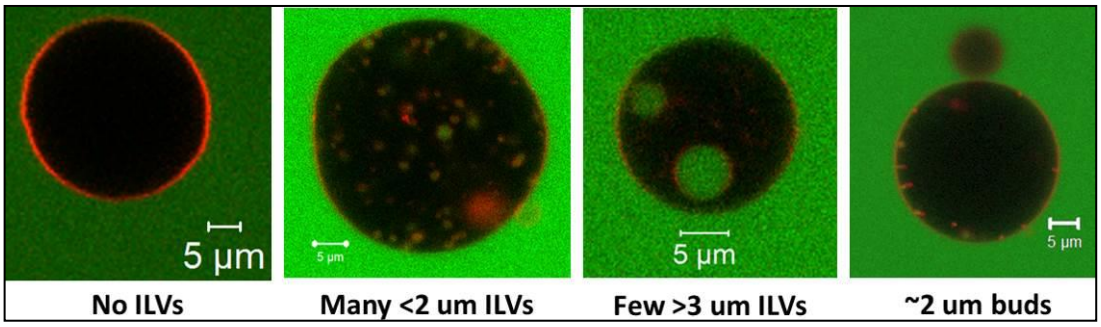

Figure 2: Examples of different ILV morphologies. Rh-DOPE (red) labels the membrane. Alexa-488 dextran (green) in the bulk phase is encapsulated with ILVs that are generated.

Having found that there was no strong correlation between vesicle size (an obvious heterogeneity in GUV samples) and these distinct ILV morphologies, other variables were sought. It is well established that considerable variation in membrane tension exists within GUV populations and therefore this was our next point for consideration. Firstly, we found that osmotic relaxation of membrane tension in a GUV population increased the number of ILVs that formed by over an order of magnitude, providing strong evidence that membrane mechanics are a significant regulating factor in ESCRT-III function. Using membrane flicker spectroscopy to determine the mechanical properties of individual GUVs, we have shown that GUVs where ILVs do not form represent that high tension population of our samples, lending further support to our hypothesis of strong mechanical regulation. This may also have significant biological implications with regards to how cells might regulate local membrane tension to exert control over ESCRT-III function.

In further work, we have early evidence to suggest that chimeric proteins can be successfully created and used to reduce the number of individual protein components in a functional complex. We have also successfully demonstrated formation of two distinct ILV populations within an individual GUV: an important step towards fabrication of complex artificial cell architectures. Ongoing and future work seeks to use membrane engineering for enhanced control over artificial cell structures and fluidic technologies are being developed to enhance the ease of fabrication and analysis of these systems.

Funding
This work was funded by the EPSRC.

Collaborators
External: B. Ciani (University of Sheffield), C. Marklew (University of Sheffield).

Enzyme engineering of aldolases

Alex Moloney, Naim Stiti, Adam Nelson and Alan Berry

Introduction

Aldolases are a class of enzyme capable of forming new carbon-carbon bonds. Coupled with their ability to accept a wide range of structurally different substrates, this makes them synthetically very appealing. We are using use these enzymes to search for new activities and engineer stereoselectivity. We do this using rational methods of chemical modification with unnatural amino acids as well as directed evolution with developed screening techniques.

Using chemically modified aldolases to yield new and interesting activities

Current methods of production for high value and rare bioactive molecules strongly rely on isolation from sources such as plants, microorganisms, chemical synthesis and the use of native biosynthetic enzymes. This can make the synthesis of novel molecules laborious, costly and environmentally unsustainable. In our lab, we use innovative, efficient, synthetic biology-based strategies with great potential for accessing novel chemistries using selected aldolases. Our knowledge of the catalytic mechanisms allows us to design and generate novel rationally engineered variants upon directed mutagenesis or/and incorporation of non-canonical amino acids. This is done through guided chemical modifications of specific amino acids side chains. Enzymatic activity screening shows that these enzyme variants open up exciting opportunities to access a wealth of new activities.

Threonine aldolase, a tool for stereoselective synthesis

Threonine aldolases are capable of synthesising β-hydroxy-α-amino acids molecules of high pharmaceutical interest. These molecules have two chiral centres resulting in four possible stereoisomers. Threonine aldolases allow extremely good stereocontrol at the α-carbon position owing to L- and D- classes of the enzyme. However, the stereoselectivity at the β-carbon is typically very poor. By developing a novel screen we were able to use combinatorial active site saturation testing (CASTing) to identify mutant enzymes with improved selectivity for a single stereoisomer. Iterative cycles of mutagenesis and screening libraries enabled us to identify several highly stereoselective enzymes without compromising the rate of the enzyme catalysed reaction (Figure 1). Current work focusses on obtaining a structural insight into how this stereoselectivity has been achieved.

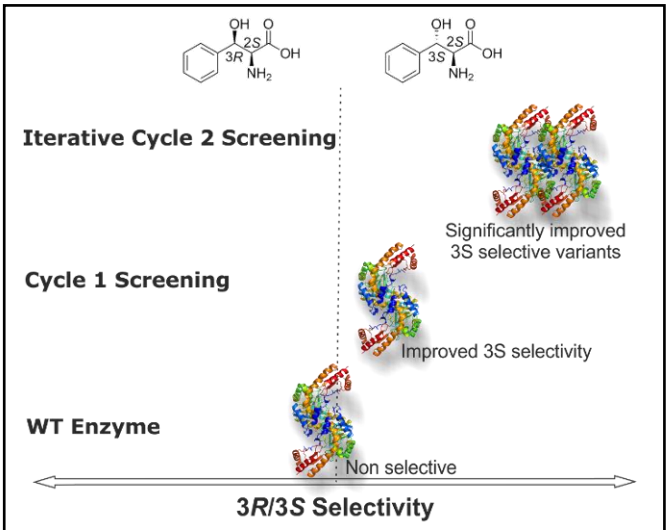

Figure 1: Iterative cycles of mutagenesis and screening allows for significantly improved stereoselective variants to be obtained.

Funding: Our work is funded by BBSRC and Dr Reddy's.

Engineering novel natural products and binding motifs

Ieva Drulyte, Jana Obajdin, Emily Turri, Adam Nelson and Alan Berry

Introduction

Natural products belong to an extensive family of diverse organic molecules: in excess of 200,000 discovered and extracted from various sources. Of particular interest are the polyketide, non-ribosomal peptide and isoprenoid classes, which contribute to the pharmaceutical, cosmetic and biofuel industries. These classes of natural products are synthesised by polyketide synthases, non-ribosomal peptide synthases and terpene synthases, respectively. Our interest lies in understanding the structure-function relationship of these enzymes; facilitating our engineering efforts to synthesise existing and novel natural products.

Structural studies in indanomycin biosynthesis

Indanomycin, an antibiotic active against Gram-positive bacteria, is produced by a hybrid nonribosomal peptide synthetase-polyketide synthase (NRPS/PKS) from *Streptomyces antibioticus* NRRL 81673. We are interested in the chemistry involved in the generation of mature polyketide. IdmH, a putative post-PKS cyclase enzyme, is thought to catalyze the indane ring formation via a Diels-Alder [4+2] cycloaddition reaction. The Diels-Alder reaction, despite being widely used in synthetic organic chemistry, is an extremely rare reaction in nature, which makes IdmH a particularly exciting enzyme to study. IdmH was cloned, heterologously expressed and purified. To aid crystallization, we made a mutant of IdmH lacking a flexible loop and solved its crystal structure to 2 Å resolution (Figure 1). We aim to use these structural data to validate the reaction mechanism of this enzyme and evaluate the suitability of IdmH to be used in rationally engineered PKS assembly lines.

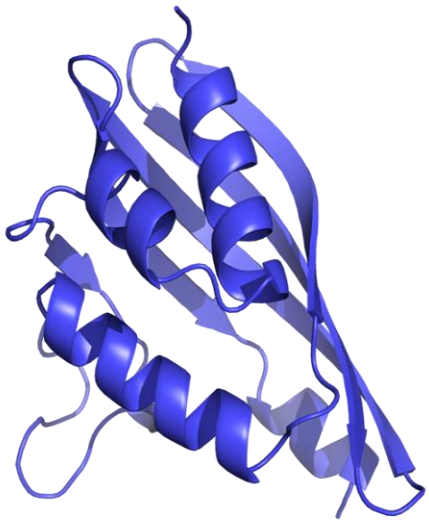

Figure 1: Atomic model of IdmH, a putative polyketide cyclase from indanomycin NRPS/PKS, monomer

Engineering selina-4(15),7(11)-diene synthase for novel activities

Selina-4(15),7(11)-diene synthase produces selina-4(15),7(11) diene and germacrene B from farnesyl pyrophosphate. Initial work has been focused on redesigning the enzyme active site to produce novel activities and novel terpenes. Previously 28 enzyme mutants have been designed and produced using site-directed mutagenesis and screened for product profile to determine their impact on the catalytic reaction. Screening is carried out using gas chromatography, mass spectrometry and any novel terpenes will be characterized using 2D NMR. The malachite green assay has been adapted to screen the mutants for pyrophosphate cleavage and has been successfully tested on wild type selina-4(15),7(11)-diene synthase. This assay utilizes an inorganic pyrophosphatase, converting pyrophosphate into two inorganic phosphate ions, which consequently form the malachite green complex.

Funding

This work is funded by the BBSRC and The Wellcome Trust.

Affimer-based immunosensor of an environmental contaminant

Elena Koutsoumpeli, Christian Tiede, James Murray, Anna Tang, Darren Tomlinson, Steven Johnson and Robin Bon

Introduction

Immunoassays rely on antibodies that recognise analytes with high affinity and selectivity. However, developing antibodies to detect non-immunogenic targets such as pharmaceuticals is challenging. Antibody mimetics such as Affimers offer the high affinity and specificity associated with antibodies, but with high stability, reduced batch-to-batch variability, and rapid *in vitro* selection against a wide range of targets. We developed an Affimer-based immunosensor of methylene blue (MB), a water-soluble dye used in biochemical research and textiles, a pharmaceutical, and an important environmental contaminant.

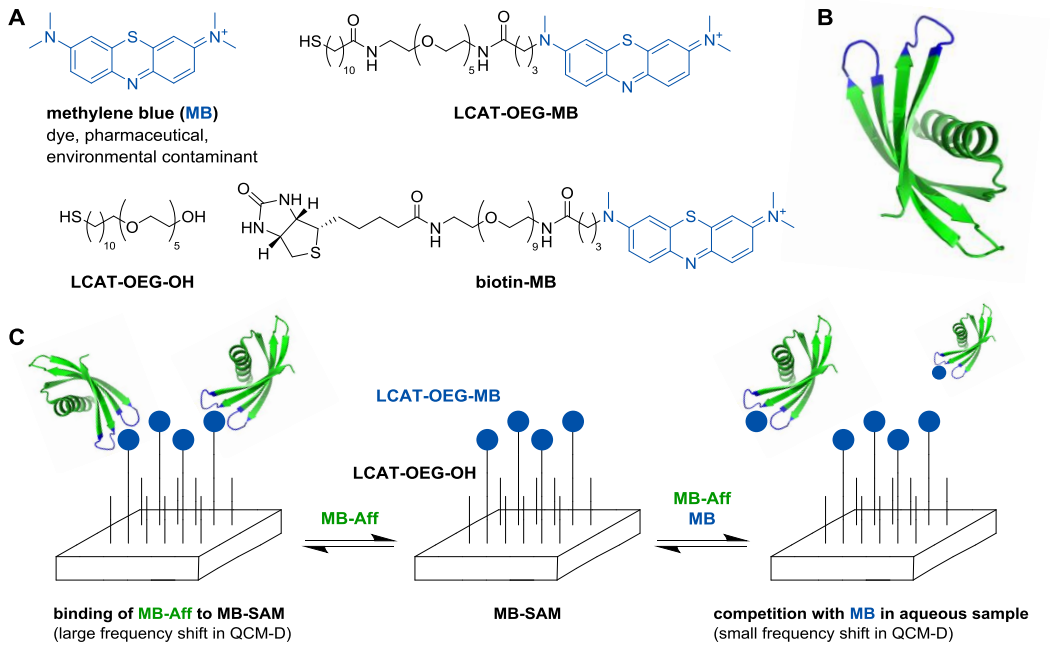

Figure 1: (A) Small molecules used in this work. (B) Structure of Affimer, with the scaffold in green and the variable loops in blue. (C) Principle of the Affimer-based MB immunosensor.

Results

Through phage display against immobilised biotin-MB, three unique MB-binding Affimers were selected from a highly diverse library (~10^{10} clones). Analysis of binding kinetics of the most promising Affimer was performed using QCM-D on well-characterised mixed self-assembled monolayers (SAMs) consisting of LCAT-OEG-MB and LCAT-OEG-OH, leading to an estimated KD of 14 nM. In competition experiments, the immunosensor could detect micromolar concentrations of MB in aqueous sample. Optimisation of sensor sensitivity and development of Affimers against other environmental contaminants is ongoing.

Publications

Koutsoumpeli E., Tiede C., Murray J., Tang A., Bon R.S., Tomlinson D.C. & Johnson S.D. (2017) Antibody mimetics for the detection of small organic compounds using a quartz crystal microbalance. *Anal Chem* **89**:3051-3058.

Funding

This work was funded by the EPSRC, EU FP7 programme and a Henry Ellison PhD studentship

Using NMR to study large RNAs at ultra-high field using direct detection of ^{15}N

Lars Kuhn, Arnout Kalverda and Alexander Breeze

Introduction

Currently available NMR methods for the study of RNAs run into difficulties when the size of the RNA exceeds approximately 150 nucleotides (nt). With long non-coding RNAs of biological relevance often exceeding 250 nt in size, there is a clear need for novel NMR approaches that can effectively address structural questions on these larger RNA species. Recently developed experiments exploiting direct detection of ^{15}N nuclei in proteins have demonstrated benefits in resolution and sensitivity for large proteins at physiologically high ionic strengths, where deuteration is not possible because of expression in non-bacterial host organisms (e.g. insect or mammalian cells). Here, we explored the potential of these methods (and novel variations thereof) for study of larger RNAs at ultra-high field (950 MHz).

Results

Together with our collaborators at the University of Frankfurt and Bruker Spectrospin, we developed an optimised version of the recently published ^{15}N-detected TROSY pulse scheme for use on large, non-deuterated proteins. This version (^{15}N-detected BEST-TROSY) incorporates band-selective ^{1}H pulses whose bandwidth was chosen to cover only the imino-chemical shift range between 15 ppm and 9 ppm (~5000 Hz) where no otherprotons of the RNA resonate. Since the ^{1}H pulses excite only a subset of the spins, the longitudinal relaxation rate of the system is enhanced, allowing a reduction in the recycle delay. Further, it ensures that the water resonance is unperturbed and aligns along the z-axis at all times during the experiment, providing a reservoir of fast-exchanging protons in magnetic equilibrium. It is necessary to achieve pure in-phase excitation with a single pulse to avoid significant phase corrections in the indirect ^{1}H-dimension. Therefore, EBurp2 shapes were used as selective 90° pulses. Carbon decoupling was carried out at a 50% reduced field strength to allow for the reduction in recycle delay to 0.2-0.3 s.

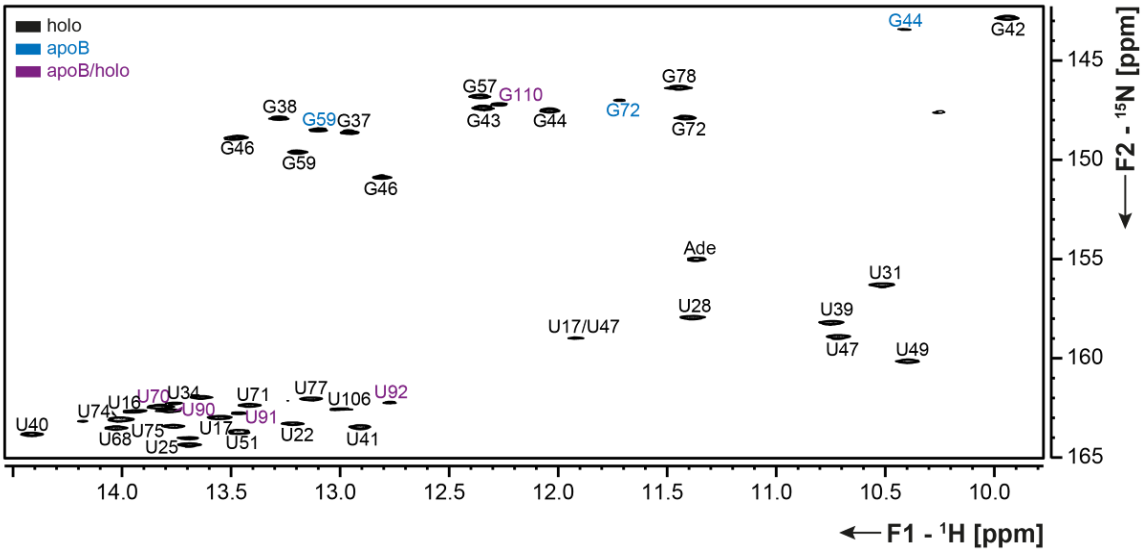

Figure 1: ^{15}N-detected 950 MHz BEST-TROSY spectrum of a 127 nucleotide adenine-sensing riboswitch RNA (^{15}N-U/G-labelled) recorded using our TXO cryoprobe (sample courtesy: R. Schnieders, U. of Frankfurt), illustrating the narrow line widths achieved in the ^{15}N dimension.

Comparing the optimised ^{15}N-detected BEST-TROSY to standard HSQC revealed an increase in relative S/N per unit time of around three-fold when tested on a well-characterised 14 nt hairpin RNA, measured at 800 MHz. However, the real benefits of ^{15}N detection and TROSY are only expected to arise with significantly larger RNAs at higher field strengths. To

investigate this, we exploited the unique 5mm TXO cryogenic probe installed on the 950 MHz spectrometer in the Astbury Biostructure Laboratory NMR facility, which, in contrast to traditional cryoprobes, is optimised for direct detection of ^{15}N (and ^{13}C) rather than ^{1}H, by reversing the positions of the probe coils in relation to the sample. Figure 1 shows the ^{15}N-detected BEST-TROSY spectrum of a 127 nt adenine-sensing riboswitch RNA in the holo state, recorded with 576 scans per ^{1}H increment and a 0.3 s relaxation delay, giving a total measuring time of 21 h. According to predictions, only minor improvements in ^{15}N-resolution (~10%) are to be expected for RNAs of a rotational correlation time of 60 ns by measuring at 950 MHz compared with 800 MHz. Those changes are below the maximal resolution of 1.7 Hz achieved in the experiment. Even for the large RNAs in our study (127 nt and 329 nt RNAs), no resolution improvement could be detected in comparison to spectra recorded at 800 MHz (not shown). The S/N-ratio, however, is increased by a factor of ~1.5 due to better ^{15}N-sensitivity. This increase in sensitivity results from the higher magnetic field strength as predicted, in combination with utilizing a ^{15}N-optimized TXO probe.

Measurements of ^{15}N-line width at different field strength hint at exchange processes in RNAs that obscure the relaxation interference benefits of ultra-high field spectrometers. However, the study does highlight that the ^{15}N line widths increase much more slowly with increasing molecular size of the RNA than do the corresponding $^{1}H_N$ line widths, and that, for all but the 329 nt RNA, it is possible directly to detect and measure trans-hydrogen-bond scalar couplings $^{2h}J_{N1N3}$/$^{2h}J_{N3N1}$ of ~6-7 Hz for Watson-Crick-type uridine and guanosine base pairs. This is facilitated by the high spectral resolution that is readily achievable in the ^{15}N dimension of ^{15}N-direct-detected BEST-TROSY experiments.

Publications

Schnieders R., Richter C., Warhaut S., de Jesus V., Keyhani S., Duchardt-Ferner E., Keller H., Wöhnert J., Kuhn L.T., Breeze A.L., Bermel W., Schwalbe H. & Fürtig B. (2017) Evaluation of ^{15}N-detected H-N correlation experiments on increasingly large RNAs. *J. Biomol. NMR* **69**, 31-44

Funding

This work was funded by DFG (Germany), iNEXT and the University of Leeds.

The role of fluid flow in causing protein aggregation

John Dobson, Amit Kumar, Leon Willis, Chloe Dickinson, Ioanna Panagi, Alison Ashcroft, Sheena Radford, Nikil Kapur and David Brockwell

Introduction

Environmental factors, such as temperature, pH and chemical denaturants, can cause proteins to unfold, mis-fold and aggregate. In addition to these, hydrodynamic forces can induce the aggregation of both model proteins and those of biopharmaceutical interest. The aggregation of biopharmaceutical proteins prevents their access to market, as the aggregates have been linked to harming patients. In the former case, a fundamental understanding of how hydrodynamic forces conformationally remodel proteins is of interest to the protein (mis-) folding field. However, this link has remained tenuous, due to the broad range of proteins investigated and differences in the type of flow field (e.g. shear vs extensional) such proteins were subjected to. In addition, the presence/absence of air-water interfaces in certain experiments has further confounded the field. In order to understand if and how hydrodynamic flow can damage proteins, we have developed, validated and characterised a flow device which subjects protein solutions to defined fluid fields. Here, we mainly discuss data characterising the flow-induced aggregation of the model protein BSA, in addition to proteins of medical (β_2m) and therapeutic (G-CSF and three monoclonal antibodies) interest.

Results

In the flow device, two Hamilton syringes are connected together *via* a glass capillary. One syringe is filled with protein solution and the plunger driven at a defined speed by a stepper motor. Where the capillary and syringe barrel meet, there is an abrupt contraction in the flow, forcing the fluid (and the proteins contained within it) to accelerate by ~238 fold (Fig. 1 i). This generates an extensional flow field, characterised by the strain rate (Fig. 1 ii). Our hypothesis was that when a protein enters an extensional flow field, hydrodynamic force is applied, causing partial unfolding of the molecule followed by aggregation. Computational fluid dynamics validated that proteins spend microseconds in this flow regime (Fig. 1 iii), before being subjected to shear flow in the capillary. Once the protein has entered the other syringe, the protein solution is shuttled back again at the same rate. Once the desired number of passes have been completed, the rig is dissembled and the protein solution analysed using an array of biochemical and biophysical techniques.

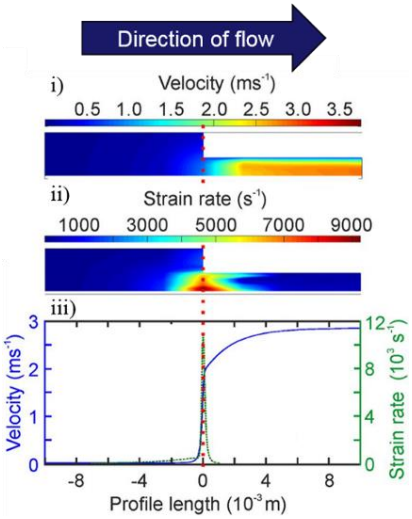

Figure 1: Overview of the flow device. i) Protein solution is driven from one syringe to the other via a thin glass capillary.The contraction in the flow generates a velocity gradient in the direction of flow (an extensional flow). ii) The magnitude of the extensional flow is characterised by the strain rate, $\dot{\varepsilon}$. At a plunger velocity of 8 mm s^{-1}, $\dot{\varepsilon}$ = 11,750 s^{-1}. iii) Computational fluid dynamics (CFD) shows that the extensional flow energy is delivered over a short distance and timescale (2 mm and 18 µs respectively). A shear flow, characterised by the shear rate $\dot{\gamma}$, then becomes the dominant flow regime in the capillary. At a plunger velocity of 8 mm s^{-1}, $\dot{\gamma}$ = 52,000 s^{-1}. Once the first syringe is empty (defined as one pass), the protein solution in the second syringe is then shuttled back in the opposite direction.

BSA was chosen as a model protein as it had been shown to unfold and aggregate under an array of different flow fields. The protein, at a concentration of 1, 2, 5 or 10 mg mL^{-1}, was

stressed in the device for 500, 1000, 1500 or 2000 passes at a plunger velocity of 8 mm s^{-1}. Following ultracentrifugation, the amount of protein left in solution was determined using UV-visible spectroscopy. These experiments revealed that as the number of passes and the concentration of protein were increased, there was a decrease in the amount of protein left in solution. Transmission electron microscopy (TEM) showed that the aggregates which form are amorphous in nature, becoming more defined as a function of pass number (Fig. 2). Importantly, quiescent samples left under ambient conditions for the length of the experiment (up to 3.5 h) showed no evidence of aggregation. In order to dissect the dispersity of the aggregates formed due to flow, Dynamic Light Scattering, Nanoparticle Tracking Analysis and Fluorescence Correlation Spectroscopy (with a 1% v/v addition of Alexa 488-labelled BSA) were employed. These techniques revealed that aggregates ranging from tens of nm to several microns form as a function of pass number and concentration. The sensitivity of FCS allowed us to determine that aggregation is detectable after as few as 10 passes for a 5 mg mL^{-1} BSA solution. Further labelling experiments and velocity variation determined the role of extensional flow in triggering BSA's aggregation.

To see if aggregation could be elicited in other proteins, several other molecules were stressed in the device of differing size and topology to the 66 kDa, α-helical BSA. The small (11 kDa) protein β_2m, the four-helical cytokine GCSF and three monoclonal antibodies (mAbs) were stressed in the device for 20 and 100 passes, then analysed biophysically. These experiments revealed that BSA and β_2m are largely resistant to flow, though the latter protein does form nano-fibrillar structures under buffer conditions where it is not usually amyloidogenic (Fig. 2). The proteins of biopharmaceutical interest were generally more susceptible to flow. Of note, the mAbs WFL and STT differ by just 6 residues in total (in CDRs 1 and 2), yet display markedly different aggregation behaviour (Fig. 2).

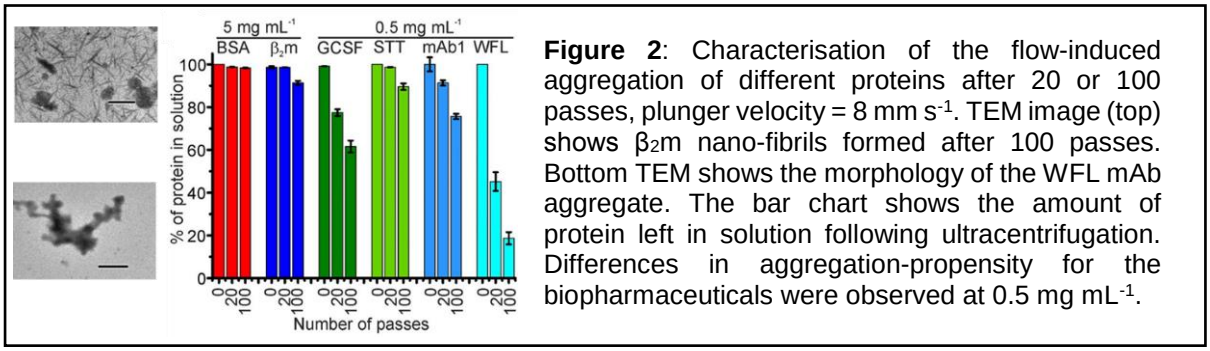

Figure 2: Characterisation of the flow-induced aggregation of different proteins after 20 or 100 passes, plunger velocity = 8 mm s^{-1}. TEM image (top) shows β_2m nano-fibrils formed after 100 passes. Bottom TEM shows the morphology of the WFL mAb aggregate. The bar chart shows the amount of protein left in solution following ultracentrifugation. Differences in aggregation-propensity for the biopharmaceuticals were observed at 0.5 mg mL^{-1}.

In summary, we now have more understanding of how extensional flow affects proteins, with a mechanistic picture of BSA's flow-induced aggregation. Current work is now focussed on utilisation of the device to map the aggregation landscapes of biopharmaceuticals, based on the sensitivity of these proteins to extensional flow. The sequence, flow rates, exposure times and buffer conditions will all play an important role in causing these proteins of pharmaceutical interest to aggregate. We hope that by understanding such factors, robust mAb candidates and manufacturing conditions can be identified.

Publications

Dobson J., Kumar A., Willis L.F., Tuma R., Higazi, D.R., Turner R., Lowe D.C., Ashcroft A.E., Radford S.E., Kapur N. & Brockwell D.J. (2017) Inducing protein aggregation by extensional flow. *Proc. Natl. Acad. Sci. U.S.A.* **114**:4673-4678.

Funding

This work was funded by MedImmune LLC, the University of Leeds and the EPSRC.

Collaborators

University of Leeds: Roman Tuma, Joanne Tipper
External: MedImmune, Adimab

Structural biology of the microtubule cytoskeleton

Joe Cockburn

Introduction

How cellular cargo molecules recruit molecular motors and regulate their activities

The cytoplasm is a highly crowded environment containing tens of thousands of different protein species, mRNA molecules, ribosomes, vesicles and organelles. Cellular function is critically dependent on the correct localisation of these components in space and time.

The movement of cellular cargoes over long distances requires dedicated motor proteins (kinesins and cytoplasmic dynein) that use ATP hydrolysis to power movement along a dynamic network of tracks called microtubules. How these motors couple ATP hydrolysis to movement is now fairly well understood, and attention in the field is now turning towards the questions of how cellular cargoes recruit molecular motors and regulate their motility. The combined action of all the kinesin and dynein motors inside your body is very powerful – if all the kinesin motors in your cells were working at full tilt all the time, they would use up somewhere in the region of 8000 kcal of energy per day! Molecular motors must therefore be carefully regulated by their cargoes to ensure that they only consume energy then they are needed.

Results

The main focus of our activity at present is on kinesin-1, which mediates the long-range transport of diverse cellular cargoes (proteins, mRNPs, vesicles, organelles and viruses). We use structural biology, biophysical and cell biology techniques to understand how kinesin-1 switches itself off when not in use, how cargo molecules bind to kinesin, and how this "switches on" kinesin-1. We have solved the crystal structure of a new kinesin-1:cargo complex and a manuscript describing this exciting work is currently being submitted for publication.

Towards a molecular-level understanding of the ciliary transition zone

Cilia are the antennae of eukaryotic cells, sensing a wide variety of environmental signals (e.g light, molecules, proteins, and fluid flow). The cilium possesses a distinct protein and lipid composition relative to the rest of the cell. This is maintained by the transition zone, a large complex of over 20 proteins at the base of the cilium that controls the exchange of material between the cilium and the rest of the cell. Mutations in transition zone genes result in a range of autosomal recessive inherited disorders, such as nephronophthisis, Joubert Syndrome and Meckel-Gruber syndrome. Around 1% of the population are genetic carriers for these conditions. Funded by a Wellcome Trust Seed Award, and in collaboration with Prof Colin Johnson at the Faculty of Medicine and Health (University of Leeds), we will use a combination of structural and cell biology approaches to begin to obtain a unified, molecular-level understanding of the function of transition zone proteins, and how mutations in transition zone genes cause diseases. This will aid in the development of gene therapies against these conditions.

Funding

Funding from the Wellcome Trust, the Royal Society and startup funding from the University of Leeds is gratefuly acknowledged.

Collaborators

University of Leeds: Prof. Michelle Peckham, Dr Stuart Warriner, Prof. Colin Johnson.

The physics of life in extreme environments

Matthew Batchelor, Ellen Kendrick, Harrison Laurent, Michael Wilson, Samuel Lenton, David Brockwell and Lorna Dougan

Introduction

We are developing single molecule manipulation techniques and neutron diffraction to explore the physics of living systems. These powerful techniques are used to study biomolecular self-assembly and the structure and dynamics of molecules in aqueous solutions, in both simple and complex systems. We are particularly interested in the physics of life under extreme environmental conditions including high and low temperatures, high salt concentrations and high and low pH.

Results

Extremophiles are organisms which survive and thrive in extreme environments. The proteins from extremophilic single-celled organisms are structurally stable and functionally active under extreme physical and chemical conditions. These proteins provide excellent model systems to determine the role of non-covalent interactions in defining protein stability and dynamics as well as being attractive targets for the development of robust biomaterials.

Cold shock proteins exist in all orders of life and are essential to protecting organisms from damage caused by sudden drops in temperature. We are using single molecule force spectroscopy and NMR to compare the stability and flexibility of these proteins from organisms adapted to survive in very cold environments, and exploring how this regulates the function of protein binding to nucleic acids.

In a new collaboration as part of a White Rose Industrial Biotechnology studentship network we are exploring *Galdieria sulphuraria,* a polyextremophile red algae, found in pHs ranging from 0-4 and temperature up to 56^{o}C, near the very limit of eukaryotic life. Proteins secreted by this organism would be expected to remain folded and active at incredible high acidity. These proteins should display enhanced acidomechanical characteristics compared to their mesophilic homologs, making them appealing candidates to be used in design of extreme biomaterials.

As well as proteins, we are interested in understanding the importance of the solvent environment, including in terrestrial and non-terrestrial conditions. The discovery of calcium and magnesium perchlorates in Martian soil samples has fuelled much speculation that flows of perchlorate brines might be the cause of the observed channeling and weathering in the surface. We have studied the structure of a mimetic of Martian water, magnesium perchlorate aqueous solution at its eutectic composition, using neutron diffraction in combination with hydrogen isotope labeling and empirical potential structure refinement. We found that the tetrahedral structure of water is heavily perturbed, the effect being equivalent to pressurizing pure water to pressures of the order of 2 GPa or more.

Neutron diffraction experiments will also be used to explore the impact of magnesium perchlorate on water structure and amino acid association, with the aim of understanding the possibility of biomolecule self-assembly on Mars. On a more macroscale, magnesium perchlorate's ability to destabilize proteins will be studied using a host of techniques, including fluorescence and circular dichroism.

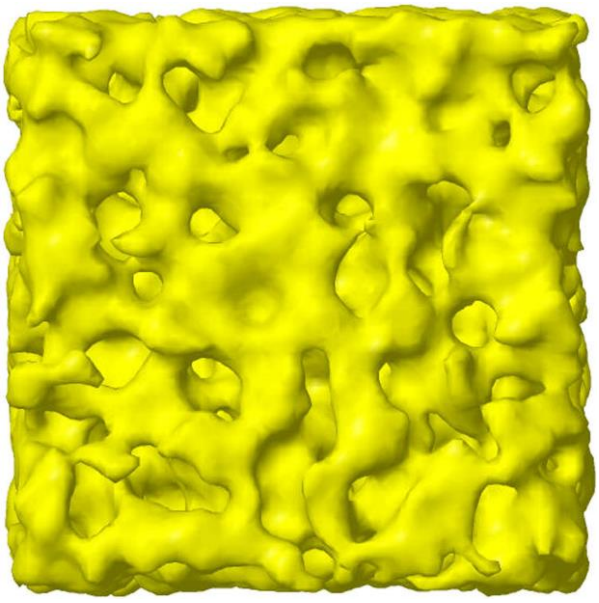

Figure 1: Highly compressed water structure observed in a perchlorate aqueous solution using diffraction and EPSR computational modelling. Distribution of water in $Mg(ClO_4)_2$ aqueous solutions. To generate the distribution of water in $Mg(ClO_4)_2$ aqueous solutions at 216 K, a Gaussian density function is placed at the center of each water oxygen atom in the EPSR simulation box with a RMS deviation (σ) of 1.5 Å (FWHM = 3.53 Å). A surface contour around the combined densities from all the water molecules is then drawn at half the maximum density. The length of one side of the cubic simulation box is 57.55 Å

Publications

Lenton S., H. Rhys N.H., Towey J.J., Soper A.K., Dougan L. (2017) Highly compressed water structure observed in a perchlorate aqueous solution. *Nature Communications*. **8**: 919

Funding

This work was funded by the EPSRC and ERC.

Collaborators

External: Alan K. Soper (ISIS Facility, Rutherford Appleton Laboratories), Natasha Rhys (University of Oxford), Prof Seth Davies (University of York), Dr Jim Gilmour & John Raffety (University of Sheffield).

Folded globular proteins as hydrogel Lego bricks

Matthew Hughes, Alexander Wright, Marcelo A. da Silva, Samuel Lenton,
David Brockwell and Lorna Dougan.

Introduction

Our aim is to develop a unique approach to the design of folded globular protein based hydrogels. Our approach involves utilising mechanical & structural techniques across multiple length scales, from single molecule techniques like atomic force microscopy to traditional rheological techniques. These methods are used to determine the major design parameters to consider when constructing a folded protein-based hydrogel. In particular we are interested in which single molecule properties scale up and which 'scale out'. This is a very powerful approach as it will allow for the specification of the physical properties (such as mechanical strength or pore size) before the gel is made and without the need for laborious exploration of the design landscape to find the desired properties.

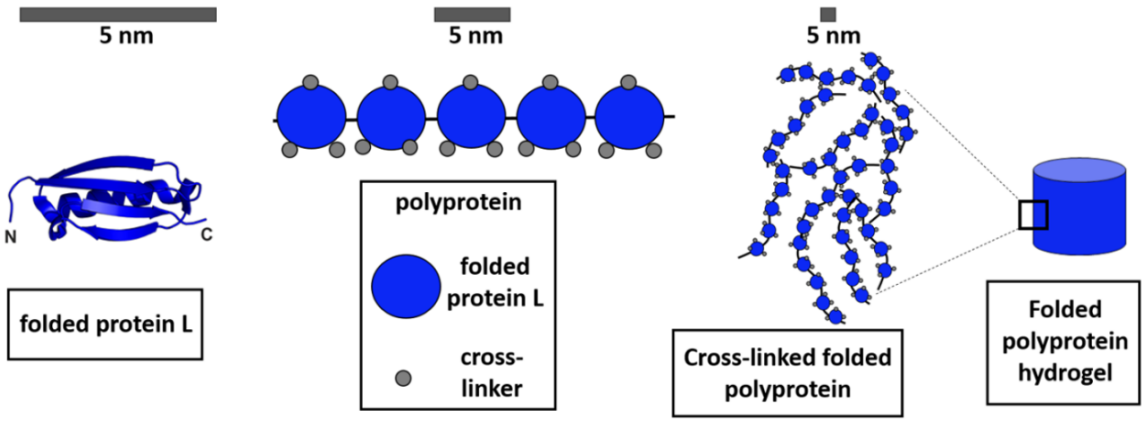

Figure 1: A visualisation of a single protein domain, formed into a polyprotein chain and crosslinked together to form a water retaining protein network.

Results

Hydrogels consist of a 3D hydrophilic, macroscopic networks swollen by large volumes of water. They are commonly made from synthetic polymers, with some research groups using unstructured peptides or the aggregation of denatured protein to produce hydrogels. In contrast, we exploit the evolutionary-optimised folded structure of globular proteins to construct a water retaining network of folded protein that preserves the innate function of the protein. Our goal is to understand the most important parameters when designing a hydrogel with regards to its physical properties such as mechanical strength or pore size. We have completed a proof-of-concept study that accesses the potential of folded globular proteins as hydrogel building blocks. In this study polyprotein constructs of the mechanically well-characterised I27 & protein L were photo-chemically crosslinked together to form a hydrogel network as depicted in Figure 1. Using shear rheometry these hydrogels were mechanically characterised to obtain storage moduli on the order of 10s of kPa (Figure 2). The internal microstructure of the gels was also probed via neutron scattering, suggesting that the polyproteins of I27 & protein L crosslink together to form a fractal structure of large interconnected scattering centres, on the order of 100-200 nm in size (Figure 3). Importantly, it was shown that the proteins remained folded once formed into these hydrogels.

This study demonstrated that tandem arrayed folded globular proteins have great potential to be used as hydrogel building blocks.

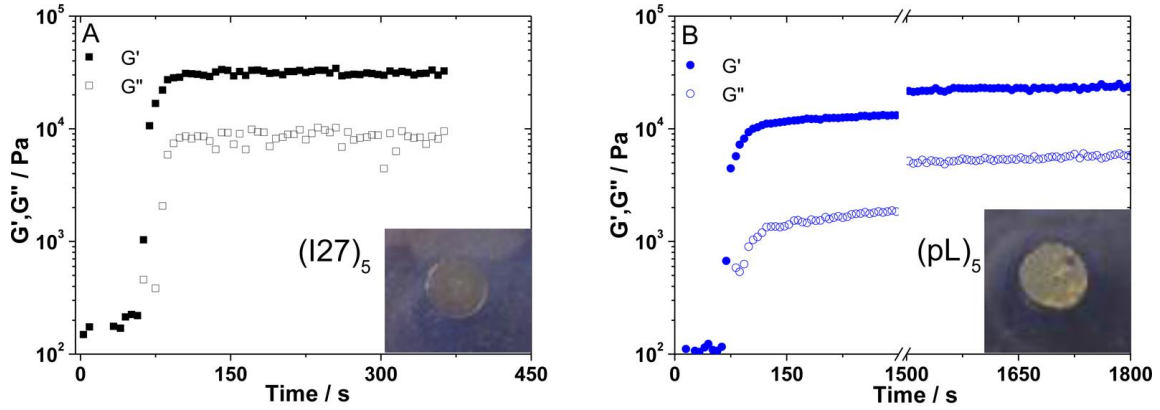

Figure 2: Time sweep curves showing the time dependence of the storage (G′) and loss (G″) moduli for the gelation of the assayed 100 mg/mL polyprotein hydrogels: (A) $(I27)_5$ and (B) $(protein\ L)_5$. G′ is shown as filled symbols and G″ as open symbols.

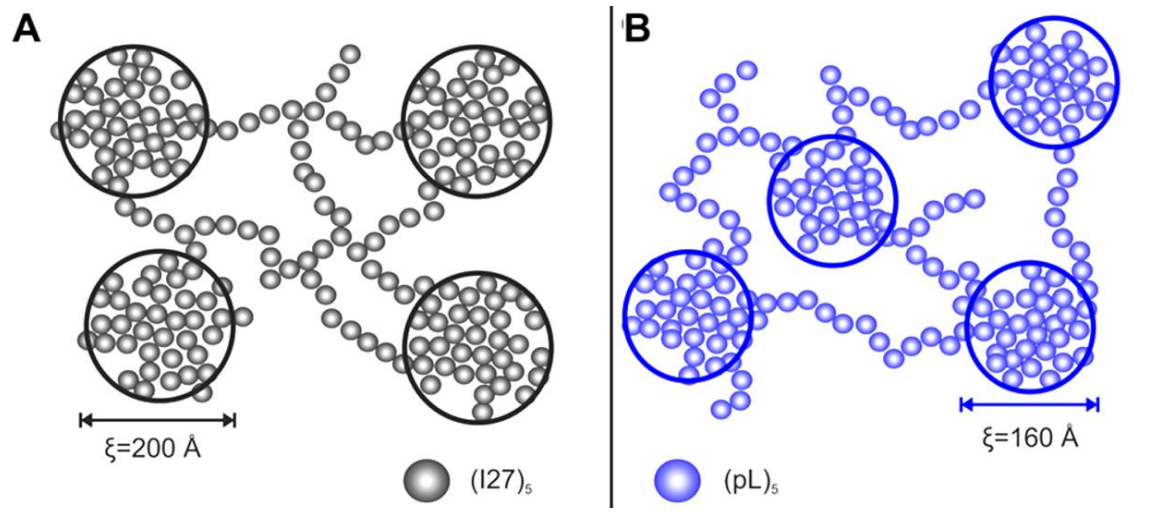

Figure 3: Schematic representation of the mesoscopic structure of the network formed by the polyprotein-based hydrogels from (A) $(I27)_5$ and (B) $(protein\ L)_5$

Publications

Da Silva M.a., Lenton S., Hughes M., Brockwell D.J., Dougan L. (2017) Assessing the Potential of Folded Globular Polyproteins as Hydrogel Building Blocks *Biomacromolecules.* **18**:636-646.

Funding

This research was funded EPSRC and ERC.

Collaborators

University of Leeds: David Head (School of Computing)

Patterned and polymer supported lipid membranes for controlling protein confinement and orientation

Peng Bao and Stephen Evans

Introduction

Supported lipid bilayers (SLBs) provide a convenient model for biological lipid membranes, facilitating direct interrogation by a broad range of spectroscopic (FTIR/Raman), structural (Neutron reflectivity, X-ray scattering, QCMD, SPR) and imaging (AFM, Fluorescence microscopy) techniques. SLBs are typically formed by the adsorption, fusion, and rupture of vesicles from an aqueous solution onto a clean glass, silica, mica or functionalised metal support and are thought to have a thin 0.5 nm -1 nm water cushion between the membrane and the support. Notwithstanding this water layer, there is evidence that the lower leaflet of the membrane interacts with the support surface and thereby influence lipid mobility but possibly also protein mobility and functionality. Thus, there has been a long-standing interest in developing supports which allow greater control over the thickness of this water cushion, thereby moving the lipid bilayer further from the solid support. There has also been significant interest in controlling the patterning of such membranes to create corrals, ratchets and structures to assess the role of confinement. In this report we present results on new ATRP-based polymer functionalised surfaces that permit patterned supported bilayer formation. Further, some have been designed to be responsive, such that they can detect changes in pH or ion gradients and hence might act as reported for functioning proteins. In a related piece of work we have also further studied the incorporation of larger integral membrane proteins into patterned bilayers and shown we can control orientation and concentration of such proteins.

Results

We developed a reaction scheme for the fabrication of binary patterned polymer brushes [1,2]. A mask was placed over an NPPOC-APTES functionalised wafer and subsequent UV irradiation (244 nm) led to deprotection of amine groups in exposed regions.

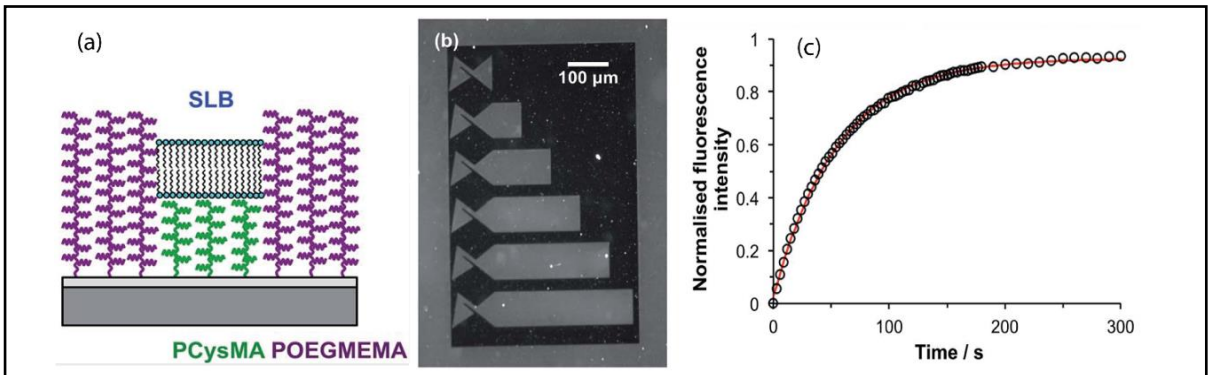

Figure 1: (A) Patterned polymer brush and SLB formation on PCysMA brushes. (B) Fluorescence microscopy of micropatterned polymer supported lipid bilayer. (C) FRAP of polymer SLB

This surface-patterned wafer was then immersed in a BIBB solution, leading to installation of ATRP initiator sites in the exposed regions. Surface ATRP was used to produce the desired patterned polymer brush (Fig. 1a). The surface is then reacted with sodium azide to end-cap the first polymer brush, and exposed to near UV light (325 nm, not damaging to the first brush) to deprotect the remaining NPPOC-APTES adsorbates. These regions are functionalised with an initiator, enabling growth of the second brush by ATRP. Using this approach patterned brushes could be made with feature sizes from several hundred nm upto the microscopic dimensions. Patterned SLBs of ternary lipid mixtures (DOPC : DOTAP : NBD–DHPE, 74 : 25 : 1) formed on PCysMA brushes via vesicle fusion (Fig. 1b) and were found to have mobile fractions and diffusion coeffiecients similar to those on glass (Fig. 1c) [1,2].

The light-activated proton pump, proteorhodopsin (pR), has seven membrane spanning domains and charged hydrophilic loops extending beyond the membrane with a molecular

weight of 29 kDa. PR can be expressed in *E. coli* and has broad potential application from photovoltaics to data storage. Here we demonstrated using fluorescently tagged pRs reconstituted into lipid bilayers that the proteins are mobile and can be concentrated via the application of an in-plane electric field (Fig. 2a,b,c and d).

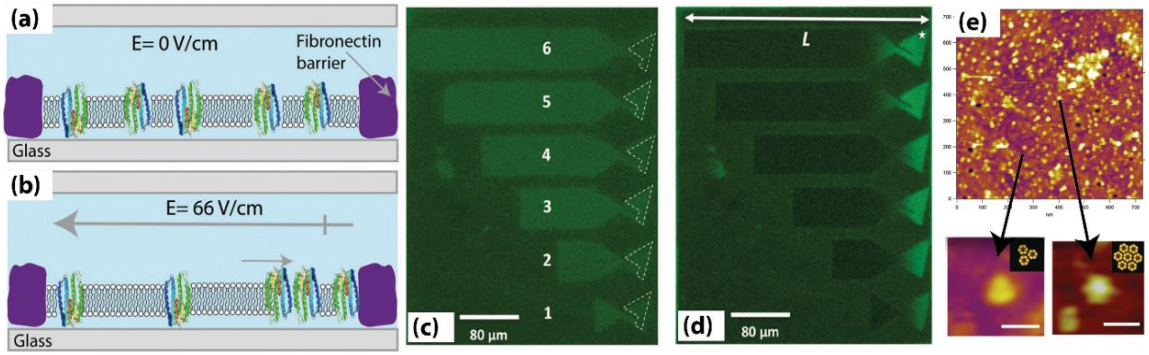

Figure 2: (A) and (B) Schematic of in-membrane electrophoretic concentration of integral membrane proteins. (C) and (D) pR distribution before and after application of E-field. €AFM height image after protein concentration.

The concentration of protein in the 'heads' of the traps was proportional to the length of the body of the trap – allowing control over protein concentration. The build-up of pR was also followed by AFM after electrophoresis, Fig. 2e. The density of pR in the 'head" of the longest trap (labelled by an asterisk in the corral 6) was ~1264 μm^{-2} after electrophoresis (Fig. 2d) compared to a density of ~50 μm^{-2} prior to the application of the field (Fig. 2c) indicating a 25 fold build-up of pR concentration.

The height data suggests two populations of pRs that protrude on average by ~0.9 and 1.4 nm, consistent with the two orientations of pR. Following the electrophoretic concentration in the trap region we find that the ratio between these populations changes from (1:1) (before E-field) to (1:9) (after E-field), with the proteins presenting higher protrusions being the dominant population (89%). This suggests that pRs with different orientations have different mobility and that the pRs with higher protrusions move more readily in SLBs. Therefore, our approach could also be potentially very useful for the separation of those membrane proteins with different orientations. This is important as, so far, little has been achieved in controlling the orientations of membrane proteins during or after reconstitution process. This was the first demonstration of the movement of integral membrane proteins using electric fields within SLBS [3].

Publications

Johnson A., Madsen J., Chapman P., Alswieleh A., Al-Jaf O., Bao P., et al. (2017) Micrometre and nanometre scale patterning of binary polymer brushes, supported lipid bilayers and proteins. *Chem Sci*. **8**:4517-4526

Johnson A., Bao P., Hurley C.R., Cartron M., et al. (2017) Simple, Direct Routes to Polymer Brush Traps and Nanostructures for Studies of Diffusional Transport in Supported Lipid Bilayers. *Langmuir* **33**:3672-3679

Bao P., Cartron M.L., Sheikh K.H., Johnson B.R.G., Hunter C.N. & Evans S.D. (2017) Controlling transmembrane protein concentration and orientation in supported lipid bilayers. *Chem Commun* **53**:4250-4253.

Funding

This work was funded by the EPSRC.

Collaborators

External: GJ Leggett , CN Hunter, S Armes (Sheffield University)

Inhibition of D-Ala:D-Ala ligase through a phosphorylated form of the antibiotic D-cycloserine

Katie Simmons and Colin Fishwick

Introduction

The increased incidence and dissemination of microbial resistance to antimicrobials point to a growing crisis in treating infectious diseases. This makes the re-evaluation and further exploration of established antimicrobial targets a potentially powerful approach to future antibacterial development. The antibacterial D-cycloserine (DCS) inhibits two sequential enzymes in the bacterial cell wall peptidoglycan biosynthetic pathway: (i) alanine racemase (Alr) and (ii) D-alanyl-D-alanine (D-Ala-D-Ala) ligase (Ddl). Unfortunately, its potential as a drug is limited as DCS is also a co-agonist of the N-methyl-D-aspartic acid (NMDA) receptor in the brain which causes seizures and peripheral neuropathy. However, its oral bioavailability, general efficacy, high gastric tolerance, and low rates of resistance means it is still of considerable interest. Ddl enzymes present an attractive target for further chemotherapeutic investigation because of their essential and universal role in bacterial cell-wall peptidoglycan biosynthesis. Although the interaction of DCS with Alr has been thoroughly studied, no comparable structural data has yet been obtained to show how DCS interacts with Ddls. We set out therefore to investigate this by elucidation of Ddl structures in complex with DCS and natural ligands to provide further mechanistic insight into the mode of inhibition.

Results

E. coli DdlB (EcDdlB) was co-crystallized with ATP and D-Ala-D-Ala (Fig. 1a), ADP and D-Ala-D-Ala (Fig. 1b), and ATP and DCS (Fig. 1c) and structures determined at < 2 Å resolution. Weighted difference maps at 1.65 Å resolution revealed the surprising discovery that phosphorylated DCS was bound in the high-affinity D-alanine binding site (D-Ala1), with the γ-5′-phosphoryl moiety of ATP having been transferred to the 3-oxygen of DCS (Fig. 1c).

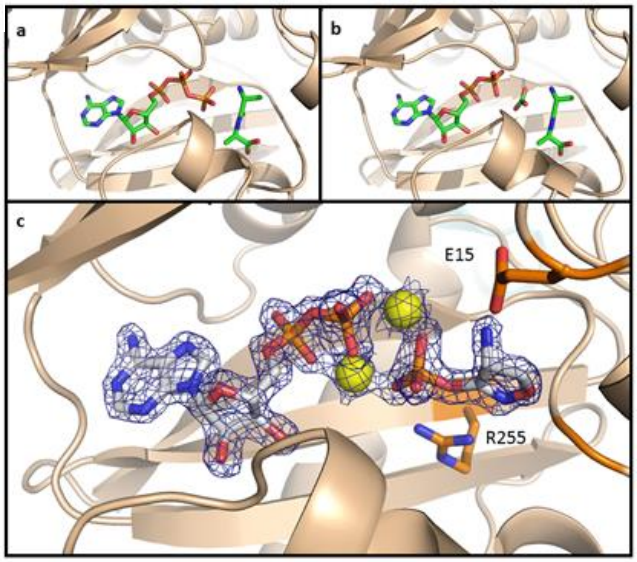

Figure 1: Active site region of EcDdlB in different complexes as described in text. EcDdlB residues Glu15 and Arg255 are within hydrogen bonding distance to DCSP.

The existence of this new chemical entity, DCSP, mimics the structure of D-alanyl phosphate, which is an obligatory intermediate formed by phosphoryl transfer during the first stage of catalysis. DCSP exploits most of the interactions that generate the high affinity site for the first D-Ala substrate (DAla1). The amino group of DCSP forms a strong hydrogen bond with the carboxylate group of Glu-15, mimicking the critical interaction made by the α-amino group of D-Ala in the first subsite. The ring oxygen of DCSP is hydrogen bonded to the backbone NH of Gly-276, in the oxyanion pocket of DdlB, while the adjacent non-protonated ring nitrogen, which occupies the position of the peptide oxygen of the dipeptide D-Ala-D-Ala product mimics

the bifurcated interactions with Gly276 NH and Arg-255 NH1 made by this atom in the product complex. The DCSP phosphate group is hydrogen bonded to Arg-255, Lys-215 and the amide nitrogen of Ser-150, replicating the interactions observed with the γ- phosphate of ATP and it forms additional links with the adjacent ADP via two coordinated magnesium ions that bridge between the DCSP and ADP molecules.

In relation to neurotoxic effects associated with the binding of DCS to the NMDA receptor, it has been documented that D-serine, DCS and glycine bind to the NR1 region of the NMDA receptor in overlapping positions. In order to explore the possibility that the phosphorylated DCS species may also bind within the NMDA receptor, we applied the docking algorithm eHiTS to the D-cycloserine binding region within the NR1 crystal structure, and modelled the resulting best docking "pose" (Fig. 2) These studies indicated that there is insufficient space in the NDMA ligand binding site to accommodate the DCSP species. Importantly, the phosphate group cannot be accommodated within the ligand binding site due to predicted steric clashes of DCSP with the wall of the NMDA ligand-binding cavity. We conclude that it is highly unlikely that DCSP or analogues developed from this structure, if able to cross the blood-brain barrier, would result in NMDA receptor activation and the side effects associated with DCS treatment. The results underscore the biochemical flexibility of this remarkably simple antibiotic.

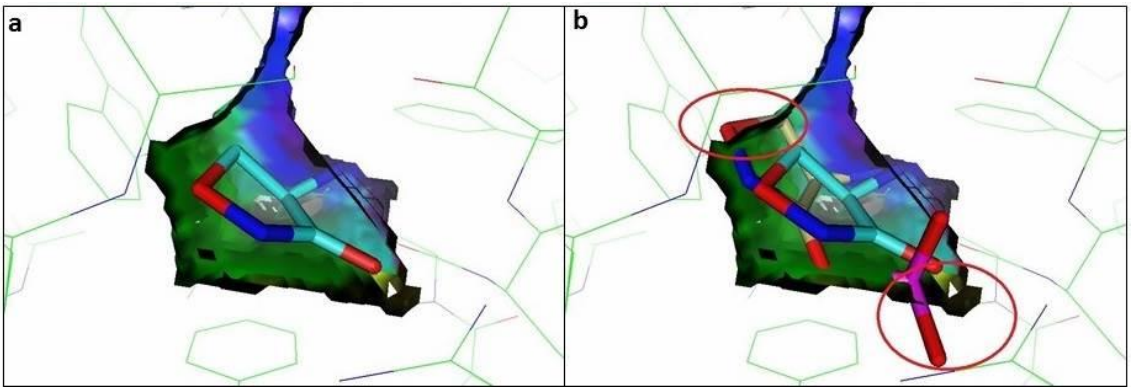

Figure 2: (A) Crystal structure of the NMDA receptor with bound DCS (cyan). Surface colour coded to indicate nature of surrounding residues; green = hydrophobic, red/blue = polar; (B) NMDA structure with best-docked pose for DCSP (beige) with location of DCS (cyan) overlayed for reference. The fit of DCSP is poor and the molecule violates the surface of the binding cavity in two places (red circles).

Publications

Batson S., De Chiara C., Majce V., Lloyd A., Gobec S., Rea D., Fulop V., Thoroughgood C., Simmons K.J.,Fishwick C.W.G., Pedro de Carvalho L. & Roper D. (2017) Antibiotic inhibition of D-Ala:D-Ala ligase through a novel phosphoryl intermediate. *Nature Comms*. **8**: 1939.

Funding

This work was funded by the Wellcome Trust and the Medical Research Council.

Collaborators

External: Sarah Batson, Cesira de Chiara, Vita Majce, Adrian J. Lloyd, Stanislav Gobec, Dean Rea, Vilmos Fülöp, Christopher W. Thoroughgood, Christopher G. Dowson, Luiz Pedro S. de Carvalho & David I. Roper

Imaging Herpes Simplex Virus life cycle using cryo-electron microscopy

Lorelai Vennard, Benjamin Chadwick, Oliver Debski-Antoniak and Juan Fontana

Introduction

HSV is a highly contagious infection endemic throughout the world that causes diseases ranging from mild skin lesions to serious encephalitis and neonatal infections. Furthermore, the ~400 million people infected worldwide with HSV type 2 have an increased susceptibility to infection by HIV and so HSV-2 infection represents an urgent public health threat. Antivirals that reduce the severity and frequency of HSV symptoms exist. However, these drugs cannot cure infection, and there is no vaccine against HSV or any other herpesvirus. Using cryo-electron microscopy (cryo-EM), an approach that allows imaging of viruses in their native state, we have been able to study two key steps of the HSV life cycle: entry to the cell and exit from the nucleus. Cryo-EM approaches include cryo-EM reconstruction (i.e. “single particle reconstruction”), for near-atomic resolution of identical particles; cryo-electron tomography (cryo-ET), for 3D imaging of unique objects; and subtomogram averaging, for molecular resolution of repeated structures within a tomogram, like fusion proteins within a virion.

Results

Viral entry is a key step of viral infection, and in enveloped viruses like HSV it is mediated by a viral transmembrane ‘fusion’ protein. Such proteins bind target membranes and transition from a pre-fusion to a post-fusion conformation, during which the merging of viral and cellular membranes is achieved. Strikingly, there is no structure available for any herpesvirus fusion protein (gB) in its pre-fusion conformation.

To characterise the different conformations of gB, we set up a system that generates vesicles displaying full-length gB from HSV type 1 on their envelope. Using this approach, we generated vesicles expressing WT gB, gB genetically tagged with fluorescent proteins (FPs), gB co-expressed with neutralizing antibodies, and gB incubated with antibodies against the fusion loops. We characterized these gB forms using cryo-ET and subtomogram averaging. This approach made the FPs, Fabs and antibodies visible, enabling us to use them as structural landmarks for localizing the different gB domains. Additionally, we showed that the different gB samples were antigenically intact, as determined by the fact that gB epitopes covering all gB domains were preserved when expressed in microvesicles. Overall, these experiments suggest that the arrangement of the initial pre-fusion gB contains its fusion loops pointing down toward the virion envelope. Our results also provide important insight into how the transition of gB from its pre-fusion to post-fusion state takes place, and therefore provide a starting point for a molecular understanding of HSV fusion process, and consequently for the development of new approaches to prevent HSV infection
(Figure 1).

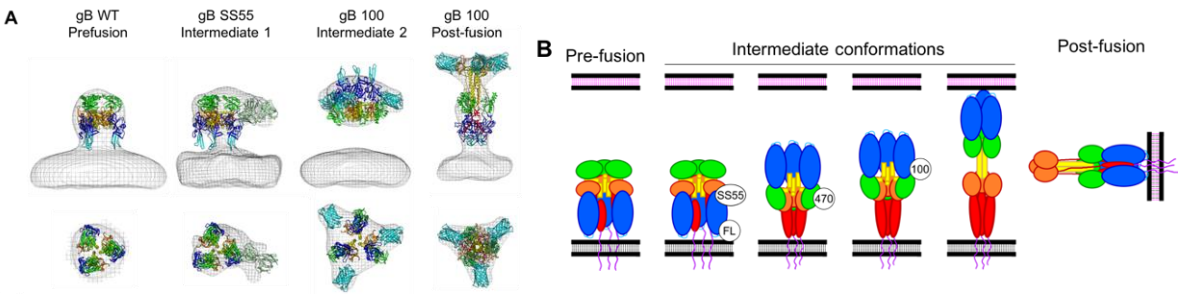

Figure 1: Model of HSV-1 fusion. (A) Models of prefusion, intermediate, and postfusion gB fitted into gB subtomogram averages. gB SS55: gB co-expressed with the SS55 neutralising Fab. gB 100 contains a FP insertion in residue 100. (B) Schematic diagram of gB transitions from the pre-fusion to the post-fusion conformation.

Herpesvirus capsids, which are produced in the nucleus, are too large to travel to the cytoplasm via the nuclear pore complexes. Therefore, they follow a two-step process of envelopment/de-envelopment. This process is based on interactions between the capsid, the inner nuclear membrane (INM), and the nuclear egress complex (NEC), a heterodimer of two viral proteins: a membrane protein (pUL34) and one with affinity for the capsid (pUL31). To characterize the NEC-capsid interactions, we employed a pUS3-null mutant. Since the viral protein kinase pUS3 is required for the HSV capsid to exit from the perinuclear space, this mutant produces an accumulation of enveloped HSV-1 capsids in the perinuclear space (which are termed Primary Enveloped Virions or PEVs). A protocol based on controlled sonication and differential centrifugation allowed us to produce an enriched sample of PEVs amenable for cryo-EM and cryo-ET experiments. This approach allowed us to characterise the native structure of the PEVs and propose a model of how the NEC interacts with the viral capsids.

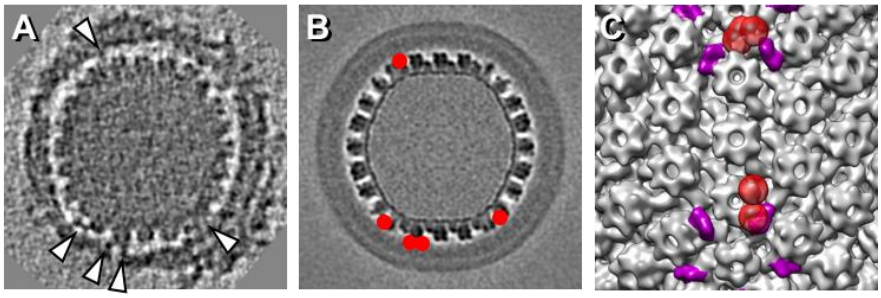

Figure 2: Densities bridging between the NEC layer and the capsid. Left panel: Central tomographic slice of a PEV. Some bridging capsid-NEC densities are labelled with arrowheads. Middle panel: Corresponding slice from a PEV cryo-EM reconstruction, with the sites of bridging densities marked with red circles. Right panel: Rendering of part of the HSV capsid surface, with the capsid densities responsible for the interactions with the NEC in magenta. The spheres represent the same bridging densities labelled in the tomographic section (left panel).

We are now expanding these results to unravel the intermediate conformations of the Influenza virus fusion protein, and the egress of Kaposi's sarcoma-associated herpesvirus.

Publications

Fontana J., Atanasiu D., Saw W.T., Gallagher J.R., Cox R.G., Whitbeck J.C., Brown L.M., Eisenberg R.J. & Cohen G.H. (2017) The Fusion Loops of the Initial Prefusion Conformation of Herpes Simplex Virus 1 Fusion Protein Point Toward the Membrane. *MBio*. **8**: e01268-17.

Newcomb W.W., Fontana J., Winkler D.C., Cheng N., Heymann J.B. & Steven A.C. (2017) The Primary Enveloped Virion of Herpes Simplex Virus 1: Its Role in Nuclear Egress. *MBio*. **8**: e00825-17.

Funding

This work was funded by the University of Leeds, the Royal Society, the Academy of Medical Sciences and the Rosetrees Trust.

Collaborators

External: D. Atanasiu, W.T. Saw, R.J. Eisenberg & G.H. Cohen (University of Pennsylvania); W.W. Newcomb, D.C. Winkler, N. Cheng, J.B. Heymann & A.C. Steven (National Institutes of Health).

Development of a novel small molecule anticoagulant with minimal bleeding risk

Roger Taylor, Robert Ariens, Colin Fishwick, Charlotte Revill, Emma Hethershaw, Helen Philippou and Richard Foster

Introduction

The underlying focus of our research is small molecule drug discovery. We are interested in the synthesis and development of small molecules as therapeutics as well as the design of chemical probes to support validation of novel biological targets in areas of unmet medical need. A priority area of research is development of new approaches to the generation of small molecule anti-coagulants with minimal bleeding risk.

Results

We have identified potent, novel small molecule inhibitors of the coagulation cascade with exceptional *in vivo* efficacy in a number of mouse models of thrombosis. The inhibitors have been identified by a number of parallel approaches incorporating virtual drug design, chemical synthesis and high-throughput screening of drug-like small molecule libraries and fragment screening. Presently, we are optimising the inhibitors for target potency, specificity and drug-like physicochemical properties using iterative rounds of medicinal chemistry development and screening using a panel of orthogonal bioassays. The compounds have been optimised for drug-likeness and demonstrate high aqueous solubility, metabolic stability, plasma stability and low levels of plasma protein binding and cardiotoxicity, including hERG inhibition. The compounds are highly potent (sub 10 nM IC50) and demonstrate >300x selectivity for 10 structurally (and functionally) related targets. Additionally the compounds demonstrate no toxicity on high concentration dosing in mice. The aim of the on-going work is to further develop the leads to generate a candidate compound with suitable pharmaceutical properties consistent with an optimised lead ready for progression to clinical trials. A second series of inhibitors identified by fragment-based screening (ligand-observed NMR and SPR) is undergoing optimisation for potency driven by structural guided design. The second series of ligands bind in a different manner to the primary series and offer a possibility to generate inhibitors with a complementary selectivity and property profile to the current leads.

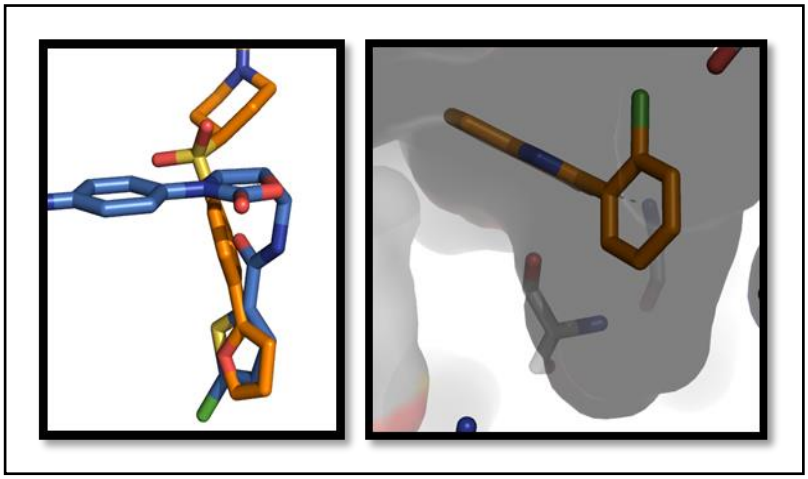

Funding

This work is funded by the Wellcome Trust, MRC and BHF.

Affimer proteins inhibit immune complex binding to FcγRIIIa with high specificity through competitive and allosteric modes of action

Maren Thomsen and Adrian Goldman

Introduction

The pathogenesis of autoimmune diseases is driven by immunoglobulins binding to Fcγ receptors (FcγR), leading to inflammation and the destruction of tissue. Targeting the responsible Fcγ receptor FcγRIIIa seems to be a valid strategy to halt or at least slow these processes. However, all Fc receptors are highly homologous, making it hard to develop specific inhibitors and increasing the likelihood of off-target effects with FcγRIIIb. These problems have so far nullified all efforts to create inhibiting therapeutic antibodies.

Results

We analysed two co-crystal structures of FcγRIIIa bound to two different adhirons to determine their mode of action and to identify the basis for their specificity. Adhiron G3 (AdG3) binds in the interface between the two ectodomains of FcγRIIIa (Figure 1A), keeping the receptor in a very restricted conformation and decreasing the angle between the two domains by 12° in comparison to IgG-bound FcγRIIIa, showing that AdG3 acts allosterically: the IgG binding site does not overlap with the AdG3 binding site. AdG3 and FcγRIIIa interact through a branched hydrogen-bond network that reaches from VR1 to VR2 and involves the FcRIIIa/b discriminating residue (a-R18/b-S18; Figure 1B). We proposed that AdG3 is specific because the network of intramolecular H-bonds around FcγRIIIa R18 stabilises a local conformation that selectively binds AdG3. S18 could not stabilise this conformation.

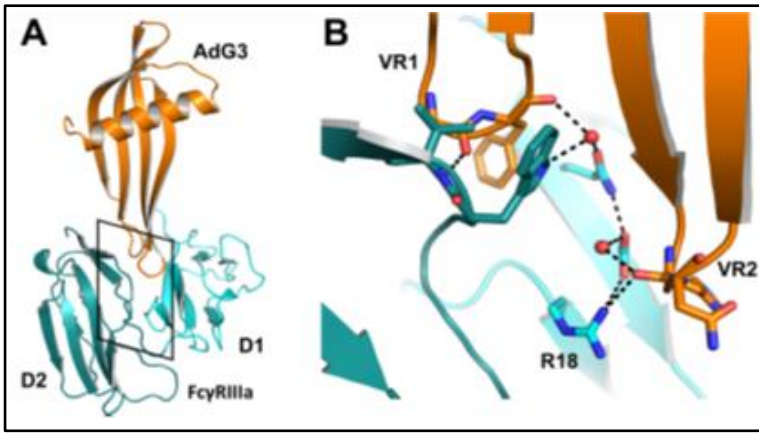

Figure 1: Molecular basis of AdG3 selectivity forFcγRIIIa. (A) Overview ofAdG3 (orange) binding to FcγRIIIa (D1 cyan, D2 teal). AdG3 binds between the domains of FcγRIIIa narrowing the D1-D2 angle by 12°. (B) Close-up view of AdG3-FcγRIIIa interactions. A hydrogen network involving water molecules and the discriminating residue R18 connects VR1 and VR2.

In contrast, adhiron F4 (AdF4) binds to the surface of D2 of FcγRIIIa, burying nearly half of the IgG binding site and so acts as a competitive inhibitor (Figure 2A). AdF4 specificity for FcRIIIa is likely focussed around the region containing the FcRIIIa/b discriminating residue (a-G129/b-D129), even though this region does not contribute to adhiron binding. However, Y132 is buried by VR2 and so locked in one specific rotameric conformation in close proximity to G129. In silico mutagenesis of G129 to D129 results in severe clashes between D129 and Y132 (Figure 2B). To prevent this clash, Y132 would have to move, thus destabilising the hydrophobic interaction with VR2 of AdF4 and disordering the loop. MD simulations in collaboration with Sarah Harris show that indeed Y132 moves away from D129, thus destroying the hydrophobic patch with VR2 (Figure 2C).

Adhirons are a promising tool for generating highly specific protein-interaction inhibitors even in highly homologues families due to their ability to explore new binding sites.

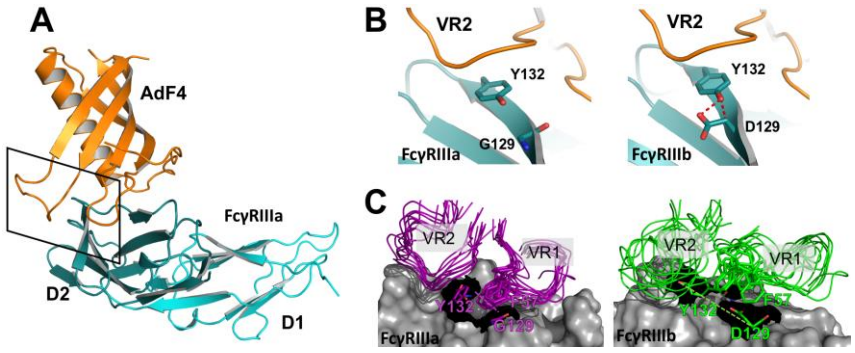

Figure 2: Structural basis explaining specificity of AdF4 for FcγRIIIa. (A) Overview of AdF4 (orange) binding to D2 of FcγRIIIa (D1 in cyan, D2 in teal). (B) Specific molecular recognition of FcγRIIIa depends on second shell binding residue at position 129. Cocrystal structure of AdF4 bound to FcγRIIIa (left with G129) and mutated in silico to resemble FcγRIIIb (right with D129). The mutation G129D results in severe clashes (red dashed lines, distances below 2.4 Å) with Y132. (C) AdF4 variable region interface in FcRIIIa and FcRIIIb from MD simulations. AdF4 VR1 and VR2 are depicted as ensembles of snapshots taken at 20 ns intervals in representative simulations of the FcγRIIIa- and FcγRIIIb-AdF4 interactions.

Publications

Kolodziejczyk R., Mikula K.M., Kotila T., Postis V.L.G., Jokiranta T.S., Goldman A. & Meri T. (2017) Crystal structure of a tripartite complex between C3dg, C-terminal domains of factor H and OspE of Borrelia burgdorferi. *PLoS One* **12**:0188127.

Saarma M. & Goldman A. (2017) Obesity: Receptors identified for a weight regulator. *Nature* **500**:195-197.

Saarenpää T., Kogan K., Sidorova Y., Mahato A.K., Tascón I., Kaljunen H., Yu L., Kallijärvi J., Jurvansuu J., Saarma M. & Goldman A. (2017) Zebrafish GDNF and its co-receptor GFRα1 activate the human RET receptor and promote the survival of dopaminergic neurons in vitro *PLoS One* **12**:0176166.

Shah N.R., Wilkinson C., Harborne S.P.D., Turku A., Li K-M., Sun Y-J., Harris S. & Goldman A. (2017) Insights into the mechanism of membrane pyrophosphatases by combining experiment and computer simulation Structural Dynamics. *Struct Dyn* **4**:032105.

Wright J., Thomsen M., Kolodziejczyk R., Ridley J., Sinclair J., Carrington G., Singh B., Riesbeck K. & Goldman A. (2017) The crystal structure of PD1, a Haemophilus surface fibril domain, *Acta Crystallogr F Struct Biol Commun* **73**:101-108.

Funding

Marie Skłodowska-Curie Individual Fellowship (HeartAtaK 708051), BBSRC (ALERT-13 and BB/M021610/1), Royal Society (Wolfson award), Wellcome Trust (091322/2/10/2), Academy of Finland (12522061), Erkko foundation

Collaborators

University of Leeds: Ann W. Morgan, Sarah Harris, Colin Fishwick
External: Seppo Meri, Henri Xhaard, Roberto Docampo, Arwen Pearson, Reijo Lahti, Jari Yil-Kauhaluoma

Flavivirus small membrane (M) proteins as potential ion channel antiviral targets

Emma Brown, Matthew Bentham, Hannah Beaumont, Abigail Bloy, Rebecca Thompson, Clive McKimmie, Richard Foster, Neil Ranson, Andrew Macdonald, Antreas Kalli and Stephen Griffin

Introduction

Flavivirus small membrane (M) proteins play a well-characterised role during virion assembly, secretion and maturation, serving as a chaperone for the envelope (E) glycoprotein as part of the pr-M-E precursor. However, unlike the pr peptide, M protein persists within the mature virion as an integral membrane protein with two short *trans*-membrane domains (TMD), yet whether it plays a further role during the virion life cycle remains unclear.

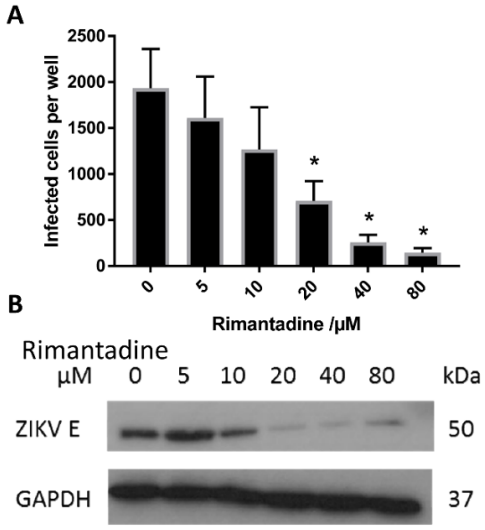

Figure 1: Rimantadine sensitive entry of ZIKV in Vero cells. (A) Vero cells were infected at a MOI of 0.1 PFU/cell ZIKV in the presence of increasing rimantadine concentrations. Infected cells were stained using anti-ZIKV E antibody and quantitated by immunofluorescence using an Incucyte. (B) Experiment identical to (A), but cells were instead lysed and probed for ZIKV E by western blotting. * p≤0.05 Student T test, three experimental repeats.

We have investigated the hypothesis that M functions as a virus-coded ion channel, or "viroporin", within virion membranes, with a potential role during entry and uncoating of infectious particles. Whilst dimeric in the mature virion, ultrastructural changes induced by endosomal acidification provide an environment in which M might rearrange into a higher order oligomer with potential to mediate protonation of the virion core, thus enabling uncoating of the virus genome as it enters the cell.

Our approach combines molecular dynamic simulations of M within membranes, combined with structural and biochemical analysis of ion channel function and the use of small molecule inhibitors against viruses in culture. Confirmation of M-specific channel activity would provide an important opportunity to develop new drugs capable of limiting or preventing infection by globally challenging *Flaviviruses* such as dengue, Yellow Fever, West Nile and Zika viruses.

Results

We first determined whether viroporin activity played a potential role during the *Flavivirus* cell entry process by using the broad-spectrum viroporin inhibitor, rimantadine. Reassuringly, rimantadine was able to reduce the infectivity of Zika virus (ZIKV) within Vero cells in a dose dependent manner, judged by both infectious titre and a reduction in viral protein expression in bulk culture (Figure 1). We are currently attempting to select rimantadine-resistant ZIKV in culture by sequential supernatant passage in the presence of increasing drug concentrations, with the aim of identifying associated polymporphisms within the M protein sequence.

Acidification of Flavivirus particles leads to dramatic rearrangments of their E glycoproteins, releasing M dimers from potentially restrictive interactions. To explore whether M proteins retain the potential to form higher order oligomers when free to migrate within the virion membrane, we undertook course-grain molecular dynamics simulations. Due to the very short TMDs present within M in the Dengue/Zika virus cryo-EM structures, previous studies have predicted that M might rearrange into a single *trans*-membrane structure, supported by peptides corresponding to such regions retaining channel activity *in vitro*. However, simulations do not support the stability of such rearrangements, instead showing that M in its

native form mediates compression of the lipid bilayer such that the M TMDs are membrane-spanning. M also readily dimerises over a relatively short time-frame, and simulations with higher order structures are ongoing. We have also created 5-, 6-, and 7-mer models for potential M channel complexes, where the channel lumen is lined by the C-terminal helix 3, which retains characteristics analogous to pore-lining peptides. These are currently being investigated for stability using simulations and will later serve as templates to guide mutagenesis and *in silico* drug design.

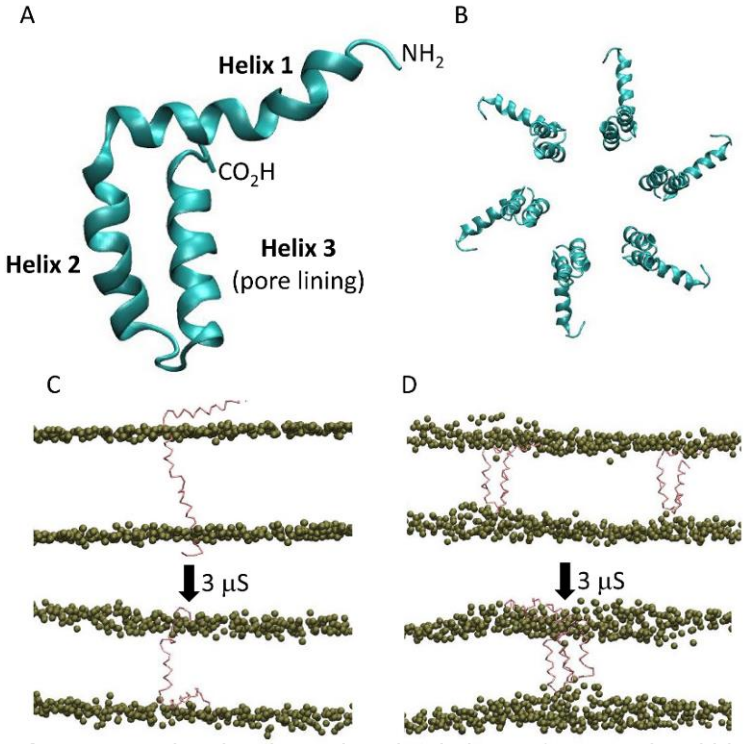

Figure 2: Molecular dynamics simulations of M protein within model membranes. (A) M protein adapted from ZIKV Cryo-EM structure showing extra-membrane helix 1 and the two TMDs, of which helix 3 is predicted to be pore-lining. (B) Hexameric model of M protomers. (C) Course-grain simulation of M forced into single TMD conformation showing partial reversion to 2 TMD structure. (D) M protein dimerization following placement of two protomers at 80 nm distance within the membrane.

Finally, we have begun structural and functional characterisation of M within both model and virion membranes. Prokaryotic expression trials of recombinant M are ongoing, and we are establishing protocols to determine the cryo-EM structure of acidified ZIKV particles to detect the presence of M channel complexes.

Funding
This work was funded by a studentship from the Leeds Institute for Cancer & Pathology, FMH, awarded to SG, CM and RF.

Collaborators
University of Leeds: A. Macdonald, N Ranson, A Kalli
External: Andres Merrits (University of Tartu, Estonia).

Towards a better understanding of oxidative biomass deconstruction

Glyn Hemsworth

Introduction

The industrial production of lignocellulosic biofuels, a greener fuel for the future, remains too costly to compete with fossil fuels at present. There has therefore been great interest in the discovery of lytic polysaccharide monooxygenases (LPMOs). These oxidative enzymes are able to introduce chain breaks into the crystalline regions of cellulose, thereby augmenting the ability of traditional enzyme cocktails to depolymerise this substrate – one of the most difficult steps in the process. We are interested in how LPMOs are activated, which could be key to ensuring that they are used optimally in the biorefinery.

Results

Working with Prof Bernard Henrissat, founder of CAZy (www.CAZy.org), we have identified a set of targets from bacteria to be studied (Figure 1A). These proteins contain X-domains, which have unknown functions but are often appended to Carbohydrarte Binding Modules (CBMs), suggesting a role in polysaccharide processing. Further analysis suggests many of these domains could harbor electron transfer functions and so we are interested in delineating whether or not they are LPMO activators, and aim to assign their function.

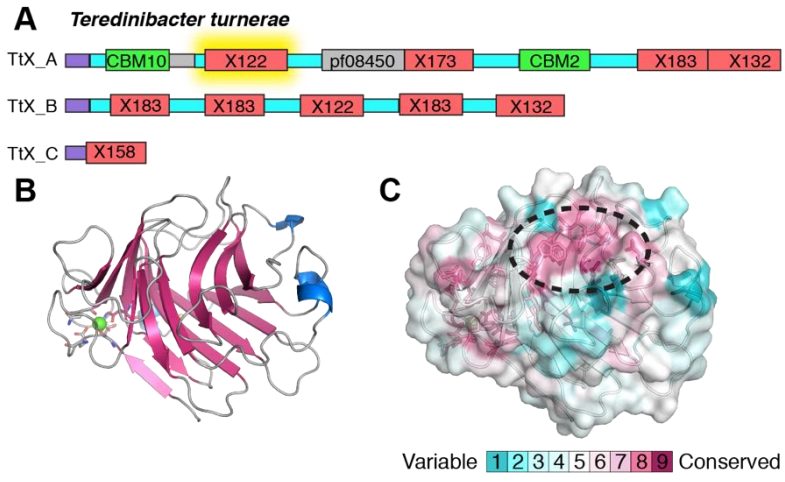

Figure 1: (A) The domain architecture of some of our targets. TtX122A is highlighted with a yellow background (B) Overall structure of TtX122A shown in cartoon representation coloured by secondary structure. (C) Consurf analysis showing sequence conservation within the X122 family on the surface of the TtX122A structure coloured according to the inlay. A conserved patch which could represent the active site of an enzyme is circled with a black dashed line.

We recently determined the structure of TtX122A at 1.5 Å resolution (Figure 1B). The structure reveals a polysaccharide lyase-like fold. Its closest structural match is the protein Cip1 (Cellulose Induced Protein-1) from *Trichoderma reesei*, which is expressed during growth on cellulose though its function is unknown. Sequence conservation analysis within the X122 family, suggests that there is a patch of conserved residues where the active site would normally be located in a typical polysaccharide lyase (Figure 1C). Initial assays are underway examining a range of poly- and oligosaccharides as enzymatic substrates in the hope of providing novel insight into the function that this domain plays in oxidative biomass degradation.

Funding

This work is funded by the BBSRC.

Collaborators

University of Leeds: Prof Alan Berry
External: Prof Bernard Henrissat (AIX Marseille Université), Prof Paul Walton (University of York), Dr Alison Parkin (University of York).

Topological dissection of a protein derived from cysteine accessibility and mass spectrometry

Antonio Calabrese, Scott Jackson, Lynsey Jones, David Sharples,
Sheena Radford, Alison Ashcroft and Peter Henderson

Introduction

Cysteine accessibility and quantitative mass spectrometry (MS) analyses have been devised to study the topological transitions of Mhp1, the membrane protein for sodium-linked transport of hydantoins from *Microbacterium liquefaciens* [1]. The workflow devised is simple and applicable to a range of systems, enabling the interrogation of protein structure, the structural changes required for function, and the structural consequences of mutations.

Results

Mhp1 has previously been crystallised in three forms (outward-facing open, outward-facing occluded with substrate bound, and inward-facing open, Figure 1). We show that one natural cysteine residue, Cys327, out of three, has an enhanced solvent accessibility in the inward-facing (relative to the outward-facing) form (Figure 1).

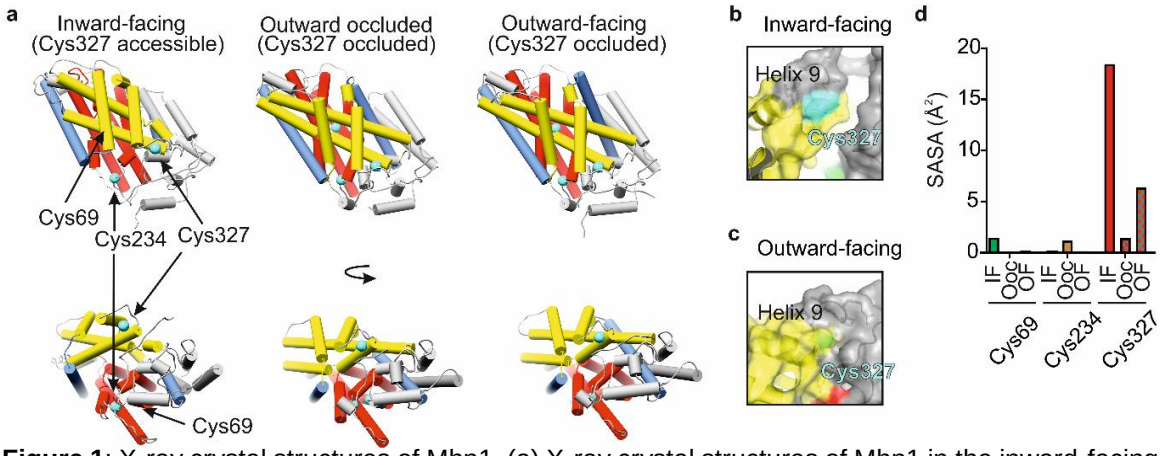

Figure 1: X-ray crystal structures of Mhp1. (a) X-ray crystal structures of Mhp1 in the inward-facing (PDB 2X79), outward-occluded (PDB 4D1B) and outward-facing (PDB 2JLN) conformations. Helices are represented as cylinders. The bundle helices (TMHs 1, 2, 6, 7) are coloured red, the hash motif helices (TMHs 3,4,8,9) are coloured yellow, the flexible helices (TMHs 5 and 10) are coloured blue, the C-terminal helices (TMHs 11 and 12) and the surface extracellular and cytoplasmic helices are coloured grey. The Cys residues are shown in cyan. (b,c). Location of Cys327 (cyan) in the (b) inward-facing and, (c) outward-facing conformations of Mhp1, showing that TMH9 protects Cys327 from solvent in the outward-facing conformation. (d) Average side-chain solvent accessible surface area (SASA) values of the three Cys residues of Mhp1 in 20 ns MD simulations started from the inward-facing (IF), outward occluded (OOc) and outward-facing (OF) crystal structures.

Reaction of the purified protein, in detergent, with the thiol-reactive *N*-ethylmalemide (NEM), results in modification of Cys327 (Figure 2), suggesting that Mhp1 adopts predominantly inward-facing conformations. Addition of either sodium ions or the substrate 5-benzyl-L-hydantoin (L-BH) does not shift this conformational equilibrium but, co-addition of the two results in an attenuation of labelling, indicating a shift toward outward-facing conformations (Figure 2). Mutations that perturb the substrate binding site either result in the protein being unable to adopt outward-facing conformations or in a global destabilisation of structure [1].

From the experiments outlined we showed that purified wild-type Mhp1 in DDM detergent is in an inward-facing conformation and remains so when either a hydantoin substrate or Na^+ is

added, but changes to outward-facing when the two are added together in a concentration-dependent manner. This is an important constraint when attempting to understand individual steps of the transport cycle. Previously, information on the conformation of the protein required crystallographic structure determination, highlighting the power of NEM-MS for a simple readout and quantification of the different conformational states of the protein ensemble.

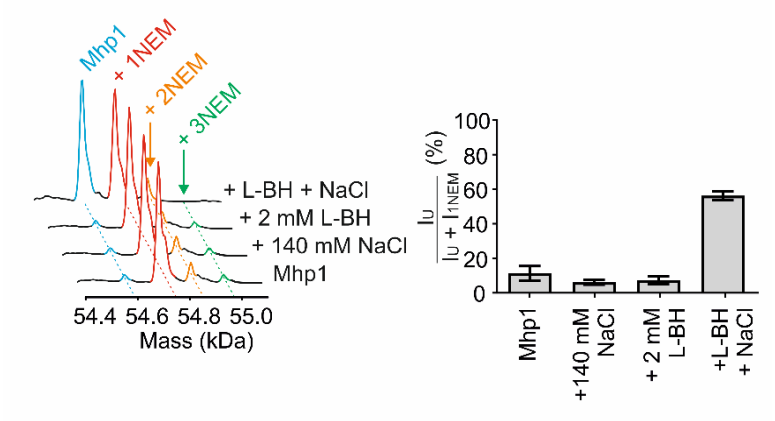

Figure 2: Mass spectrometry of wild-type Mhp1 after labelling with NEM under different conditions of substrate and/or Na^+ inclusion. (Left) Deconvoluted mass distributions of Mhp1 after NEM labelling under varied solution conditions. (Right) Relative abundances of unlabelled Mhp1 (I_U) relative to Mhp1 with 1 NEM label (I_{1NEM}) in the mass spectra. Data are shown as mean ± SEM of three independent experiments.

For other proteins for which only a single structure is available, this MS-based strategy could be implemented to discriminate hypotheses about conformational changes, identify residues important for structural maintenance, and to screen a number of variants quickly. Even when no structure is available, a model of the structure of any protein and its conformational flexibility can be tested using the strategy described, which requires only µg quantities of protein and provides rapid insights about the relative population of different conformational states that is not possible using crystallography. The NEM-MS strategy described can be readily implemented to interrogate conformational transitions, elucidate ion-substrate coupling stoichiometry, screen widely for ligand specificity and illuminate mechanistic features of membrane protein structure- function that have eluded characterisation to date.

Publication

Calabrese A.N., Jackson S.M., Jones L.N., Beckstein O., Gsponer J., Sans M., Kokkinidou M., Pearson A.R., Radford S.E., Ashcroft A.E. & Henderson P.J.F. (2017) Topological dissection of the membrane transport protein Mhp1 derived from cysteine accessibility and mass spectrometry. *Anal. Chem.* **89**:8844-8852.

Funding

This research was funded by the BBSRC (grant BB/K000659/1) to AEA, SER and PJFH including support for ANC and DS. ANC was also supported by the Wellcome Trust Institutional Strategic Support Fund (ISSF) (Grant number 015615/Z/14/Z). AEA and SER are also supported by the ERC under the EU's Seventh Framework Programme (FP7.2007-2013/Grant number 322408) and PJFH by an Emeritus Research Fellowship from the Leverhulme Trust (Grant number EM-2014-045).

Cellular interactions with amyloid

Matthew Jackson, Michael Davies, Madeline Brown, Atenas Posada Borbon, Chalmers Chau, Sheena Radford and Eric Hewitt

Introduction

The formation of insoluble amyloid fibrils is associated with a spectrum of devastating human disorders, including Alzheimer's, Parkinson's, type 2 diabetes and dialysis related amyloidosis (DRA). In these disorders the formation of amyloid fibrils results in cellular dysfunction and tissue destruction. Understanding the mechanisms of amyloid toxicity is a priority if we are to develop new therapeutics for the amyloidoses.

Overview

Our goal is to determine how the structure and physical properties of amyloid fibrils and their assembly intermediates affects the function and viability of cells. This involves a highly collaborative and multidisciplinary approach in which information obtained structural biology techniques is integrated with cell biological analyses. Currently, we are studying the oligomeric assembly intermediates and fibrils formed by the amyloidogenic sequences, α-synuclein (Parkinson's), amyloid-β (Alzheimer's) and β_2-microglobulin (DRA). We are examining the uptake of amyloid aggregates by cells, the interactions between amyloid and cellular components, the induction of inflammatory responses, and the effects of amyloid on cellular physiology and cell viability. These cell biological experiments use an array of techniques, including plate-based assays for cell viability and metabolism, live cell confocal microscopy, flow cytometry, subcellular fractionation and proteomics. In addition, we are exploring a novel single molecule platform for the delivery of amyloid aggregates into the cytoplasm of cells with colleagues in the School Electrical and Electronic Engineering.

Publications

Jackson M.P. & Hewitt E.W. (2017) Why are Functional Amyloids Non-Toxic in Humans? *Biomolecules* **7**:71.

Funding

This work was funded by the BBSRC, MRC, Wellcome Trust, EPSRC and ERC

Multilayered lipid membrane stacks for biocatalysis using bacterial membrane extracts

George Heath, Mengqiu Li, Valentin Radu and Lars Jeuken

Introduction

Multilayered membranes, along with their associated membrane proteins, are an integral part of the energy producing pathways of eukaryotic cells, gram-negative bacteria and chloroplasts. In addition to greater control over compartmentalization, the extra layering of membranes gives the organisms increased area for membrane proteins. The inner membranes of mitochondria for example, are folded into cristae to greatly increase the surface area available for the electron transport chain proteins, packing high concentrations into a small volume. Similarly, chloroplasts employ the stacking of interconnected thylakoid membranes to greatly enhance the concentrations of photosynthetic protein complexes required to efficiently harness solar energy. These structures and many others show how the lamellar stacking of membranes and their proteins hold substantial technological potential for biomimicry, where the stacking of membranes may allow the design of novel protein arrangements with possible applications in catalysis, photonics, sensing and the 3D crystallization of membrane proteins.

Here, we engineered a lipid multilayer matrix in which native electron mediators (i.e. membrane quinones like co-enzyme Q) can freely diffuse for electrocatalytic applications. Mimicking the function of cristae and thylakoid stacks in mitochondria and chloroplasts, respectively, the assembly increases the concentration of membrane enzymes per electrode surface area in a stepwise manor. We created multilayers of membrane enzymes in a native-like lipid environment using a Layer-by-Layer (LbL) technique with bacterial membrane extracts. Assemblies with two different membrane proteins are demonstrated: a membrane-bound hydrogenase from *Ralstonia eutropha*, which oxidises H_2 and an ubiquinol oxidase, cytochrome bo_3, from *Escherichia coli* which reduces oxygen. With each deposition of a membrane layer, we see the catalytic activity increasing as the total amount of enzyme on the surface increases. This biomimetic system demonstrates how the stacking of membranes can proportionally increase the concentration of active membrane proteins at surfaces.

Results

Assembly of the multilayered bacterial membrane extracts is schematically shown in Figure 1. Polycations (Poly-L-Lysine, PLL) is allowed to bind to a negatively charged 'base' membrane layer which is formed by fusion of membrane extracts with an electrode surface partly modified

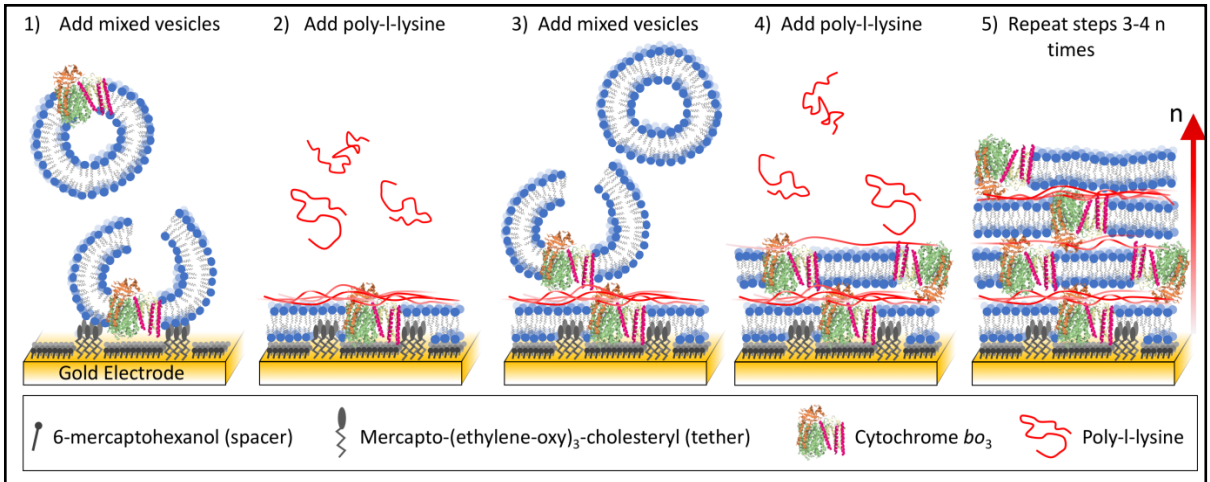

Figure 1: A schematic representation of the formation of a multilayer membrane stack using layer-by-layer assembly of negatively charged lipid vesicles that rupture on the surface to form planar membranes and positively charged PLL.

with cholesterol 'tethers' which aid the formation of a planer membrane on the electrode. Excess PLL is then rinsed away and a second membrane is formed on top via a solution of negatively charged membrane extract. This process is then repeated for each additional layer: binding of PLL followed by membrane extract in an LbL fashion.

Cyclic voltammetry (CV) reveals a linear increase in biocatalytic activity with each additional membrane layer. Figure 2 shows an example of oxygen reduction by ubiquinol oxidase from *E. coli*. Similar results were observed for hydrogen oxidation when membrane extracts from *R. eutropha,* which over-express a membrane-bound hydrogenase, are absorbed. Electron transfer between the enzymes and the electrode is mediated by the quinone pool that is present in the lipid phase. We deduce by atomic force microscopy, CV and fluorescence microscopy that quinones are able to diffuse between the stacked lipid membrane layers via defect sites where the lipid membranes are interconnected (schematically seen in Figure 2A). This assembly is akin to that of interconnected thylakoid membranes or the folded lamella of mitochondria and have significant potential for mimicry in biotechnology applications such as energy production or biosensing.

Our study shows how a simple layer-by-layer method can be used to create biomimetic interconnected lipid multilayers, which allow the concentration of active membrane enzymes at surfaces to be multiplied. The ability to incorporate a high density of active membrane enzymes using mixed membrane extracts highlights the system's adaptability (as long as there is sufficient negatively-charged lipid).

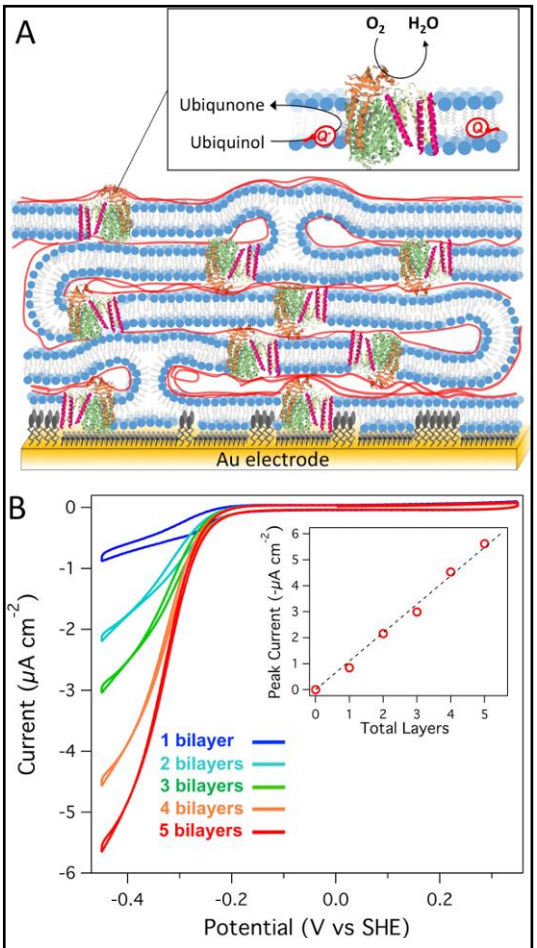

Figure 2: (A) Illustration of the possible interconnected multilayer membrane structure. The ubiquinone-10 (co-nezyme Q) is reduced at the electrode to ubiquinol-10, which is then reoxidized by ubiquinol oxidase present in the bacterial membrane extract, catalyzing the reduction of oxygen to water. (B) Cyclic voltrammograms s of 1-5 bilayer stacks. The current observed at potentials < -0.2 V is due to catalytic electroreduction of oxygen. (Inset) Catalytic current measured at -450mV vs SHE as a function of the number of bilayers.

Publications

Heath G.R., Li M., Rong H., Radu V., Frielingsdorf S., Lenz O., Butt J.N. & Jeuken L.J.C. (2017) Multilayered lipid membrane stacks for biocatalysis using membrane enzymes. *Adv. Funct. Mater* **27**:1606265

Funding

This work was funded by the BBSRC and the ERC.

Collaborators

External: S. Frielingsdorf and S. Lenz, (Technical University Berlin, Germany) J.N. Butt (Universtiy of East Anglia, Norwich, UK)

The Band 3 anion exchanger in a lipid bilayer

Antreas Kalli

Introduction

Band 3 (AE1, SLC4A1), a member of the Solute Carrier 4 family of bicarbonate transporters (SLC4), is a major glycoprotein found in red blood cells. Band 3 is responsible for the electro-neutral exchange of chloride and bicarbonate across the red blood cell plasma membrane. Mutations on Band 3 lead to inherited diseases such as Southeast Asian Ovalocytosis, hereditary spherocytosis and distal renal tubular acidosis. Human Band 3 consists of a N-terminal cytosolic domain (residues 1-360) and a C-terminal membrane domain (residue 361-911) that is responsible for its transport function. Recently, a crystal structure of the transmembrane region of the human Band 3 confirmed that Band 3 is predominantly a dimer in the membrane and showed that each Band 3 subunit consists of 14 transmembrane segments arranged in an inverted 7 + 7 topology. Each Band 3 monomer consists of two sub-domains: a core domain and a gate domain. It is the relative moment of these two sub-domains that allows transport of chloride and bicarbonate across the red blood cell plasma membrane but the molecular details of this moment are largely unknown. Additionally, it has been shown that Band 3 function is also regulated by lipids, e.g. enriched levels of cholesterol deceased Band 3 anion transport activity.

Band 3 interaction with Glycophorin A (GPA) promotes Band 3 trafficking from the endoplasmic reticulum to the cell surface. In mature red blood cells this interaction also forms the Wright (Wr) blood group antigen but the molecular details of this complex are elusive. In this study, we have used molecular dynamics simulations at different resolutions (i.e. coarse-grained and all-atom simulations) to insert the dimeric membrane domain of human Band 3 in an asymmetric lipid bilayer containing a full complement of phospholipids, cholesterol, and its partner membrane protein Glycophorin A (Figure 1). These simulations allowed us to gain novel insights into the dynamic interactions of Band 3 with lipids and with GPA.

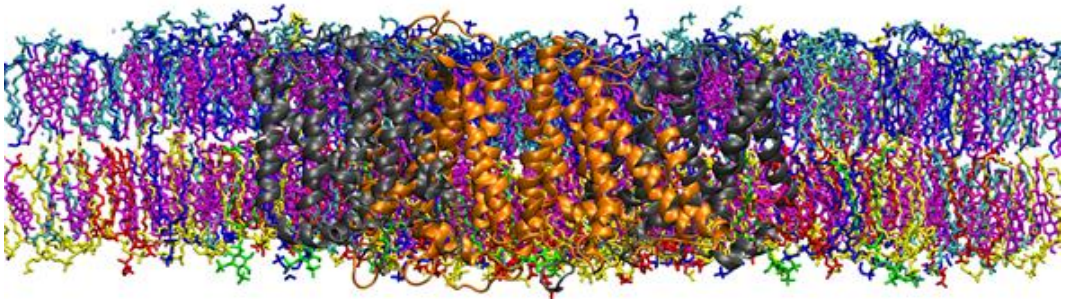

Figure 1: Structure of the dimeric Band 3 membrane domain embedded in a complex asymmetric model membrane. The different lipid types are shown in different colours. The Band 3 core domain is shown in grey and the gate domain in orange.

Results

To study the interactions of Band 3 with different lipids, we first inserted the transmembrane region of Band 3 in an asymmetric bilayer containing 45% POPC and 5% POPE lipids in the outer leaflet and 12% POPC, 23% POPE, 15% POPS lipids in the inner leaflet. Analysis of the interactions of Band 3 with the different lipids revealed that a discontinuous anionic annulus was formed around Band 3 in the inner bilayer leaflet. The POPS lipids interacted mainly with arginines and lysines on the Band 3 surface. The anionic annulus around Band 3 was retained after the addition of other anionic lipids in the bilayer, i.e. PIP_2 molecules but in this case the annulus was formed mainly by PIP_2 molecules and not POPS. Additionally, PIP_2 were more specifically-localized in their interactions with Band 3 compared to POPS. Cholesterol also

interacts preferentially with Band 3. The crystal structure of Band 3 revealed a rather loose packing of the two Band 3 monomers with some space between the two monomers. Interestingly, in our simulations this space was filled mainly with cholesterol and with the lipids tails of other phospholipids. This suggests that lipids may regulate the interaction between the Band 3 monomers.

As mentioned above the interactions of Band 3 with GPA is critical for the trafficking of Band 3 to the cell surface and also creates the Wright (Wr) blood group antigen. To gain molecular understanding for the Band 3/GPA complex we have inserted the transmembrane helical region of the GPA and two Band 3 dimers in a complex bilayer that resembles the native red blood cell plasma membrane. Our simulations showed that the GPA dimer interacts with the two Band 3 dimers, forming a bridge between them. It is, therefore, possible that GPA may promote the clustering of Band 3 dimers. To test this hypothesis further, we have run large-scale coarse-grained simulations in which 64 Band 3 dimers or 64 Band 3/GPA complexes were inserted in a POPC bilayer. At the end of the simulation with the Band 3 alone, the largest cluster contained 5 Band 3 dimers but approximately ~45% of the Band 3 dimers in this simulation were not part of a cluster. In contrast, in the simulation with the Band 3/GPA complexes the largest cluster consisted of 8 proteins and in this case only ~20% of the Band 3/GPA complexes were not part of a cluster. Interestingly, in most cases the interaction between Band 3 dimers is mediated via the GPA as predicted by our simulations above (Figure 2).

In summary, our results provide a realistic model of the dimeric membrane domain of human Band 3 in an asymmetric lipid bilayer that mimics the native red blood cell membrane. Using simulations, we were also able to provide new knowledge for the Band 3/GPA interaction and to show that GPA promotes the clustering of Band 3 in red blood cell membranes. This clustering may facilitate Band 3 trafficking to the cell surface.

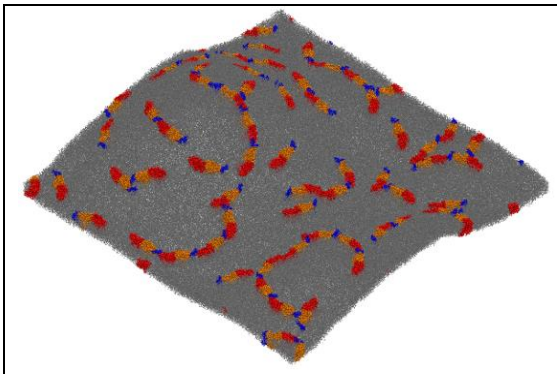

Figure 2: Final snapshot of the large-scale simulations with the Band 3/GPA complexes showing the GPA-mediated clustering of Band 3. The Band 3 monomers are shown in orange and red and the GPA in blue. The POPC lipids are shown in grey.

Funding
This work was funded by the Academy of Medical Sciences.

Collaborators
External: Reinhart Reithmeier (Dept. of Biochemistry, University of Toronto).

Accurate determination of optimal reaction coordinates from atomistic simulations

Sergei Krivov

Introduction

Recent advances in simulation and experiment have led to dramatic increases in the quantity and complexity of produced data, which makes the development of automated analysis tools very important. A powerful approach to analyze dynamics contained in such datasets is to describe/approximate it by diffusion on a free energy landscape - free energy as a function of reaction coordinates (RC). For the description to be quantitatively accurate RCs should be chosen in an optimal way. Recent theoretical results show that such an optimal RC exists and it can be used to compute exactly important dynamical quantities. Determining such RCs for practical systems is a very difficult unsolved problem.

Results

We have found a solution to this problem. We developed an adaptive nonparametric approach to accurately determine the optimal RC (the committor) for an equilibrium trajectory of a realistic system. In contrast to alternative approaches, which require a functional form with many parameters to approximate a RC and thus an extensive expertise with the system, the suggested approach is nonparametric and can approximate any RC with high accuracy without system specific information and minimal input from the user. To avoid overfitting for a realistically sampled system, the approach performs RC optimization in an adaptive manner. The power of the approach was illustrated on a paradigmatic system - a long equilibrium atomistic folding simulation of HP35 protein. We have determined the optimal folding RC - the committor, which was confirmed by passing the committor validation test. It allowed us to determine a first quantitatively accurate protein folding free energy landscape. We have confirmed the theoretical result that diffusion on such free energy profile can be used to compute exactly the equilibrium flux, the mean first passage times, the mean transition path times. We showed that the mean squared displacement along the optimal RC grows linear with time as for simple diffusion. The free energy profile allowed us to obtain a first direct rigorous estimate of the pre-exponential factor for the folding dynamics.

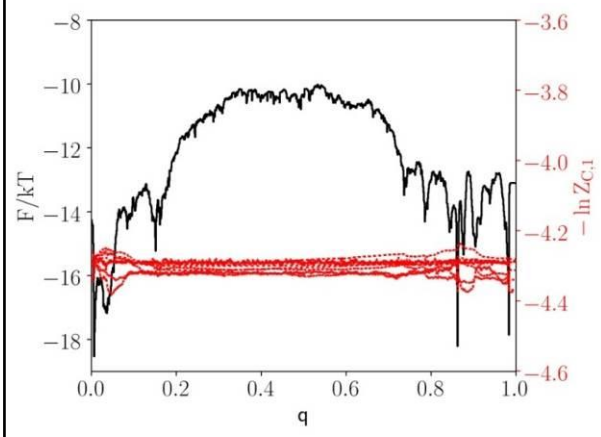

Figure 1: Black line shows the free energy landscape of HP35 Nle/Nle mutant as a function of the committor. Red lines show $Z_{C1}(q,\Delta t)$ profiles, which are all equal to a constant (up to statistical error of 0.08). It validates that the determined coordinate is the committor, for which $Z_{C1}(q,\Delta t)=N_f$, the number of folding events.

Funding

This work was partially supported by the BBSRC.

Receptor tyrosine kinase signalling in the absence of growth factor stimulation: response to cellular stress

Eleanor Cawthorne, Janne Darell, Christopher Jones, Sabine Knapp,
Chi-Chuan Lin, Dovile Milonaityte, Arndt Rohwedder, Caroline Seiler and John Ladbury

Introduction

Receptor tyrosine kinases (RTKs) expressed on the plasma membrane of cells in normal tissue are rarely exposed to high concentrations of extracellular growth factors. Nonetheless they express proteins associated with kinase-mediated signalling. We are interested in the signalling associated with these protein that occurs under basal conditions (which are close to the conditions experienced by normal tissue. In the absence of extracellular stimulation or genetic mutation, an oncogenic response can be driven by the competitive binding of SH3 domain-containing downstream effector proteins to proline-rich sequences on growth factor receptors. Of the approximately 50 plasma membrane receptor tyrosine kinases (RTKs) the majority have proline-rich sequences in their C-termini. These have a propensity to bind to the >300 proteins expressed in human cells which contain SH3 domains. These interactions occur in the absence of any extracellular stimulation (e.g. growth factors, cytokines). Proline-rich sequence binding to SH3 domains are promiscuous and the observed interactions with RTKs are dependent on the relative concentrations of the proteins involved.

We previously established that under non-stimulatory conditions the fibroblast growth factor receptor 2 (FGFR2) recruits the adaptor protein, growth factor receptor binding protein 2 (Grb2) through its C-terminal SH3 domain. In cells depleted of Grb2 other proteins can access the proline-rich motif on FGFR2. One of these proteins, phospholipase C(gamma)1 (Plcγ1) is activated on binding and through turnover of plasma membrane phospholipids to produce second messengers, raises cellular calcium levels which are responsible for increased cell motility and invasive behaviour. In ovarian and lung adenocarcinoma patients with low levels of Grb2 and increased expression of Plcγ1, higher incidence of metastasis leads to greatly reduced survival outcomes.

The dependence of signalling described above on respective concentrations of RTKs and SH3 domain-containing proteins mean that there is no on-off switch for this form of signalling. The outcomes are dictated solely by fluctuations of protein concentrations. As a result, one key driver for this form of signalling is cellular stress. We are working to establish how stresses experienced by tissue (e.g. pH change associated with acid reflux in the oesophagus) can lead to cancer outcomes.

Results

We have extended our studies in this area to explore other RTK-SH3 domain-containing protein interactions to establish whether the up-regulation of signal transduction through these interactions is a general phenomenon. This leads to the hypothesis that two tiers of intracellular signalling can be derived from receptors with intrinsic protein kinase activity:
1) Ligand-induced elevation in kinase activity resulting in tyrosylphosphate-mediated effector protein recruitment and committal to a defined cellular outcome (e.g. proliferation).
2) Receptor phosphorylation-independent activation of downstream effectors through SH3 domain/proline-rich sequence interactions, which appear to be required for cell homeostasis/metabolic control.

Hyperactivity of the tier 1 signalling is a feature of receptor tyrosine kinase-related cancers arising from genetic mutation. Although the tier 2 signalling mechanism occurs under basal conditions, and is thus likely to be associated with cellular maintenance, we have shown that fluctuations in expression levels of SH3-containing proteins can drive cells into pathological phenotypes including proliferation and metastasis.

We are testing this hypothesis with a range of methods, extending from cell-based assays (including fluorescence lifetime imaging microscopy), through to structural and in vitro biophysical analysis.

We are optimising a screening protocol to establish the extent of tier 2 signalling in a range of cells and conditions. We have identified novel interactions involving well studied proteins as well as less understood systems. These are being validated and phenotypic outcomes of knocking down these interactions are being explored to establish the effects of signalling in normal tissue.

We have focused on gastro-intestinal cancers and have begun to explore the effects of stress on intracellular protein expression and the outcomes on tier 2 signalling. We have shown that by mimicking conditions experienced in the GI tract we can affect expression of receptor tyrosine kinases.

In addition to identifying the signalling pathways which are initiated as a result of fluctuations in protein concentrations in cell-based assays, we are exploring the interactions associated with up-regulation of Tier 2 signalling using both biophysical and structural biological methods. High resolution structural detail on the receptor-ligand interactions are providing invaluable detail on the mode of recruitment of signalling proteins as well as information towards potential inhibition of aberrant pathways that lead to pathogenic outcome.

Funding
This work is funded by Cancer Research UK.

Collaborators
University of Leeds: Prof. Phillip Quirke, Prof. Susan Short, Prof. Alex. Breeze, Dr. Darren Tomlinson
External: Prof. Zamal Ahmed, Prof. Mien-Chie Hung, Swathi Arur, Mikhail Bogdanov (University of Texas, MD Anderson Cancer Center, USA) and Richard Grose (Barts Cancer Institute, London).

Studies of small DNA tumour viruses that cause disease in humans

Ethan Morgan, Christopher Wasson, Daniel Hurdiss, Margarita Panou, David Kealy, Gemma Swinscoe, Michelle Antoni, Eleni-Anna Loundras and Andrew Macdonald

Introduction

Members of the Papillomavirus and Polyomavirus families are the causative agents of a number of severe diseases in humans. Notable examples include cervical cancer, which is exclusively associated with infection with human papillomaviruses, and polyomavirus-associated nephropathy (PVAN) and Merkel cell carcinoma (MCC) caused by the BK and MCV polyomaviruses, respectively. Current therapeutic strategies to treat these virus-associated maladies are lacking. We undertake a broad ranging analysis of these viruses in an effort to identify new targets for therapeutic intervention. Our studies have revealed novel information about these viruses.

Results

Human papillomavirus: Infection with HPV causes ~6% of human cancers, including nearly all cervical carcinomas, as well as many other anogenital tract tumours. The past decade has also witnessed an epidemic of head and neck squamous carcinomas (HNSCC), primarily in white, middle aged men, which are also associated with HPV. Despite FDA-approved prophylactic vaccines, the burden of HPV-associated malignancy will remain high for decades due to their limited availability in low income countries, poor coverage where access is possible, and the long latency period separating infection from carcinogenesis. Although HPV-specific antivirals are needed, their development is hindered by an incomplete understanding of the virus life cycle and essential interactions with host factors within the infected keratinocyte.

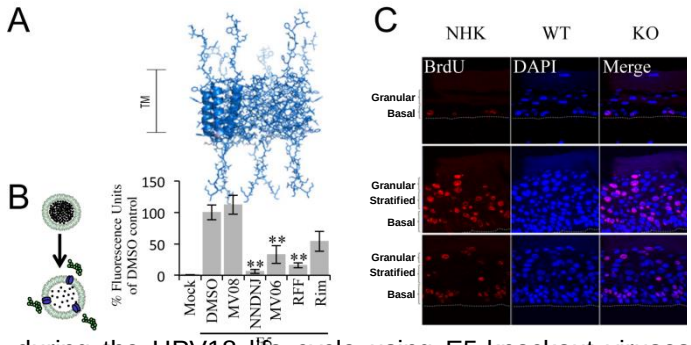

Figure 1: (A) *In silico* modelling of the HPV16 E5 proteins. Energy minimisation models depicting a hexameric channel structure. (B) Screen for novel inhibitors of E5 viroporin activity. Panel of known viroporin inhibitors and bespoke compounds generated from the *in silico* model were tested for the ability to prevent E5-mediated dye release. (C) Genetic studies of E5 function during the HPV18 life cycle using E5-knockout viruses in primary 3D organo-typic raft culture models. BrdU incorporation measures the levels of unscheduled DNA replication in the suprabasal layers of the epithelium (red stain) in normal human keratinocytes (NHK), cells infected with wild-type HPV18 (WT) and cells infected with an HPV18 genome lacking E5 expression (KO). Loss of E5 results in a significant reduction in DNA replication.

Using an approach incorporating molecular and cellular biology with cutting edge cell culture and cancer models we explore the roles of the HPV encoded E5, E6 and E7 oncoproteins in the virus life cycle and in transformation. Our studies have revealed new information on these proteins, in particular how they interact with host factors that are essential for virus replication. For example, we identified the E5 protein as an ion channel or viroporin. This has opened up the possibility of developing small molecule inhibitors targeting the channel function of E5. In addition, we have shown that E5 hijacks the epidermal growth factor receptor (EGFR) to drive keratinocyte proliferation, which is necessary for both virus replication and transformation (2).

Human polyomaviruses: Members of this family, including BK and Merkel cell polyomavirus (MCV), are associated with disease in humans. Despite their clear association with disease there is a paucity of understanding of their basic biology and as such we are using a wide-ranging series of experiments to understand their life cycles and to identify novel targets for

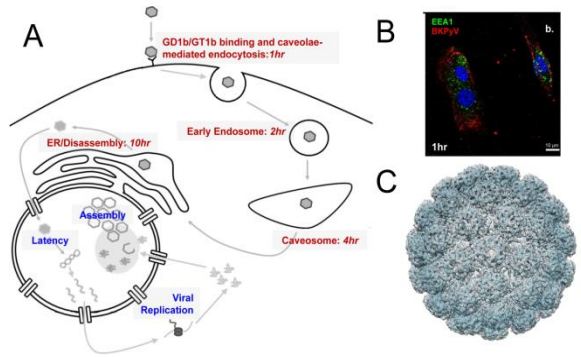

Figure 2: (A) Schematic of the current understanding of BK polyomavirus (BKPyV) life cycle. (B) Immunofluorescence with Alexafluor954 labelled BKPyV infected human renal proximal tubular epithelial (RPTE) cells. (C) Cryo-electron microscopy structure determination of the native BKPyV virion.

antiviral therapeutics. We have described roles for MCV proteins in immune evasion (1) and in collaboration with Prof. Adrian Whitehouse identified mechanisms of MCV-mediated cancer metastasis (3). With Prof. Neil Ranson we are using the latest advances in cryo-electron microscopy to gain an unprecedented understanding of the fundamental make-up of polyomavirus particles and how they mediate their interactions with host receptor molecules. This information may herald crucial advances in antiviral drug design. In more recent studies we have focussed on BK virus entry and egress mechanisms and identified a vital role for a host ion channel in polyomavirus entry to primary kidney cells. Importantly, a commonly available drug targeting this channel prevents BK infection. Further work will validate this channel as a novel therapeutic strategy to target BK-associated disease and mechanistic studies will shed light on why it is needed for virus infection.

Publications

Abdul-Sada H., Muller M., Mehta R., Toth R., Arthur J.S.C, Whitehouse W. & Macdonald A. (2017) The PP4R1 sub-unit of protein phosphatase PP4 is essential for inhibition of NF-κB by Merkel polyomavirus small T antigen. *Oncotarget* **8**:25418-25432.

Wasson C.W., Morgan E.L., Müller M., Ross R.L., Boxall S., Hartley M, Roberts S. & Macdonald A. (2017) Human papillomavirus type 18 E5 oncogene supports cell cycle progression and delays epithelial differentiation by modulating growth factor receptor signalling. *Oncotarget.* **8**:103581-103600.

Funding

This work was supported by Kidney Research UK, BBSRC, Wellcome Trust and Yorkshire Kidney Research Fund.

Collaborators

University of Leeds: Neil Ranson and Adrian Whitehouse (FBS), Stephen Griffin (LICAP), Richard Foster and Andrew Wilson (School of Chemistry).
External: Sally Roberts (Birmingham), Nick Coleman (Cambridge), Sheila Graham (Glasgow) and Simon Arthur (Dundee).

Virus requirement for endosomal K^+ reveals new roles of cellular ion channels during infection

Samantha Hover, Becky Foster, Juan Fontana, John Barr and Jamel Mankouri

In order to multiply and cause disease a virus must transport its genome from outside the cell into the cytosol, most commonly achieved through the endocytic network. Endosomes transport virus particles to specific cellular destinations and viruses exploit the changing environment of maturing endocytic vesicles as triggers to mediate genome release. Previously we demonstrated that several bunyaviruses, which comprise the largest family of negative sense RNA viruses, require the activity of cellular potassium (K^+) channels to cause productive infection. Specifically, we demonstrated a surprising role for K^+ channels during virus endosomal trafficking. In this study, we have used the prototype bunyavirus, Bunyamwera virus (BUNV), as a tool to understand why K^+ channels are required for progression of these viruses through the endocytic network. We report three major findings: First, the production of a dual fluorescently labelled bunyavirus to visualize virus trafficking in live cells. Second, we show that BUNV traffics through endosomes containing high [K^+] and that these K^+ ions influence the infectivity of virions. Third, we show that K^+ channel inhibition can alter the distribution of K^+ across the endosomal system and arrest virus trafficking in endosomes. These data suggest high endosomal [K^+] is a critical cue that is required for virus infection, and is controlled by cellular K^+ channels resident within the endosome network. This highlights cellular K^+ channels as druggable targets to impede virus entry, infection and disease.

Publications

Hover S., Foster B., Barr J.N. & Mankouri J. (2017) *J Gen Virol* **98**:345-351.

Funding

Jamel Mankouri is funded by a Royal Society Fellowship (RG110306 & UF100419)

Collaborators

University of Leeds: Andrew Tuplin, Ade Whitehouse, Andrew Macdonald, Jon Lippiat, Juan Fontana, John N Barr.
External: Alain Kohl (CVR Glasgow), Steve Goldstein (Loyola University Chicago), Stefan Finke (Friedrich-Loeffler-Institut).

Electron microscopy of membrane proteins to underpin structure guided inhibitor design

Shaun Rawson, Rachel Johnson, Paul Beales, Colin Fishwick and Stephen Muench

Introduction

Structure based drug design is dependent upon structural information from either experimentally derived structures or modeling. However, the determination of membrane protein structures, which are key targets for therapeutic development has lagged behind that of their soluble counterparts due to the complications of expressing, stabilising and crystallising membrane proteins. The development of more native lipid environments to house membrane proteins would also be beneficial to biophysical characterization. A further area for development in structure based drug design approaches is in moving beyond the static snapshot that is often available through conventional structural techniques and trapping proteins and protein complexes in defined catalytic states using time-resolved methodologies. Our group have been tackling these issues through the use of single particle cryo-EM to study membrane protein structures and in the development of new membrane protein scaffolds and time-resolved EM approaches.

Results

The group have been looking at new ways of studying membrane proteins in more “native” environments through the use of styrene maleic acid (SMA) co polymers, which cut up the membrane into lipid particles (SMALPs) enclosing the membrane protein by native lipid, which often results in higher activity than detergent solubilized counterparts. This year we determined the structure of the *Escherichia coli* multidrug efflux transporter AcrB in a SMALP scaffold to sub-nm resolution using single particle cryo-EM (**Fig. 1A**). This work has shown the potential of an SMA approach for single particle cryo-EM studies and in parallel with have been studying new SMA based polymers which will have applications in other biophysical techniques. The group have also worked with the Beales group who have developed new proteo-hybrid vesicles which offer significant extended functional lifetimes (months) for membrane proteins.

Through our studies we aim to further our structural and mechanical understanding of proteins and protein complexes to drive the design of novel modulators of function. We are currently studying a wide range of targets including, V-ATPase, cytochrome *bc*1, Enoyl Reductase, P2X7 and IGPD. In collaboration with the University of Liverpool we have now used single particle cryo-EM to determine a number of inhibitor bound structures of cytochrome *bc*1 to a resolution where we can identify the inhibitor binding site (**Fig. 1B**). This work will feed into our ongoing work on developing new anti-malarial and Toxoplasmosis therapies. Through single particle cryo-EM we have also determined the IGPD structure from both yeast and arabidopsis to understand the difference in inhibitor potency between the two systems (**Fig. 1C**).

To understand biological mechanisms, structural biologists aspire to visualise dynamic changes in macromolecules at atomic resolution; ‘time-resolved structural biology.’ Such capability would increase mechanistic understanding of protein(s) and how mutations cause disease states. Recent advances in the resolution obtainable by electron microscopy (EM) and the broad range of samples that can be studied (from ~65kDa proteins to protein complexes and cells) makes it ideally suited to time-resolved studies. The progress of time-resolved methodologies within EM has been slow due to limitations with microscope design, data collection throughput, resolution and reproducibility of the grids. On the back of recent developments in the EM field our group (in collaboration with Prof White and Dr Trebbin) are developing one of a handful of pre-existing time-resolved apparatus and re-designing its setup to become a universal system for time-resolved studies.

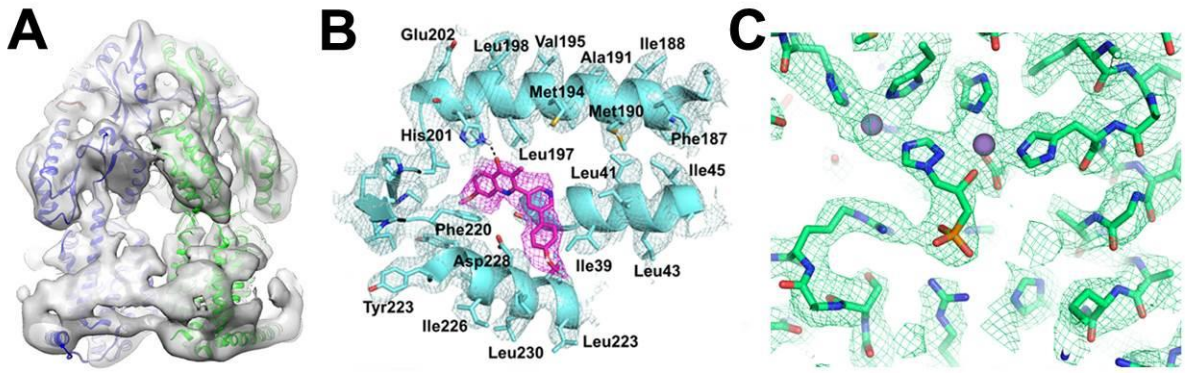

Figure 1:(A) Single particle cryo-EM map of AcrB which had been extracted using an SMA polymer as appose to conventional detergent approaches, highlighting the promise of SMA technology for single particle cryo-EM. (B) The single particle cryo-EM map of bovine cytochrome *bc1* with inhibitor bound (pink mesh). (C) Cryo-EM map of IGPD, showing strong density which accommodates the inhibitor, surrounding residues and the two Mn^{2+} ions (purple spheres).

Publications

Wanjun Q.I., Manfield I.W., Muench S.P. & Baker A. (2017) AtSPX1 affects the AtPHR1 dimer-DNA binding equilibrium by binding monomeric AtPHR1 in solution. Biochem J **474**:3675-3687.

Muench S.P (2017) Everyone needs good neighbours – the intricate relationship between the acetylcholine-receptor channel and its membrane environment. *IUCrJ* **4**:306-307.

Rawson S., McPhillie M.J., Johnson R.J., Fishwick C.W.G. & Muench S.P. (2017) The potential use of single-particle electron microscopy as a tool for structure-based inhibitor design. *Acta Crystallographica D Struct Biol* **73**:534-540.

Beales P.A., Khan, S., Muench S.P. & Jeuken L.J.C. (2017) Durable vesicles for reconstitution of membrane proteins in biotechnology. *Bioch. Soc. Trans* **45**:15-26.

Caseley E.A, Muench, S.P. & Jiang L.H. (2017) Conformational changes during human P2X7 receptor activation examined by structural modelling and cysteine-based corss-linking studies. *Purinergic Signalling* **13**:135-141.

Funding

This work was supported by the BBSRC, MRC, Wellcome Trust and NIH.

Collaborators

External: Prof. Tim Dafforn - University of Birmingham, Prof. Rima McLeod - University of Chicago, Prof Howard - White Eastern Virgina Medical School, Martin Trebbin – University of Hamburg. Prof Samar Hasnain & Dr Svetlana Antonyuk - University of Liverpool.

Unified synthetic approaches to diverse biologically-relevant molecular scaffolds

Joan Mayol-Llinas, Mark Dow, Francesco Marchetti, Daniel Foley, Philip Craven, Richard Doveston, Anthony Aimon and Adam Nelson

Introduction

The discovery of biologically-active small molecules is an enduring theme in chemical biology and medicinal chemistry. However, the historical exploration of chemical space has been highly uneven and unsystematic: a sixth of known cyclic organic compounds are based on just 30 (of 2.5 million) known molecular scaffolds! This uneven exploration stems, in large part, from the narrow toolkit of reliable reactions that currently underpins molecular discovery. We have an ongoing and vibrant research programme that is focused on the development of unified approaches to explore novel and diverse regions within chemical space.

We developed a unified synthesis of thirty lead-like molecular scaffolds for CNS drug discovery (Scheme, left panel). Specifically, we demonstrated that decoration of the molecular scaffolds would yield compounds with appropriate properties to serve as high-quality leads for CNS discovery. Crucially, the approach enabled variation of the nature of the fusion between two rings, as well as independent variation of the size and heteroatoms within both rings.

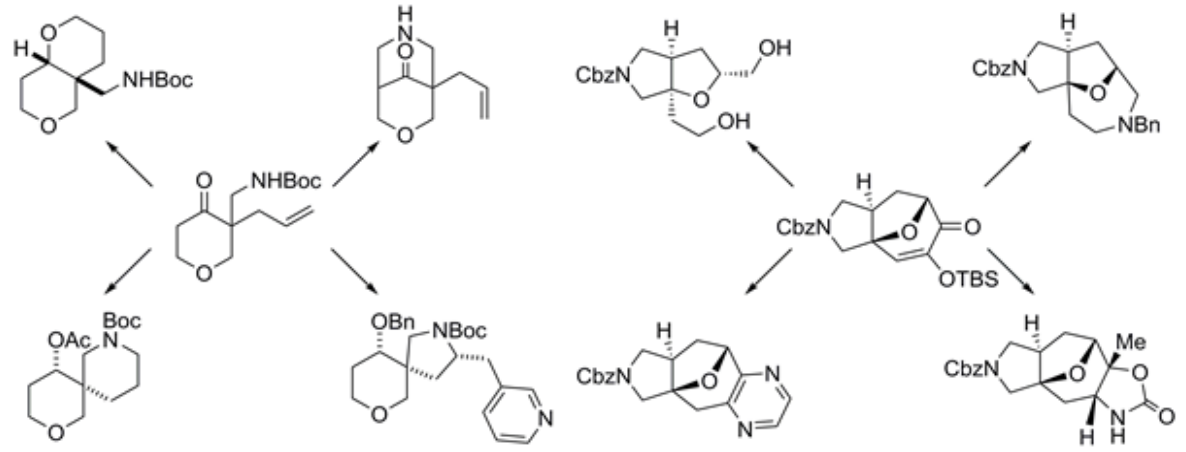

Exemplar unified synthetic approaches to diverse molecular scaffolds. Left: Synthesis of lead-like scaffolds for CNS drug discovery. Right: Synthesis of natural product-like molecular scaffolds.

We have also developed a "top-down" synthetic approach which enables complex intermediates to be converted into a wide range of alternative molecular scaffolds (Scheme, right panel). Here, the complex intermediates were converted into diverse natural product-like scaffolds via ring cleavage, ring expansion and annulation. To demonstrate biological relevance, we designed and prepared a fragment set based on the scaffolds, and used X-ray crystallography to identify hits against three distinct protein targets (for example, see Figure). Although the scaffolds have frameworks that are not found in specific natural products, they can nonetheless provide biologically-relevant and distinctive starting points for bioactive molecule discovery.

The development of unified strategies that are able to deliver skeletally diverse scaffolds is demanding. In addition, it is critical to demonstrate the biological relevance of novel scaffolds that are prepared, for example through fragment screening (see above) or phenotypic screening (e.g. for antimycobacterial activity). We have translated many of our unified diversity-oriented synthetic approaches into the €196M European Lead Factory in which Leeds is a partner. Publications from this programme, and other programmes under active development in the group, are listed below. Further details of research within the Nelson group may be found at www.asn.leeds.ac.uk.

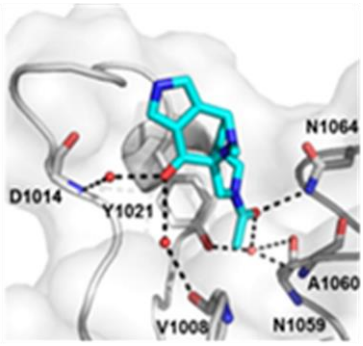

Figure 1: Exemplar fragment hit in complex with the ATAD2 bromodomain.

Publications

Mayol-Llinas J., Ayscough A., Nelson A., Farnaby W. (2017) Assessing molecular scaffolds for CNS drug discovery. *Drug Discov. Today* **22**:965-969.

Chow S. Y., Nelson A. (2017) Embarking on a Chemical Space Odyssey. *J. Med. Chem* **60**:3591-3593.

Dow M., Marchetti F., Abrahams K. A., Vaz L., Besra G. S., Warriner S., Nelson A. (2017) Modular Synthesis of Diverse Natural Product-like Macrocycles: Discovery of Hits with Antimycobacterial Activity. *Chem. Eur. J* **23**:7207-7211.

Foley D. J., Craven P. G. E., Collins P. M., Doveston R. G., Aimon A., Talon R., Churcher I., von Delft F., Marsden S. P., Nelson A. (2017) Synthesis and Demonstration of the Biological Relevance of sp^3-rich Scaffolds Distantly Related to Natural Product Frameworks. *Chem. Eur. J* **23**:15227-15232.

Mayol-Llinas J., Farnaby W., Nelson A. (2017) Modular synthesis of thirty lead-like scaffolds suitable for CNS drug discovery. *Chem. Commun* **53**:12345-12348.

Funding

We thank EPSRC, BBSRC, the EU, Takeda, AstraZeneca and GSK for support

Collaborators

University of Leeds: Professor Steve Marsden
External: Dr Ian Churcher (GSK), Luis Vaz (AstraZeneca), Will Farnaby and Dr Andy Ayscough (Takeda), Dr Frank von Delft (Diamond Light Source and Oxford University) and Professor Del Besra (University of Birmingham).

We also acknowledge other scientific collaborators who have also contributed strongly to other aspects of our on-going research programme.

Revisiting unexploited antibiotics in search of new antibacterial drug candidates

Nada Nass, Nicola Ooi, Christopher Randall, Ryan Seipke and Alex O'Neill

Introduction

The emergence and spread of antibiotic resistance in pathogenic bacteria is severely eroding our ability to manage infection. Central to an effective response to this problem will be the development of new antibacterial drugs with activity against bacteria resistant to existing antibiotics. Unfortunately, progress towards this end has been hampered by the technically-challenging nature of antibacterial discovery; the field is now 30 years into a 'Discovery Void', from which no novel drug class effective against the most problematic bacterial pathogens has emerged to reach the clinic.

One strategy that we have been pursuing to identify new antibacterial drug candidates involves revisiting known antibiotic classes that have not to date been exploited for the treatment of bacterial infection. The underpinning hypothesis is that amongst the *c*. 3000 antibiotics discovered to date - of which only a handful of classes have been employed clinically – there may reside a wealth of compounds with untapped potential as antibacterial drugs. By initiating the discovery process with compounds about which something is already known, this approach offers a potential fast-track through the challenging early stages of drug discovery. Whilst a proportion of these unexploited antibiotics will likely have been considered and rejected for development because they possess liabilities that went unreported in the scientific literature, it is also conceivable that many have not been properly evaluated as potential drug candidates. Furthermore, there are several examples of antibiotics that were initially dismissed as drug candidates, but which were later re-evaluated and successfully developed for clinical use (e.g. daptomycin, fidaxomicin). Thus, we consider a systematic re-evaluation of known antibiotics to identify antibacterial drug candidates a worthwhile endeavor. However, to redress the opacity of past antibacterial drug discovery efforts and to prevent future duplication of effort, it is vital that the scientific record comprehensively captures the details both for compounds that such an analysis reveals to have potential as antibacterial drug candidates, as well as those it does not.

Results

In the first instance, we revisited MSD-819 (6-chloro-2-quinoxalinecarboxylic acid 1,4-dioxide), a natural product antibiotic first isolated in the late 1960's that has been reported to exhibit antibacterial activity *in vitro* and *in vivo*. We obtained MSD-819 by chemical synthesis, and subjected it to detailed *in vitro* characterization of its antibacterial properties. MSD-819 demonstrated broad-spectrum bactericidal activity, and had the desirable property that resistance to the compound could not be readily selected. The antibacterial mode of action was shown to result from perturbation of the cytoplasmic membrane. Unfortunately, MSD-819 was found to exert a similar effect on mammalian cells, mediating loss of membrane integrity in both equine erythrocytes and human kidney cells. In view of this lack of selective toxicity against bacteria, we concluded that MSD-819 does not represent a useful candidate for clinical development. Subsequently, we evaluated the actinorhodins, a class of natural dimeric benzoisochromanequinone antibiotics first reported in the late 1940's. In conjunction with colleagues in the School of Chemistry at Leeds, we devised a scalable method for targeted isolation and purification of γ-actinorhodin (γ-ACT)(Figure 1). Purified γ-ACT displayed potent bactericidal activity against key Gram-positive pathogens (including Staphylococcus aureus and enterococci), exhibiting an antibacterial activity at least 10-fold greater than that reported in earlier studies of this class. The antibacterial mode of action of γ-ACT was found to be unlike that of any antibacterial drug in clinical use, involving collapse of the proton motive force and the generation of reactive oxygen species, both effects apparently resulting from γ-ACT-mediated interference with correct functioning of the electron transport chain in bacteria.

Crucially, and in contrast to MSD-819, γ-ACT exhibited selective toxicity against bacteria, with toxic effects against mammalian cells only becoming apparent at concentrations >50-fold higher than those inhibiting bacterial growth. No resistance to γ-ACT could be selected in bacteria, even upon extended challenge to the antibiotic, implying a desirably-low resistance potential. γ-ACT also demonstrated a degree of *in vivo* efficacy, improving host survival in an invertebrate model of bacterial infection. Thus, this antibiotic possesses many of the requisite properties of an antibacterial drug. Our findings regarding γ-ACT underscore the utility of revisiting unexploited antibiotics as a source of novel antibacterial drug candidates, and further such antibiotics are currently under investigation.

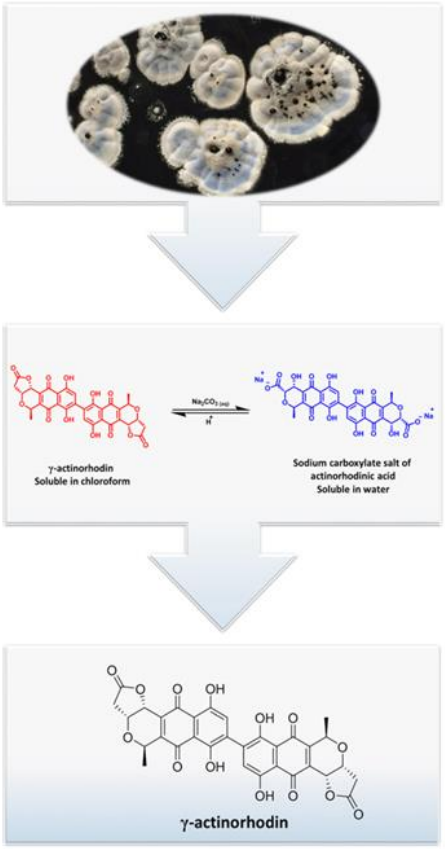

Figure 1: The antibiotic γ-actinorhodin, and its purification from Streptomyces coelicolor. During growth on agar, S. coelicolor strains L646 secretes γ-ACT (blue) into the medium. Purification of γ-ACT was achieved by formation of the carboxylate salt of actinorhodinic acid, a compound with high water solubility. The identity and purity (>95%) of γ-ACT were confirmed using mass spectrometry, 1-D NMR, 2-D NMR, infrared spectroscopy and analytical HPLC.

Publications

Nass N. M., Farooque S., Hind C., Wand M. E., Randall C. P., Sutton J. M., Seipke R. F., Rayner C. M., O'Neill A. J. (2017) Revisiting unexploited antibiotics in search of new antibacterial drug candidates: the case of γ-actinorhodin. *Sci Rep* **7:**17419.

Ooi N., O'Neill A. J. (2017) Revisiting unexploited antibiotics in search of new antibacterial drug candidates: the case of MSD-819 (6-chloro-2-quinoxalinecarboxylic acid 1,4-dioxide). *J Antibiot* **70:**317-319.

Funding

This work was funded in large part by the Medical Research Council, with sponsorship from the Saudi Government to support NN.

Collaborators

University of Leeds: Sannia Farooque, Christopher Rayner (School of Chemistry)
External: Charlotte Hind, Matthew Wand, Mark Sutton (PHE, Porton Down, UK)

Transcellular stress signalling: How proteotoxic stress is communicated between different tissues in *C.elegans*

Daniel O'Brien, Rebecca Aston, Vijay Shanmugiah, David Westhead and Patricija van Oosten-Hawle

Introduction

In all biological systems, cells throughout their lifetime are exposed to different physiological and environmental stress conditions that lead to protein damage and cellular dysfunction – and ultimately disease. Cumulative protein misfolding and aggregation is one of the hallmarks implicated in the pathologies of misfolding diseases associated with neurodegeneration, including Alzheimer's disease, amyotrophic lateral sclerosis, Huntington's disease and Parkinson's disease, as well as cancer, diabetes and several myopathies. Maintaining a healthy cellular proteome is crucial to cellular viability. This is achieved by the proteostasis network, which integrates protein biogenesis, protein folding by molecular chaperones, as well as clearance mechanisms and stress response pathways.

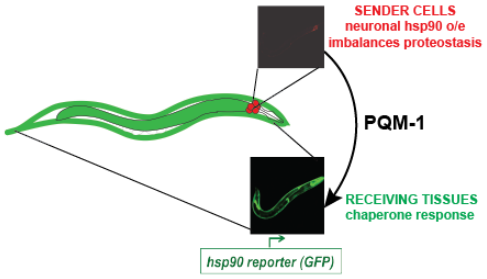

Figure 1: Model explaining transcellular chaperone signalling (TCS) in *C. elegans.*

In metazoans, tissues experiencing proteotoxic stress induce "transcellular chaperone signalling" (TCS), that activates molecular chaperones, such as *hsp-90*, in distal tissues. Thus, conserved stress responses such as the heat shock response initiate inter-cellular communication that allows protective chaperone expression to be signalled and spread from one tissue to another, a process known as transcellular chaperone signalling (TCS). One key observation of TCS is that an imbalance of proteostasis in only one tissue (e.g. neurons) through altered expression of the major chaperone *hsp-90*, can lead to an upregulated *hsp-90* chaperone response in receiving tissues that is spread throughout the organism (Figure 1). How this form of intertissue communication is mediated to upregulate systemic chaperone expression and whether it can be utilised to protect against protein misfolding diseases remains an open question to date.

Results

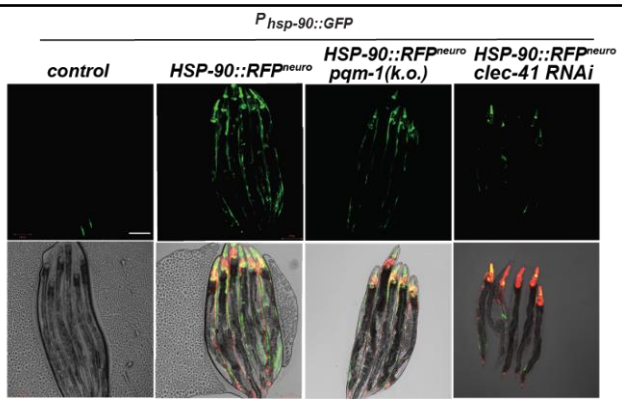

Figure 2: Overexpression of HSP-90::RFP in the neurons induces transcriptional activity of a *hsp-90::GFP* reporter fusion in muscle cells. Knockout of the transcription factor PQM-1 (*pqm-1k.o.*) and knockdown of *clec-41* by RNAi abolishes this induction

Using *C. elegans*, we identified key nodes of a neuronal induced transcellular signalling cue that couples the PQM-1 zinc finger transcription factor and components of the innate immune response with the regulation of systemic proteostasis. We show that perturbation of proteostasis in the neurons, via neuron-specific overexpression of HSP-90, activates TCS via PQM-1 and the innate immunity-associated transmembrane protein CLEC-41. This activation of neuronal PQM-1/CLEC-41 signalling is required to induce transcellular *hsp-90* expression in muscle cells (Figure 2).

Using a *C. elegans* model for Alzheimer's disease that expresses $A\beta_{1\text{-}42}$ in the muscle, we show that TCS-induced *hsp-90* expression via PQM-1/CLEC-41 signalling ameliorates muscle-expressed $A\beta_{1\text{-}42}$ associated toxicity (Figure 3). Thus our results reveal elements of a novel neuronal signalling cue that promotes cell nonautonomous *hsp-90* chaperone expression and protects against age-associated proteostasis dysfunction (See Figure 4 for a model).

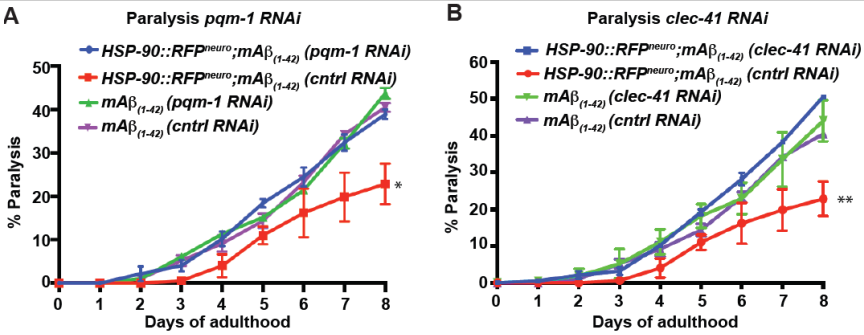

Figure 3: Overexpression of HSP-90::RFP in the neurons (HSP-90::RFP^{neuro}) suppresses muscle-expressed Abeta(1-42) associated toxicity. (A) Knockdown of *pqm-1* by RNAi abolishes this beneficial effect in HSP-90::RFP^{neuro}, Abeta(1-42) animals as does (B) knockdown of *clec-41* by RNAi

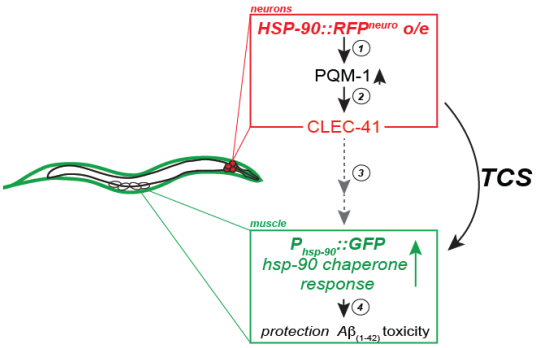

Figure 4: Model for transcellular chaperone signalling activated in the neurons which induces protective *hsp-90* expression in the muscle, mediated through PQM-1/CLEC-41 signalling.

Funding

We are grateful for support from the Wellcome Trust, the NC3Rs, and a BBSRC and MRC doctoral studentship.

Collaborators

University of Leeds: David Westhead.

Proteins under the computational microscope: folding, binding, disorder, mechanics, kinetics.

Emanuele Paci

Introduction

Our research focuses on the development and application of novel computational tools to investigate structure and functional dynamics of biomolecules. One of our aims is fully exploit the wealth of structural data obtained with the advanced experimental probes available at Astbury. Most of our research involves experiments performed in collaboration with colleagues from the Astbury Centre and further afield.

One topic where models and simulations provided information that experiments cannot provide and suggestions for more insightful experiments relates to the structural propensity of polypeptides with specific sequence patterns. These range from the simplest repeat, a homopolypeptide, i.e., repeats of the same aminoacid, or repeats short patterns of amino acids. While polymer theory suggests that most of these sequences are unstructured we found evidence of the emergence of structural preferences and unique, sequence and length dependent, dynamical properties. In collaboration with Michelle Peckham at Astbury we have been exploring the properties of polyampholyte repeat sequences that are strongly helical using experiment and simulation (Wolny 2017, Batchelor 2017).
Characterization kinetics and thermodynamics of disordered states is one of the current focuses of our group. We recently published a paper (Gowdy 2017) where we explore the rate of contact formation in a number of peptides and proteins. Results explain and reconcile experimental results that show an anomalous time dependence of the contact formation rate. The anomalous kinetics turns out to be in part due to the ruggedness of the free energy landscape, and in part due to the polymeric nature of peptides and proteins.

Much of our work involves molecular simulation of the dynamics and interactions within and between protein systems. Data generated from simulation are used to interpret and direct experimental measurements such as hydrogen-deuterium exchange probed by mass spectroscopy, NMR and SAXS.

Among our current interests is the development of *ab initio* methods to determine the structure of proteins and protein complexes, the use of sparse experimental data to select the most likely correct, and simulation to assess their stability. The approach has led to a submitted publication in collaboration with the group of Andreas Plückthun at University of Zurich where we could determine the correct structure of designed antibody analogs interacting with domain IV of Human Epidermal Growth Factor Receptor 2 (Radom 2018).

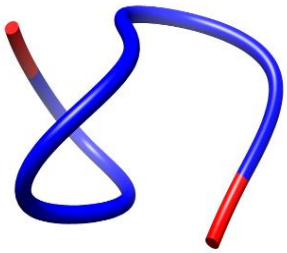

Figure 2: The kinetics of loop formation, i.e., the occurrence of contact between two atoms of a polypeptide, remains the focus of continuing interest. One of the reasons is that contact formation is the elementary event underlying processes such as folding and binding. More importantly, it is experimentally measurable and can be predicted theoretically. for ideal polymers. Deviations from single exponential kinetics have sometimes been interpreted as a signature of rugged, protein-like, free energy landscapes.

Results

In our group we also develop and implement methods to determine free energy changes along pathways connecting different conformational states of proteins. One particular topic on which we have been working for the past 20 years is that of interpreting single molecule force spectroscopy experiments. We are currently collaborating with David Brockwell and Colin Kleanthous to dissect the import of nutrients and

proteins through bacterial TonB-dependent transporters. The energy required for the process is provided by inner membrane proteins in the form of mechanical force through a mechanism that atomistic simulation are helping elucidating. We addressed the import of vitamin B_{12} (Hickman 2017) and are currently studying how killer proteins produced by other bacteria hijack a TonB-dependent transporter to penetrate bacterial outer membranes.

Publications

Wolny M., Batchelor M., Bartlett G. J., Baker E. G., Kurzawa M., Knight P. J., Dougan L., Woolfson D. N., Paci E., Peckham M. (2017) Characterization of long and stable de novo single alpha-helix domains provides novel insight into their stability. *Sci Rep* **7**:44341.

Hickman S. J., Cooper R. E., Bellucci L., Paci E., Brockwell D. J. (2017) Gating of TonB-dependent transporters by substrate-specific forced remodelling. *Nature Communications* **8**:14804.

Gowdy J., Batchelor M., Neelov I., Paci E. (2017) Nonexponential Kinetics of Loop Formation in Proteins and Peptides: A Signature of Rugged Free Energy Landscapes? *J Phys Chem B* **121**:9518-9525.

Collaborators

University of Leeds: B. Turnbull, D. Brockwell, L. Dougan, R. Tuma, D. Donnelly, M. Peckham
External: J. Clarke (Cambridge), A. Plückthun (Zurich), D. Glowacki (Bristol), C. Kleanthous (Oxford).

Understanding the stability of Single Alpha Helical (SAH) domains

Marcin Wolny, Matthew Batchelor, Marta Kurzawa, Lorna Dougan, Emanuele Paci, Peter Knight and Michelle Peckham

Introduction

Our research interests focus on the cytoskeleton in both muscle and non-muscle cells. As part of our research efforts this year, we have been investigating what underlies the stability of stable single alpha helical (SAH) domains, which we discovered in various different myosin isoforms just over 10 years ago (Knight et al., J. Biol. Chem. 2005), and have since discovered to be widespread and found in many different proteins (Knight & Peckham, Soft Matter, 2009).

SAH domains are rich in Glutamate (Glu, E), Lysine (Lys, K) and Arginine (Arg, R) residues. While α-helices are commonly stabilised as part of a tertiary protein fold, or by binding to other proteins, SAHs remain stable and soluble as single α-helices in isolation. Their remarkable stability is considered to arise by the formation of multiple salt bridges between oppositely charged residues (E-K, or E-R) either 3 (i, i+3) or 4 (i, i+4) residues apart along the helix (Fig. 1A).

However, understanding how salt bridges promote their stability is challenging as SAHs can be very long and their sequences are highly variable. In particular, the relative contribution of Lys or Arg to the salt bridge is of interest given the different properties of the side chains of these two residues: is Lys more stabilising than Arg or vice versa?

To address this question, we designed and tested simple *de novo* 98-residue polypeptides containing 7-residue repeats (AEEEXXX, where X is K or R), which we expected to promote salt-bridge formation between Glu and Lys/Arg to generate SAH domains, and in parallel, we performed a range of molecular dynamics simulations and an interrogation of helical structure in the Protein Database (PDB) to investigate the nature and dynamics of Glu-Lys and Glu-Arg salt-bridges.

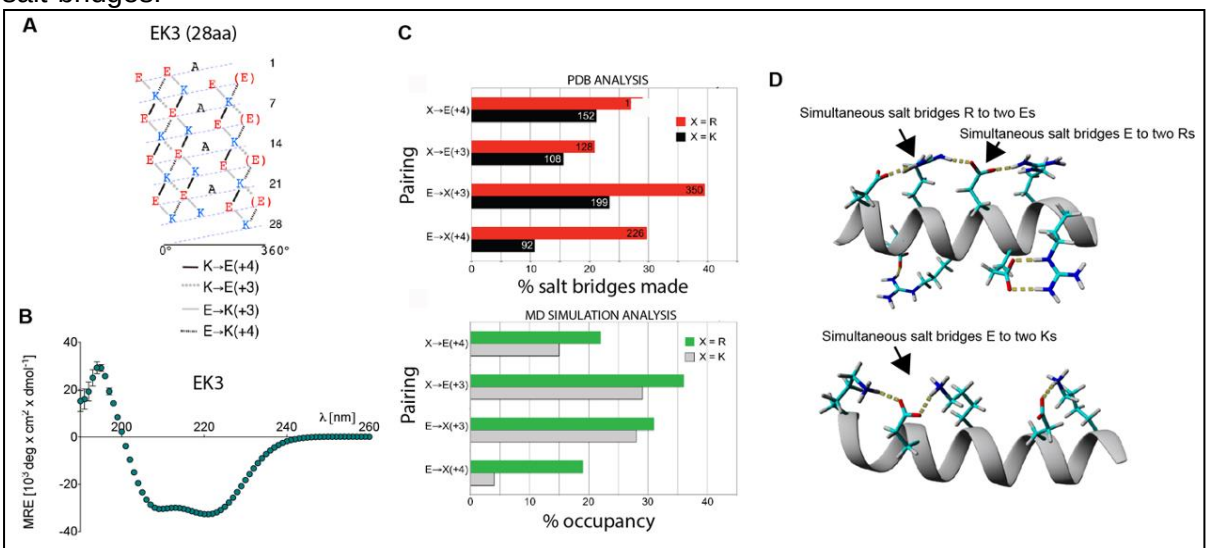

Figure 3: (A) Heptad net for part of the 96 residue EK3 sequence, shows potential interactions between oppositely charged residues. (B) Circular dichroism shows the highly helical nature of SAH domains. (C) A PDB analysis (top: red is R, black is K) and molecular dynamics simulation (MD) analysis (bottom: green is R, grey is K) shows R forms more salt bridges than K. (D) Molecular dynamics simulations show a higher propensity for simultaneous salt bridges between Glu (E) and Arg (R), than between Glu (E) and Lys (K).

Results
We first tested Lys-rich sequences, and found that only EK3 (AEEEKKK)) formed a stable SAH in solution (Fig. 1B). Decreasing the number of EK pairs (e.g. EK2 (AEEAKKA) or EK1 (AAEAAK) did not result in SAH domain formation: EK1 aggregated, and EK1 was only soluble at low (<50mM NaCl) ionic strength. Surprisingly, none of the Arg-rich sequences (ER3, ER2 or ER1) formed SAH domains, and ER3 aggregated. However, substituting in an Arg for a single Lys in EK3, to generate EK2R1 (AEEEKRK) did result in a stable SAH, which was more helical and thermo-stable suggesting Arg increases stability. Substituting Lys with Arg (or *vice versa)* in the naturally-occurring myosin-6 SAH similarly increased (or decreased) its stability.

Combining a PDB analysis with molecular modelling provides a rational explanation for these findings. This analysis demonstrated that Glu and Arg form salt bridges more commonly than Glu and Lys (Fig. 1C), and that Glu-Arg salt bridges utilize a wider range of rotamer conformations and exhibit a more dynamic behaviour than Glu–Lys. Shared salt bridges between Glu and Arg are also more common than between Glu and Lys (Fig. 1D). This promiscuous nature of Arg helps explain the increased propensity of *de novo* Arg-rich SAHs to aggregate. Importantly, the specific K:R ratio is likely to be important in determining helical stability in *de-novo* and naturally-occurring polypeptides, giving new insight into how single α-helices are stabilized.

Other work in the lab has investigated the role of the divergent tubulin Tuba8, and the use of Affimers as alternatives to antibodies in super-resolution imaging.

Publications
Wolny M., Batchelor M., Bartlett G. J., Baker E. G., Kurzawa M., Knight P. J., Dougan L., Woolfson D. N., Paci E., & Peckham M. (2017) Characterization of long and stable de novo single alpha-helix domains provides novel insight into their stability. *Sci Rep* **7**:44341

Tiede C., Bedford R., Heseltine S. J., Smith G., Wijetunga I., Ross R., AlQallaf D., Roberts A. P., Balls A., Curd A., Hughes R. E., Martin H., Needham S. R., Zanetti-Domingues L. C., Sadigh Y., Peacock T. P., Tang A. A., Gibson N., Kyle H., Platt G. W., Ingram N., Taylor T., Coletta L. P., Manfield I., Knowles M., Bell S., Esteves F., Maqbool A., Prasad R. K., Drinkhill M., Bon R. S., Patel V., Goodchild S. A., Martin-Fernandez M., Owens R. J., Nettleship J. E., Webb M. E., Harrison M., Lippiat J. D., Ponnambalam S., Peckham M., Smith A., Ferrigno P. K., Johnson M., McPherson M. J., & Tomlinson D. C. (2017) Affimer proteins are versatile and renewable affinity reagents. *Elife* **6**:e24903

Diggle C. P., Martinez-Garay I., Molnar Z., Brinkworth M. H., White E., Fowler E., Hughes R., Hayward B. E., Carr I. M., Watson C. M., Crinnion L., Asipu A., Woodman B., Coletta P. L., Markham A. F., Dear T. N., Bonthron D. T., Peckham M., Morrison E. E., & Sheridan E. (2017) A tubulin alpha 8 mouse knockout model indicates a likely role in spermatogenesis but not in brain development. *PLoS One* **12**:e0174264

Bedford R., Tiede C., Hughes R., Curd A., McPherson M. J., Peckham M., & Tomlinson D. C. (2017) Alternative reagents to antibodies in imaging applications. *Biophys Rev* **9**:299-308

Funding
Our work was funded by BBSRC, MRC and the British Heart Foundation.

Collaborators
External: Dek Woolfson, Emily Baker and Gail Bartlett, Schools of Chemistry and Biochemistry, (University of Bristol)

Non-covalent complexes studied by mass spectrometry: Examples of amyloid assembly and membrane protein structure and function

Samuel Bunce, Antonio Calabrese, Owen Cornwell, Paul Devine, Jim Horne, Patrick Knight, Esther Martin, Tom Watkinson, Lydia Young, Martin Walko, Andrew Wilson, Alison Ashcroft and Sheena Radford

Introduction

Non-covalent electrospray ionisation mass spectrometry (ESI-MS) is a powerful method to interrogate complex reactions in protein assembly. Combined with tandem mass spectrometry (MS/MS) and ion mobility spectrometry (IMS)-MS the mass, conformation, stoichiometry, stability, and ligand binding of biomolecules and their complexes can be determined (Figure 1). We are using MS-based methods to analyse protein folding and aggregation mechanisms, protein function and ligand binding [1-4]. We are also using chemical labelling methods (Figure 1) together with MS to interrogate protein conformation and to characterise non-covalently bound assemblies [5, 6].

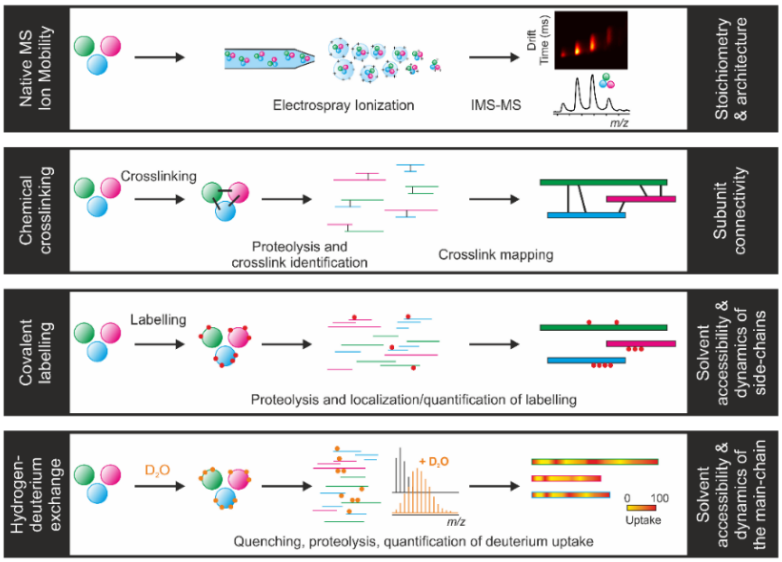

Figure 1: Summary of structural mass spectrometry methods, workflows, and the information obtained from each experiment (from Calabrese and Radford, Methods, in press).

Results

We have used ESI-IMS-MS to study the co-polymerization of related sequences of islet amyloid polypeptide (IAPP) (Figure 2a) [1]. Subtle alterations in sequence have been shown to influence dramatically the rate of assembly of IAPP into amyloid (Figure 2b). ESI-IMS-MS showed that the sequences have different abilities to co-assemble (Figure 2c,d). Combined, the data demonstrate that co-polymerization of IAPP sequences tunes the rate of amyloid assembly, with the most rapidly assembling sequence determining the aggregation rate. This is achieved by altering the conformational properties of the mixed oligomers that form.

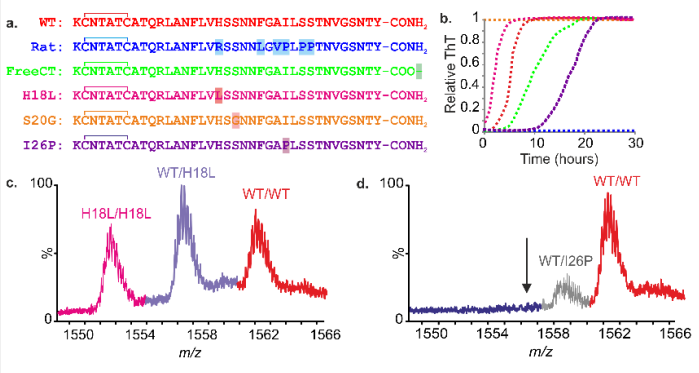

Figure 2: Sequence and amyloid formation of IAPP variants. (A) Sequence of peptides studied. (B) ThT fluorescence shows different lag times for different sequences (coloured as in (A)). (C,D) Mass spectra of 1:1 (C) WT:H18L and (d) WT:I26P, showing that homo- and hetero-dimers form for WT:H18L, but I26P homodimers do not form. The position at which I26P 5^{+} homodimers would be observed is indicated with an arrow. From ref [1].

We have also used MS-methods to study the effects of the detergent n-dodecyl-D-maltoside (DDM) and the amphipol A8-35, on the structure and function of the outer membrane protein, OmpT. A hydroxyl radical footprinting technique (FPOP) was used to label the solvent accessible amino acid side-chains of OmpT. The protein was then proteolysed and the resulting peptide fragments were subjected to LC-MS/MS for identification of the individual modification sites. The data showed that whilst the detergent DDM protects only the trans-membrane region of OmpT, the amphipol A8-35 protects both the trans-membrane and the extra-membrane regions [6].

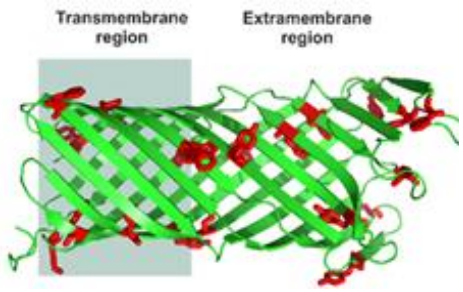

Figure 3: Structure of OmpT showing the transmembrane and extra-membrane regions. FPOP labelled residues are shown in red [6].

References

Young L. M., Tu, L.H., Raleigh D.P., Ashcroft A. E., Radford S. E. (2017) Understanding co-polymerization in amyloid formation by direct observation of mixed oligomers. *Chem. Sci.* **8**:5030-5040

Young L.M., Ashcroft A. E., Radford S. E. (2017) Small molecule probes of protein aggregation. *Curr. Opin. Chem. Biol* **39**:90-99

Schiffrin B., Calabrese A.N., Higgins A.J., Humes J.R., Ashcroft A.E., Kalli A.C., Brockwell D.J., Radford S.E. (2017) Effects of periplasmic chaperones and membrane thickness on BamA-catalysed outer membrane protein folding. *J. Mol. Biol* **429**:3776-3792

Devine P.W.A., Fisher H.C., Calabrese A.N., Whelan F., Higazi D.R., Potts J.R., Lowe D.C., Radford S.E., Ashcroft A.E. (2017) Investigating the structural compaction of biomolecules upon transition to the gas-phase using ESI-IMS-MS. *J. Am. Soc. Mass Spec* **28**:1855-1862

Calabrese A.N., Jackson S.M., Jones L.N., Beckstein O., Heinkel F., Gsponer J., Sharples D., Sans M., Kokkinidou M., Pearson A.R., Radford S.E., Ashcroft A.E., Henderson P.J.F.H. (2017) Topological dissection of the membrane transport protein Mhp1 derived from cysteine accessibility and mass spectrometry. *Anal. Chem* **89**:8844-8852

Watkinson T. G., Calabrese A. N., Ault J. R., Radford S. E., Ashcroft A. E. (2017) FPOP-LC-MS/MS suggests differences in interaction sites of amphipols and detergents with outer membrane proteins *J. Am. Soc. Mass Spectrom* **28**:50-55

Funding

Our research is funded by the BBSRC, EPSRC, Wellcome Trust, Human Frontiers Science Programme, European Research Council, Waters UK Ltd., LGC, UCB and Medimmune.

Collaborators

University of Leeds: D. J. Brockwell, R. J. Foster, S. A. Harris, P. J. F. Henderson.
External: Dr D. P. Raleigh (Stonybrook, NY, USA), Prof. J-L. Popot and Dr M. Zoonens (CNRS Paris, France), Prof. E. Deuerling (Konstanz, Germany), Prof Judith Frydman (Stanford, USA).

Effects of periplasmic chaperones and membrane thickness on BamA-catalysed outer-membrane protein folding

Jim Horne, Bob Schiffrin, Antonio Calabrese, Anna Higgins, Julia Humes, Alison Ashcroft, Antreas Kalli, David Brockwell and Sheena Radford

Introduction

The biogenesis of Gram-negative bacterial outer membrane proteins (OMPs) depends on periplasmic chaperones and a dedicated folding catalyst at the outer membrane (OM), the β-barrel assembly machinery (BAM) complex. BamA, the major subunit of BAM, is essential, surface-exposed and highly conserved, making it an attractive target for the development of novel antibiotics. In previous work, we investigated the structure of chaperone:OMP complexes and found that a 2-fold excess of the chaperone Skp could completely prevent folding of a model OMP, tOmpA – the β-barrel of OmpA, into synthetic liposomes. This raises the questions of how OMPs are released to allow folding in the OM from their high affinity (K_d ~nM) complexes with Skp, and *in vivo* how are OMPs inserted and folded into the OM by the BAM complex on release from chaperones? *In vitro* studies have shown that the physical properties of the membrane affect OMP folding rates and yields. BamA may function by causing membrane thinning and lipid disordering around a membrane-facing 'gate' in its barrel domain. Our work aims to gain mechanistic understanding of the OMP biogenesis pathway through *in vitro* biochemical and biophysical techniques, as well as *in silico* simulations.

Results

To investigate the role of BamA in releasing OMPs from their complex with periplasmic chaperones we used kinetic assays to follow the folding of tOmpA into *di*$C_{11:0}$PC (DUPC) liposomes in the presence or absence of combinations of Skp, SurA, and BamA (Figure 1). We observed that the presence of pre-folded BamA is necessary for release and folding of tOmpA from Skp. Combined with data from native mass spectrometry we showed that the presence of the other major periplasmic chaperone in *E. coli*, SurA, cannot release tOmpA from its complex with Skp. Together these results provide direct evidence for a BamA-mediated mechanism of substrate release from Skp, and rules out models in which the Skp and SurA chaperones cooperate in an obligate sequential pathway (at least for this substrate).

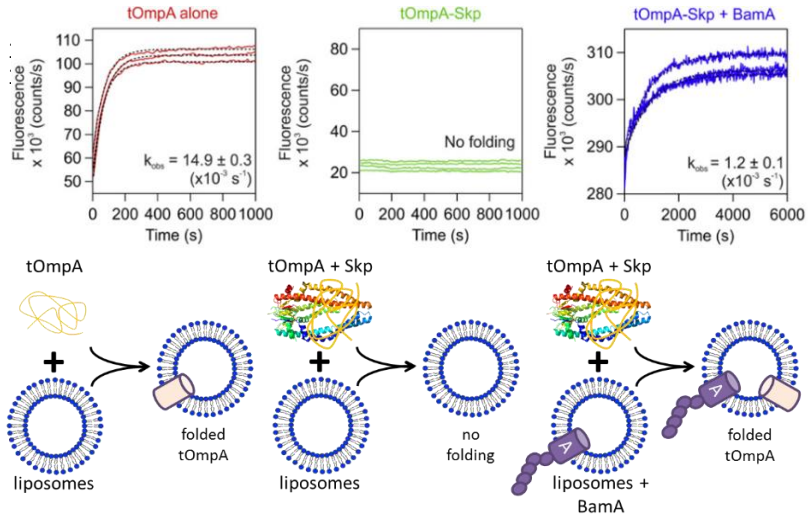

Figure 1: The presence of BamA pre-folded into di$C_{11:0}$PC liposomes allows OMPs to fold from a pre-assembled Skp:tOmpA complex. Top: folding of tOmpA observed by tryptophan fluorescence in the presence of liposomes and 1) no other components, 2) Skp, 3) Skp and BamA pre-folded into liposomes. Bottom: schematic illustrating the experimental setup and results. Numbering as in top row image.

To test the hypothesis that BamA functions through the creation of lipid disorder and thinning of lipid bilayers, we examined the effect of BamA on the folding kinetics of tOmpA, and on the lipid structure in bilayers of different hydrophobic thickness. If BamA functions by lowering the kinetic barrier imposed by hydrophobic thickness and acyl-chain packing it would be expected that its catalytic effect would be greater in thicker bilayers. Measurement of tOmpA kinetics

using tryptophan fluorescence allowed us to extract and compare t_{50} values (the time it takes to reach 50% of maximum fluorescence) for tOmpA folding into bilayers composed of 12, 13, or 14 carbon acyl chain lipids (DLPC, DTPC, and DMPC, respectively). The presence of BamA accelerated folding in all cases, but the effect was greatest in thicker membranes with a ~2-fold change in t_{50} in DLPC (C12) compared to a ~12-fold change in DMPC (C14) (Figure 2). Consistent with this, coarse-grained molecular dynamics simulations of the transmembrane domain of BamA inserted into lipid bilayers of different thicknesses showed increased membrane thinning and lipid disordering in thicker bilayers, in particular at the seam between the first and last strand of the BamA barrel. Together, these results provide compelling evidence to support a lipid 'disruptase' mechanism for BamA *in vitro*, suggesting that modulation of the bilayer architecture is important in the mechanism by which the BAM complex accelerates OMP folding *in vivo*.

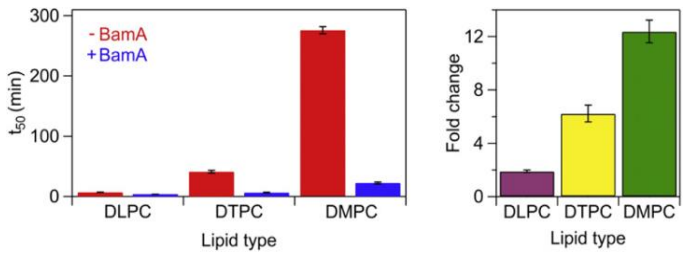

Figure 2: The catalytic effect of BamA is dependent on bilayer thickness. Left: t_{50} values of tOmpA folding measured by tryptophan fluorescence in the absence or presence of BamA in lipids with acyl-chain lengths C12-C14. Right: the enhancement of tOmpA folding kinetics (uncatalyzed/catalyzed) by BamA increases with bilayer thickness.

We are currently building on this work to tie together our mechanistic and structural understanding of the OMP biogenesis pathway through two major threads: 1) the chaperoning of OMPs by SurA and their delivery to BamA/BAM, and 2) the effect of the lipid environment on BamA and the BAM complex and conversely, the details of how BamA and the BAM complex remodel lipid membranes in order to catalyse OMP folding.

Publications

Schiffrin B., Calabrese A.N., Higgins A.J., Humes J.R., Ashcroft A.E., Kalli A.C., Brockwell D.J. & Radford S.E. (2017) Effects of periplasmic chaperones and membrane thickness on BamA-catalyzed outer-membrane protein folding. *J. Mol. Biol* **429**:3776-3792.

Schiffrin B., Brockwell D.J. & Radford S.E. (2017) Outer membrane protein folding from an energy landscape perspective. *BMC Biology* **15**:123-138.

Funding

This work was funded by the BBSRC, the NIH, and The Wellcome Trust.

Collaborators

University of Leeds: Neil Ranson, Matt Iadanza.

High resolution Cryo-EM to study virus-receptor interactions

Daniel Hurdiss and Neil Ranson

Introduction

In the last decades, there have been millions of cases of acute haemorrhagic conjunctivitis (AHC) worldwide, a painful and contagious eye disease which is associated with ocular swelling, watering and extensive subconjunctival haemorrhaging. The main causative agent of AHC is Coxsackievirus A24v (CV-A24v), an Enterovirus within the *Picornaviridae* which emerged from a non-pathogenic form of the virus, CV-A24. At present, there are no available vaccines or antivirals for prevention or treatment of viral AHC. Receptors are important determinants of viral tropism and as such, we wanted to elucidate the receptor repertoire of CV-A24v and identify possible explanations for the switch from non-pathogenic CV-A24 to disease-causing CV-A24v.

Results

Intracellular adhesion molecule 1 (ICAM-1) was identified as an essential proteinaceous receptor for CV-A24v using neutralisation assays and confirmed by CRISPR-Cas9 knockout of the ICAM-1 gene. To determine the interaction of ICAM-1 and CV-A24v we used single-particle cryo-EM analysis on a complex between a recombinant D1-D2 fragment of ICAM-1 and purified CV-A24v virions. A recombinant D1-D2 fragment of ICAM-1 was applied to CV-A24v virions immobilized on a lacey carbon support. This on-grid binding was performed for 30 s at 8 °C prior to blotting away excess sample and plunge freezing. This approach allowed us to determine the cryo-EM structure of the ICAM-1-CV-A24v complex (Figure 1A-B), whereas incubation of the components in solution resulted in the loss of particle integrity, likely due to destabilization of the particle following receptor binding. The EM structure had a global resolution of 3.9 Å, the viral capsid proteins were resolved to ~3.6–3.8 Å, and the interface between the ICAM-1 D1 domain and virion surface was ~3.7 Å, with side chain density visible in the EM density map. The exterior of enterovirus particles is comprised of 60 copies of the capsid proteins VP1, VP2, and VP3. A canyon is formed by a depression which encircles the fivefold axis of symmetry, which provides the binding site for previously identified uncoating receptors. Our structure shows that the ICAM-1 D1 domain is bound in the canyon located at the quasi-threefold axis. However, unlike earlier studies where resolution was limited to ~8-20 Å, the capsid-ICAM-1 D1 interface in our map is well resolved, with clear secondary structure and side chain density visible.

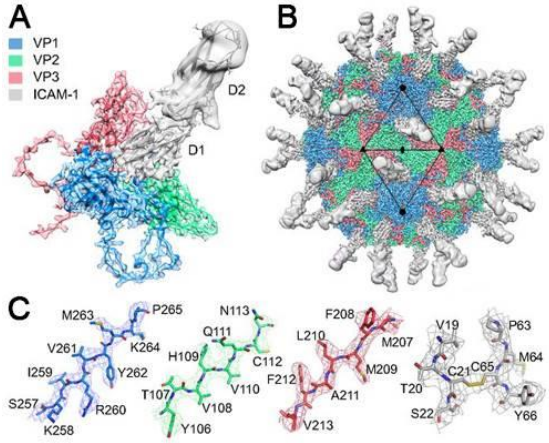

Figure 1: (A) An enlarged and tilted view of the quasi-threefold of the CV-A24v capsid and bound ICAM-1 D1-D2 domains, indicated by a black triangle in B, with the corresponding atomic model fitted in the density. The D1 domain binds in the "canyon" located at the interface between VP1, VP2 and VP3. (B) Isosurface representation of CV-A24v in complex with ICAM-1 (D1D2) with the capsid viewed down the icosahedral twofold axis. D1 (1σ), D2 (0.6σ) and VP1-3 (3.6σ). (C) Representative cryo-EM density of VP1-3 and D1 domain.

The interaction between ICAM-1 and CV-A24v is largely mediated by electrostatic complementarity. The capsid residues VP3 Asp^{181} and VP1 Asp^{238} interact with Lys^{29} located on the FG loop of ICAM-1. In addition, VP1 Arg^{168} forms a salt bridge with Asp^{71} on the tip of the FG loop of ICAM-1. Finally, the VP1 residues Asp^{228} and Asp^{225} located on the GH loop interact with Lys^{50}(strand C) and Lys^{39} (strand D) of ICAM-1 (Figure 2A-C). In addition, a

hydrogen bonding network tethers VP1 (Tyr^{230}) and VP2 (Ala^{138}, Lys^{139} and Thr^{140}) to the DE loop of ICAM-1 D1 (Arg^{49}, Asn^{47} and Pro^{45}). There is a high level of sequence conservation for these residues among other ICAM-1–binding viruses which belong to the enterovirus C species, indicating a conserved interaction with ICAM-1. In contrast, VP1 Asp^{238} and VP3 Asp^{181} are only conserved residues present in rhinoviruses which bind ICAM-1.

In addition to the interaction with ICAM-1, we also identified an adaptation which improves binding of CV-A24v to sialic acid which serves as an additional attachment receptor. This may have contributed to the pathogenicity and pandemic nature of CV-A24v thus highlighting the sialic acids importance for viruses with ocular tropism e.g. influenza A virus and some adenoviruses.
Current work now aims to characterise the conformational changes in the CV-A24v capsid associated with genome release and whether this can be blocked by capsid binding compounds which have been
identified for other Enteroviruses. If these compounds prove effective in a cell culture model of infection, the mode of binding will be elucidated using cryo-EM.

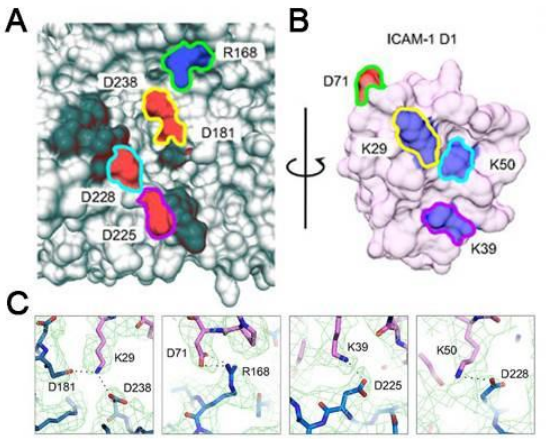

Figure 2: (A-B) Surface representation of the ICAM-1 binding site (grey) and D1 (pink), the residues involved in formation of salt bridges are labeled and colored according to their interacting partners. Capsid residues that hydrogen-bond with ICAM-1 are dark gray and residues involved in electrostatic interactions are colored according to charge (red = negative, blue = positive). (C) Cryo-EM density (green mesh) for the interactions shown in A & B between ICAM-1 (pink) and CV-A24v (blue). Possible hydrogen bonds are shown as black lines.

Funding
This work was funded by the Wellcome Trust, the Netherlands Organization for Scientific Research and the German Research Foundation.

Collaborators
External: J. Baggen, R.W. Roberts, J.J. Slager, H. Guo, A.L.W.v. Vliet, M. Wahedi, C.A.M.d. Haan, E.d. Vries, R.J.d. Groot, H.J. Thibaut & F.J.M.v. Kuppeveld (Utrecht University). G. Zocher & T. Stehle (University of Tübingen) N. Mistry & N. Arnberg (Umeå Univeristy). K. Benschop & E. Duizer (National Institute for Public Health and the Environment, the Netherlands). J.M. Casasnovas (Centro Nacional de Biotecnología, Madrid).

Controlling multivalent binding through surface chemistry

Ralf Richter

Introduction

Multivalent binding, through multiple interactions between specific ligand/receptor pairs, underpins many biological interactions (*e.g.*, antigen/antibody, cell/cell, cell/virus) and cellular processes (*e.g.*, adhesion, chemotaxis, inflammation, secretion). Multivalent interactions are also an attractive tool for the design of supramolecular architectures: they enable strong but reversible attachment, and drastically increase binding selectivity as compared to monovalent bonds. Defining the factors governing multivalent binding at interfaces thus is important for understanding biological systems and the design of supramolecular nanomaterials. We aim to understand how multivalent binding depends on surface properties - chemistry, packing and lateral mobility of binding moieties. This question has traditionally been difficult to assess, and quantitative information about the residual valency and orientation of surface-bound molecules is often missing.

Results

To address these questions, we study streptavidin (SAv; a tetravalent biotin binder) on commonly used biotinylated surfaces such as supported lipid bilayers (SLBs; a model of cell membranes that displays laterally mobile biotinylated lipids) and self-assembled monolayers (SAMs; displaying immobile biotins). Stability and kinetics of SAv binding was assessed by quartz crystal microbalance (QCM-D), while the residual valency of immobilized SAv was quantified using spectroscopic ellipsometry (SE) by monitoring binding of biotinylated probes. Purpose-designed SAv constructs having controlled valencies (mono-, di-, trivalent) are studied to rationalize the results obtained on regular (tetravalent) SAv (Figure 1).

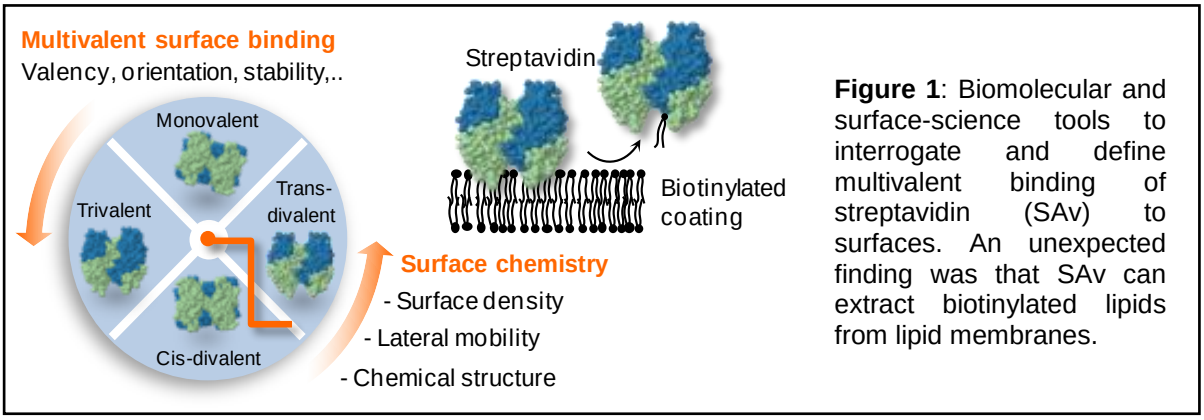

Figure 1: Biomolecular and surface-science tools to interrogate and define multivalent binding of streptavidin (SAv) to surfaces. An unexpected finding was that SAv can extract biotinylated lipids from lipid membranes.

We found that the divalent interaction of SAv with biotinylated surfaces is a strict requirement for stable immobilization. Despite the high intrinsic affinity of SAv-biotin bonds, monovalent attachment is reversible and, in the case of SLBs, leads to the extraction of biotinylated lipids from the bilayers (Figure 1). SAv binds to surfaces in multiple orientations (divalent in trans and cis, and trivalent; Figure 2). The surface density and lateral mobility of biotin, and the SAv surface coverage are all found to influence the average orientation and residual valency of SAv on a biotinylated surface. We demonstrate how the residual valency can be adjusted to one or two biotin binding sites per immobilized SAv by choosing appropriate surface chemistry. The obtained results provide means for the rational design of surface-confined supramolecular architectures involving specific biointeractions at tunable valency. This knowledge can be used for the development of well-defined bioactive coatings, biosensors and biomimetic model systems.

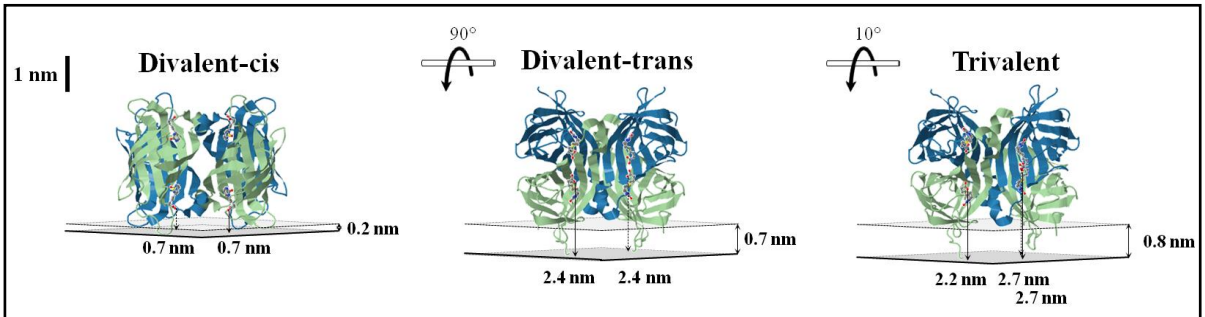

Figure 2: Possible orientations of SAv on biotinylated surfaces.

Publications

Dubacheva G. V., Araya-Callis C., Geert Volbeda A., Fairhead M., Codee J., Howarth M. & Richter R. P. (2017) Controlling Multivalent Binding through Surface Chemistry: Model Study on Streptavidin. *J. Am. Chem. Soc* **139**:4157-4167.

Funding

This work was funded by the European Union (Marie Curie Actions and European Research Council), the BBSRC, and the Spanish Ministry of Competitiveness and Innovation.

Collaborators

External: G. V. Dubacheva (CIC biomaGUNE, now Ecole Nationale Superieure, Paris, France), C. Araya-Callis (CIC biomaGUNE), A. Geert Volbeda & J. Codee (Leiden University, The Netherlands), M. Fairhead & M. Howarth (University of Oxford, UK).

Heterologous production of neoantimycins

Divya Thankachan and Ryan Seipke

Introduction

Streptomyces species produce an incredible array of high-value specialty chemicals and medicinal therapeutics. Neoantimycins are 15-membered ringed depsipeptides produced by *Streptomyces orinoci* (Figure 1). Neoantimycins were recently identified as downregulators of GRP78/BiP expression. Growth of cancerous cells is energetically expensive and as a result often exist in a state of hypoxia, which necessitates the overproduction of the molecular chaperone GRP78/BiP for survival. Thus, modulating the activity or indeed the level of cellular GRP78/BiP represents an exciting therapeutic target for the treatment of diverse cancers. Despite being known for >50 years, remarkably little is known about the biosynthesis of neoantimycins and thus the opportunity for bioengineering new drug variants is limited. Here we identified and cloned the neoantimycin biosynthetic gene cluster and engineered its overproduction by *Streptomyces coelicolor.* This expression chassis can be used in the future to bioengineer neoantimycin analogues and evaluate structure-activity relationships.

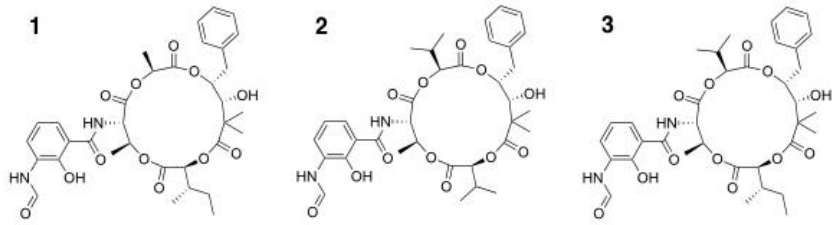

Figure 1: Chemical structures of neoantimycins

Results

We sequenced the genome of the neoantimycin producer, *Streptomyces orinoci* using Pacific Biosciences SMRT RSII platform and identified a ~38 kb biosynthetic gene cluster (BGC) composed of 18 genes whose deduced functionalities were consistent with a pathway that may proudce neoantimycins. A key aim of this study was to first determine if this BGC does indeed confer the production of neoantimycins and then develop an expression system by which new variants could be bioengineered in the future. To achieve this, the BGC was into two plasmids harbouring orthologous phage integrate sites so that they could stablely be maintained in a *Streptomyces* host without selection. Next, a suite of promoter engineering recombineering templates were developed and used these to replace native promoters with strong constitutive ones such that the entire BGC would be overexpressed. The engineered neoantimycin plasmids were moved to *Streptomyces coelicolor* and the resulting strains were examined for their ability to produce neoantimycins using liquid chromatography high resolution electrospray ionisation mass spectrometry (LC-HRESIMS). As anticipated, molecular formulae for neoantimycins were observed in chemical extracts prepared from the *S. coelicolor* double integrant (Figure 2). Current work is now aimed at using this platform to bioengineer new neoantimycin analogues.

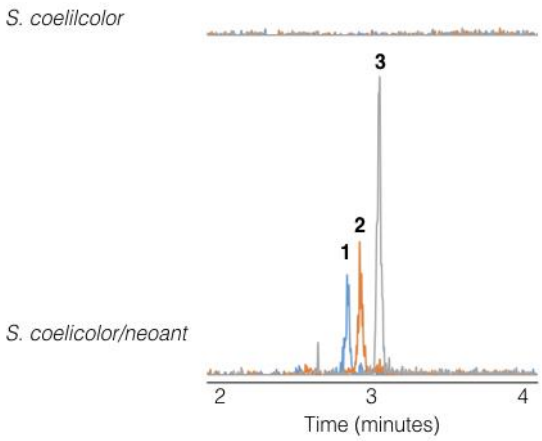

Figure 2: Engineered heterologous production of neoantimycins by *Streptomyces coelicolor* M1146. The empty *S. coelicolor* host (top) does not produce neoantimycins while neoantimycins are readily detectable from chemical extracts prepared from *S. coelicolor* harbouring the engineered neoantimycin plasmids (bottom). Shown are extracted ion chromatograms $[M+H]^+$ for **1, 2, 3** depicted in Figure 1.

Funding
This work was funded by the BBSRC.

Collaborators
External: W. Zhang (University of California at Berkeley).

Microfluidic droplets enabling study of atmospheric science in a high throughput way

Mark Tarn, Sebastien Sikora, Grace Porter, Daniel O'Sullivan, Mike Adams, Thomas Whale, Alexander Harrison, Benjamin Murray and Jung-uk Shim

Introduction

Ice-nucleating particles (INP) play a significant role in the climate and hydrological cycle by triggering ice formation in super-cooled clouds thereby causing precipitation and affecting cloud lifetimes and their radiative properties. However, despite their importance they often comprise only 1 in 10^3 to 10^6 ambient particles, making it difficult to ascertain and predict their type, source and concentration. They can originate from various sources such as desert dust plumes, marine sources, and anthropogenic activities and their relative contributions can vary depending on timeframe and location. The typical techniques for quantifying INP concentrations tend to be highly labour intensive, suffer from poor time resolution or are limited in sensitivity to low concentrations. Microfluidic technology enables the generation of very monodisperse droplets at high production rates for a range of applications, but while such devices have been employed successfully in environmental monitoring, their application to the atmospheric sciences has been largely neglected. The microfluidic continuous flow freezing studies require complex and careful preparation and operation to ensure accurate measurements in such a dynamic system. An alternative approach is to generate the droplets before containing them in a static system that can be cooled. A method of monitoring droplets in a static system is to simply collect the microfluidic droplets and dispense them directly onto a substrate on a cold stage. However, there is a lack of microfluidic data for atmospherically relevant INPs. Here, we employ the simple microfluidic strategy of combining microfluidic droplet generation and collection with a Peltier-based cold stage for the analysis of atmospheric INP (Figure 1). In order to validate the platform, we performed measurements of known INP present in desert dust (K-feldspar mineral particles) and biological species (i.e. pollen and fungal-based nanoscale INPs, and *P. syringae* in the form of Snomax®) sources.

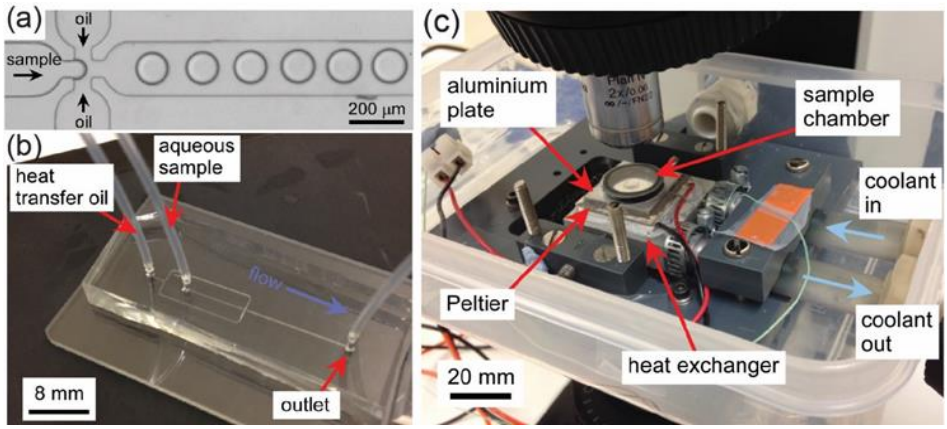

Figure 1: (A) Generation of water-in-oil droplets in the microfluidic device. (B) Microfluidic device. (C) Collected water-in-oil droplets were pipetted into a sample chamber and placed onto a Peltier-based cold stage for freezing experiments.

Results

Droplets generated via the microfluidic device were collected and then cooled via the Peltier-based cooling stage (Figure 1). Images and temperature measurements were taken every second, from which the temperatures at which each aqueous droplet froze could be determined. 250−500 droplets were analysed per sample. The fraction of droplets frozen, $f_{ice}(T)$, by temperature T for a range of atmospherically relevant INP was calculated; $f_{ice}(T) = n_{ice}(T)/n_{tot}$ where $n_{ice}(T)$ is the total number of frozen droplets at temperature T, and n_{tot} is the total number of droplets (Figure 2). Droplets containing purified water without the addition of INP were used as a blank. The $f_{ice}(T)$ results demonstrate the range over which

different atmospheric INP trigger the freezing of water, from the highly active *P. syringae* bacteria (in the form of Snomax®) at −4.2 to −7.8 °C, to K-feldspar mineral at −17.5 to −24.4 °C. Purified water, in the absence of any added INP, was shown to freeze homogeneously between −34.1 to −35.6 °C. A sample of tap water was analysed to demonstrate the difference between purified and non-purified water, with the results showing the presence of some INP that triggered ice formation as high as −25.6 °C. However, the amount of INP in the tap water sample was actually quite low, with only a small fraction (~3 %) of the droplets freezing at temperatures higher than the pure water sample. Assuming a singular approximation, in which ice nucleation is assumed to be a temperature dependent and time-independent process, each droplet containing INP will freeze at a characteristic temperature that will depend upon the nature of the INP. According to the singular model, the cumulative number of ice nucleation sites per unit volume of water, *K(T)*, on cooling to temperature *T* can be calculated from the fraction frozen curves according to (2), where V is the volume of a droplet: $K(T) = -\ln(1 - f_{ice}(T))/V = -\ln(f_{water}(T))/V$ where f_{water} is the fraction of droplets that remain liquid by temperature *T*. The results for *K(T)* (per mL) of the various samples are shown in Figure 2. From *K(T)*, a number of INP properties can be determined regarding the number of active sites on the particles between 0 °C and temperature *T*, based on the mass concentration, C_m, of INP: $K(T)/C_m = n_m(T) = n_s(T) \cdot S = n_n(T) \cdot N$ where $n_m(T)$ is the active site density per unit mass of INP, $n_s(T)$ is the number of active sites per surface area, S, is the surface area of INP per droplet, $n_n(T)$ is the active site density per particle number, and *N* is the specific particle number. These various active site density values provide a standard by which measurements of the efficiency with which a material nucleates ice can be compared between instruments. We present the novel application of microfluidic devices to the study of atmospheric INP via the simple and rapid production of monodisperse droplets and their subsequent freezing on a cold stage. This device offers a high-throughput testing of INP concentrations in aqueous samples with high sensitivity and high counting statistics. The ability to detect INP from atmospheric aerosol was demonstrated via the analysis of field campaign samples, which we believe is a first for a microfluidic platform.

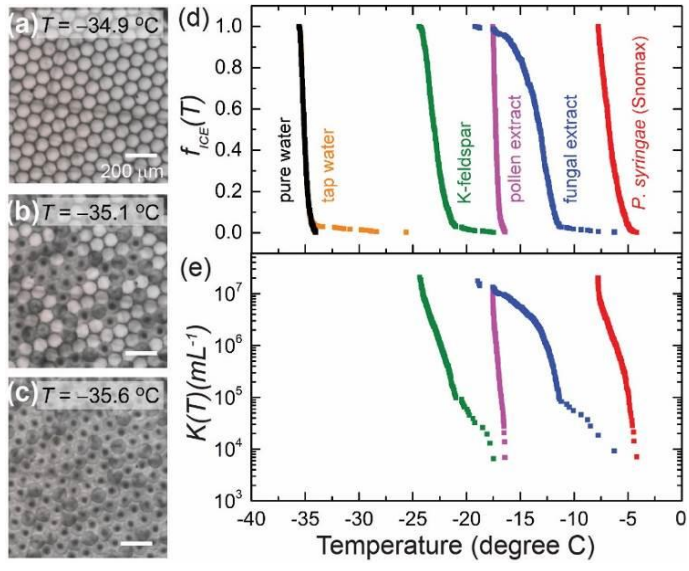

Figure 2: (A-C) Photographs showing the freezing of pure water droplets on the cold stage. (A) Before freezing, (B) with half of the droplets frozen (C) with all of the droplets frozen. (C-D) Ice-nucleation studies for water and a range of atmospherically relevant INP of dust and biological origins. (d) Fraction frozen ($f_{ice}(T)$) curves. (E) The cumulative number of ice nucleation sites per millilitre (*K(T)*) for the various INP. The temperature uncertainty was estimated to be ± 0.9°C.

Funding
This work was funded by the ERC.

Liquid-liquid phase separation of RNA-binding proteins

Albert Konijnenberg and Frank Sobott

Introduction

Liquid-liquid phase separation (LLPS) of RNA-binding proteins plays an important role in the formation of multiple membrane-less organelles involved in RNA metabolism, including stress granules. Defects in stress granule homeostasis constitute a cornerstone of ALS/FTLD pathogenesis. Polar residues (tyrosine and glutamine) have been previously demonstrated to be critical for phase separation of ALS-linked stress granule proteins. We now identify an active role for arginine-rich domains in these phase separations. Moreover, arginine-rich dipeptide repeats (DPRs) derived from C9orf72 hexanucleotide repeat expansions similarly undergo LLPS and induce phase separation of a large set of proteins involved in RNA and stress granule metabolism. Expression of arginine-rich DPRs in cells induced spontaneous stress granule assembly that required both eIF2α phosphorylation and G3BP. Together with recent reports showing that DPRs affect nucleocytoplasmic transport, our results point to an important role for arginine-rich DPRs in the pathogenesis of C9orf72 ALS/FTLD.

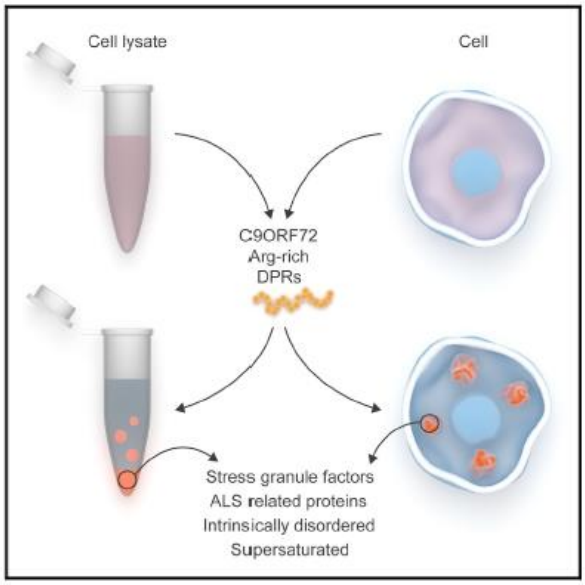

Figure 1: Proteins high in arginine content are enriched in stress granules. We show that arginine-rich peptides can actively mediate liquid-liquid phase separation, a process underlying liquid organelle formation. Toxic C9orf72 DPRs change the arginine content and alter the properties of stress granules.

Results

Global hydrogen-deuterium exchange (HDX) experiments were used to show that arginine-rich peptides phase separate in vitro. HDX shows full accessibility of the free peptide, which is compatible with its disordered state. Following the addition of polyU RNA, accessibility drops only slightly (to 80% of its initial value), indicating that the peptide is still largely accessible, and suggesting that it stays disordered after LLPS. Together with a large range of other biophysical data, this indicates the basis of stress granule formation is liquid-liquid phase separation. Depending on in vitro conditions, liquid-like protein-rich droplets can form. The intrinsically disordered prion-like domains of these proteins by themselves are sufficient in inducing LLPS. Interestingly, these liquid-like droplets can mature over time to more fibrillar states, and this process is accelerated by disease-causing mutations.

Collaborators

External: Steven Boeynaems, Elke Bogaert, Denes Kovacs, Evy Timmerman, Alex Volkov, Mainak Guharoy, Mathias De Decker, Tom Jaspers, Veronica H. Ryan, Abigail M. Janke, Pieter Baatsen, Thomas Vercruysse, Regina-Maria Kolaitis, Dirk Daelemans, J. Paul Taylor, Nancy Kedersha, Paul Anderson, Francis Impens, Joost Schymkowitz, Frederic Rousseau, Nicolas L. Fawzi, Wim Robberecht, Philip Van Damme, Peter Tompa, Ludo Van Den Bosch.

A Novel Conserved Assembly Mechanism in ssRNA Viruses

Nikesh Patel, Emma Wroblewski, Simon White, Daniel Maskell, Rebecca Thompson, Neil Ranson, Roman Tuma and Peter Stockley

Introduction

Positive sense, single stranded RNA viruses encompass a large fraction of all known viruses, these causing major current epidemics such as the alphavirus Chikungunya Virus. An obligate step in the lifecycles of all of these viruses is the specific packaging of their RNA genomes within a protective capsid shell comprised of coat protein (CP) subunits.

Recently we showed that the model viruses Satellite Tobacco Necrosis Virus (STNV) and Bacteriophage MS2; as well as Human Parechovirus-1 one of the major causes of infant death by sepsis, that virion assembly is mediated by multiple, sequence-degenerate RNA packaging signals (PS) dispersed along the respective genomes. PSs typically encompass sequence motifs with high (nM) affinities for cognate CPs that are presented in the loops of stem-loop (SLs). The multiple PS-CP contacts act co-operatively to make virion assembly highly efficient *in vivo*. Single molecule fluorescence correlation spectroscopy (smFCS) assays with STNV have been used to confirm many of the features of this PS-mediated assembly mechanism. PS-CP contacts are positioned along the genome in such a way that they facilitate the formation of the CP-CP contacts of the protein capsid, simultaneously compacting the RNA genome so it fits within the confined space of the virion. These observations at the nanomolar concentrations in smFCS assays explain the outcomes of natural infections in terms of genome specific encapsidation.

We describe some of these data below. There are many potential selective advantages to viruses assembling via the PS-mediated mechanism. This is consistent with its occurrence in many viral families including human Hepatitis B Virus (HBV), a para-retrovirus of the hepadnavirus family which packages a pre-genomic RNA (pgRNA) within its nucleocapsid (NC). HBV is the major cause of liver cancer worldwide and these data open a novel set of potential drug targets that could be exploited in its clinical management.

Results

The most 5′ 5 PSs on the STNV-1 genome (PS1 through 5) are crucial for assembly of the STNV virion, being the likely site of assembly initiation *in vivo*. Each of these SLs presents an

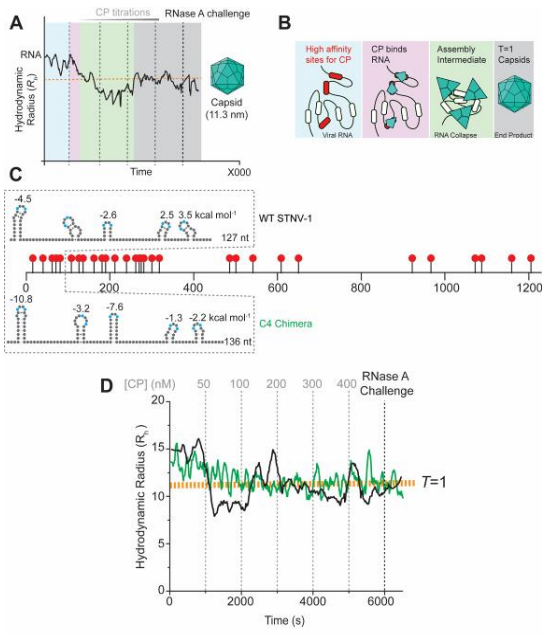

Figure 1: (A) Schematic of events during smFCS assays of *in vitro* assembly. The hydrodynamic radius (R_h) of CP-free RNA (blue background) is too large to fit in a viral shell. As CP is added it binds to PSs dispersed throughout the genome (pink), forming the CP-CP contacts of the capsid and collapsing the R_h (green). As CP concentration increases the R_h increases as the T=1 particles form (grey). **(B)** Cartoon of events described in (A). **(C)** Cartoons of PS1-5 and the C4 cassette above and below the wild-type genome with the positions of the PSs shown as red lollipops. **(D)** Comparison of smFCS assays with STNV CP and labelled RNAs encompassing wild-type (black) or with a 5´ C4 cassette (green). RNase is added at the end of the titrations to confirm complete capsid assembly. The artificial initiation site triggers a more rapid formation of the protein shell since the collapse in R_h is not seen.

AXXA motif in their loops, presumed to be the CP recognition motif. The precise determinants of this recognition have been determined using a series of variant SLs and an smFCS displacement assay. This revealed that the 5´A is not essential although the adenine at the 3´ of the motif is an absolute requirement. We also explored the optimal spacing and stability of these five PSs, and the minimum number of PSs required to generate co-operative assembly. The folding propensity of each SL is the critical factor in their functioning. Using this information we designed synthetic RNA cassettes lacking viral sequences that are superior assembly substrates than the natural genome (Figure 1). When the C4 sequence variant cassette was grafted on to 128-1293nt of the wild-type genome the chimeric RNA formed nuclease resistant *T*=1 particles more rapidly and at a higher yield compared to wild-type. This result confirms that we understand the self-assembly instructions underlying the PS-mediated assembly mechanism. Such information could enable the design of superior assembly substrates, crucial for optimising virus-like particle (VLP) manufacture for vaccine or drug delivery.

HBV packages a ss pgRNA into its NC converting it to the dsDNA of the mature virus particles using a single co-packaged polymerase. We investigated the assembly of NC around the pgRNA to see if it also made use of PS-mediated assembly.

HBV NC is a polymorphic protein shell, existing as either *T* = 3 or 4 surface lattices, made up of 90 or 120 core protein dimer (Cp) subunits, respectively. RNA SELEX was performed upon these Cp dimers to identify preferred RNA sequences that bind the Cp. Comparing the aptamer sequences against the HBV genome revealed multiple regions that matched both the aptamers and each other. Nine such sites are conserved across multiple HBV strains. The most stable folds for these genomic putative PSs were SLs presenting an RGAG motif in the loop and with a single stranded bulge within the middle of the stem. smFCS binding assays between RNA oligos encompassing the most conserved genomic PS revealed a high affinity interaction, with binding beginning at low nM concentrations and leading to the assembly of mainly *T*=4, nuclease resistant NCs (Figure 2). RNA sequence variant experiments established that this assembly reaction is highly sequence-specific, i.e. HBV seems to have many of the same features as the PS-mediated assembly of ssRNA viruses.

The structures of the PS oligo-containing VLPs from the smFCS assays were determined using cryo-election microscopy in the Astbury Biostructure Laboratory. 2D class averages revealed a subset of *T*=4 particles in which density corresponding to the RNA used for assembly was visible. A C1 asymmetric reconstruction to a resolution of 11.5 Å (Figure 2B), reveals density for the presumed PS-mediated assembly initiation complex, the first such complex ever observed directly. This structure represents a novel anti-viral drug target.

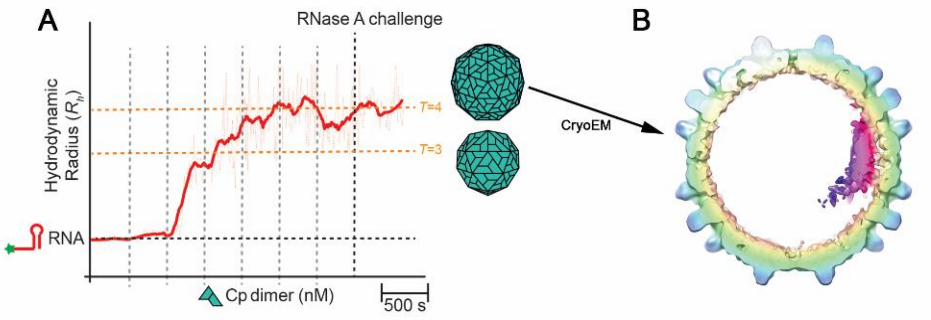

Figure 2: (A) smFCS binding assay between HBV Cp dimer and an RNA PS. The faint red trace represents the real time, raw signal while the thicker red line represents the data following smoothing. The time scale is indicated in the bottom right. (B) Asymmetric EM reconstruction of the RNA containing *T*=4 VLPs. A ~40-Å-thick slab through the asymmetric HBV VLP reconstruction shows an asymmetric feature bound to one region of the Cp shell, ascribed to a complex of PS oligo(s) and the C-terminal domain of HBV Cp (bright cerise, magenta and purple).

Publications

Patel N., White S. J., Thompson R. F., Bingham R., Weiss E. U., Maskell D. P., Zlotnick A., Dykeman E., Tuma R., Twarock R., Ranson N. A., Stockley P. G. (2017) The HBV RNA pre-genome encodes specific motifs that mediate interactions with the viral core protein that promote nucleocapsid assembly. *Nature Microbiology* **2**:17098.

Patel N., Wroblewski E., Leonov G., Phillips S. E. V., Tuma R., Twarock R., Stockley P. G. (2017) Rewriting nature's assembly manual for a ssRNA virus. *PNAS* 114:12255 – 12260.

Funding

This work was supported in part by the BBSRC (BB/J00667X/1, BB/L021803/1, BB/J004596/1 and BB/L022095/1), the Leverhulme Trust (LT130088 and ECF-2013-019), the NIH (R01-AI118933), the EPSRC (EP/K028286/1), the MRC (MR/N021517/1), and the Joint Investigator Award from the Wellcome Trust to Peter Stockley and Reidun Twarock (University of York) (089311/Z/09/Z, 090932/Z/09/Z, 106692, 110145 and 110146).

Collaborators

University of Leeds: Neil Ranson and Roman Tuma
External: Reidun Twarock, German Leonov & Eric Dykeman (University of York), Simon Phillips (Harwell/University of Oxford), Adam Zlotnick (Indiana University, Bloomington, USA)

A chemical genomics approach to drug reprofiling in oncology: antipsychotic drug risperidone as a potential adenocarcinoma treatment

Colin Fishwick and Paul Taylor

Introduction

In the search for new cancer treatments, the potential of existing drugs that have been or are being used for non-cancer indications remains under-investigated. Herein, we demonstrate that our Magic Tag® chemical genomics tool has the potential to systematically screen known drugs to identify reprofiling opportunities. Specifically, we present the widely used antipsychotic therapy risperidone as a possible treatment for prostate cancer and other adenocarcinomas.

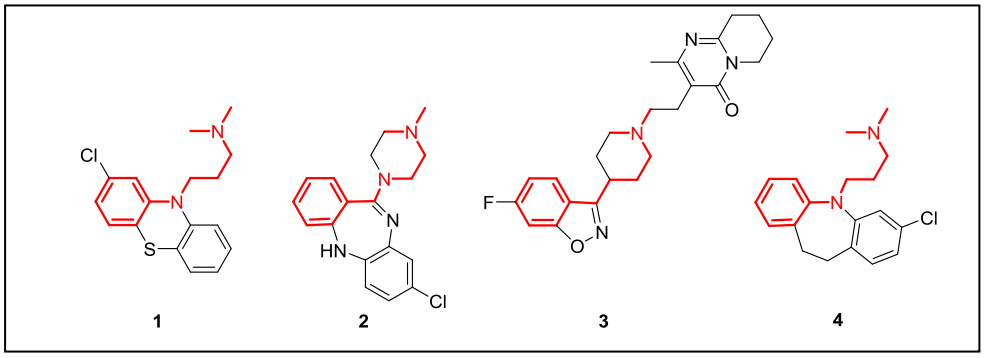

Results

Magic Tag® immobilized chlorpromazine **1** was exposed to a *D. melanogaster* phage-displayed library of polypeptides in three rounds of biopanning. 35 clones of interest were submitted to a selective elution experiment. Eight clones were judged to merit further study on this basis. Broadly in accordance with the extent of homology between humans and our chosen model *D. melanogaster*, six of the eight clones had DNA inserts that corresponded to sections of orthologous human genes, of which one had previously been proposed as a therapeutic "target". 17-β-Hydroxysteroid dehydrogenase 10 (17HSD10, also known as ABAD, ERAB, Type II HADH, SCHAD *etc.*) is an intracellular binding partner for Amyloid β-Peptide (Aβ); Kissinger *et al.* have suggested inhibiting 17HSD10 as a new approach to treatment of Alzheimer's Disease. Additionally, 17HSD10's function in dihydrotestosterone synthesis led some authors to propose it as a prostate cancer target. The enzyme is highly expressed in prostate cancer bone metastases, as compared with non-malignant and primary tumor tissues. Recently, it has become apparent that 17HSD10 is overexpressed in many cancerous cells, particularly those of adenocarcinoma types, with the enzyme's multifunctional nature contributing more broadly to the stabilisation of cancer cells.

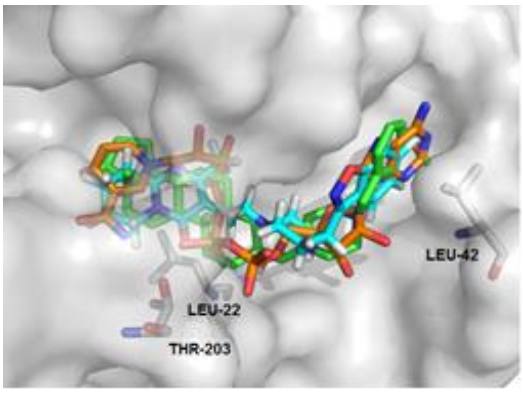

Figure 1: Predicted binding of risperidone 3 to 17-HSD10: overlay of risperidone (cyan), RM-532-46 (green) and NAD co-factor (orange), modelled in the active site of 17-HSD10 (PDB-ID: 1U7T).

To test whether antipsychotic drugs such as chlorpromazine would interact with normally expressed human 17HSD10 in vitro, we studied their effects on the recombinant 17HSD10 catalyzed oxidation reaction of estradiol and corresponding reduction of (acetylaceto) coenzyme A. As well as chlorpromazine **1**, we investigated two further antipsychotic drugs, clozapine **2** and risperidone **3**. Chlorpromazine was shown to have virtually no effect on the 17HSD10-catalyzed dehydrogenation of estradiol. The other drugs tested showed higher levels of inhibition. To better understand why risperidone was the best inhibitor of 17HSD10 we undertook a computational study. This is a similar mode of binding to that predicted and observed for RM-532-46 6 (Fig. 1).

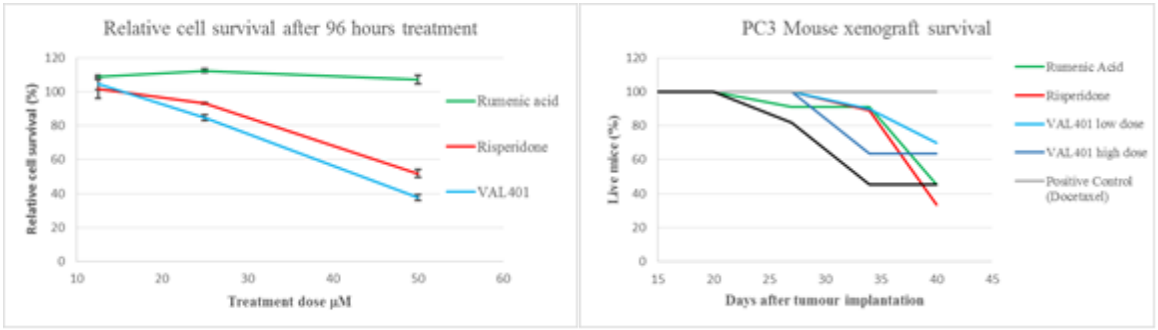

Figure 2: Effects of risperidone, rumenic acid and the VAL 401 formulation on prostate cancer cells and xenografts: (a) survival of PC3 prostate cancer cells at varying dose after 96 hours continuous treatment; and (b) survival of mice with PC3 orthotopic prostate cancer xenografts after daily oral treatment.

Given the literature observations on the importance of 17HSD10 expression in both Alzheimer's disease and in prostate cancer, we designed VAL401, a formulation of risperidone in rumenic acid. *In vitro* and *in vivo* assays were promising (Fig. 2). Subsequent commerical development of VAL401 led to a small scale Phase 2B clinical trial in patients with late stage non-small cell lung cancer, where improvements both in overall survival and in quality of life were observed.

Publications

Dilly S.J., Clark A,J., Marsh A., Mitchell D.A., Cain R., Fishwick C.W.G., Taylor P.C. (2017) A chemical genomics approach to drug reprofiling in oncology: Antipsychotic drug risperidone as a potential adenocarcinoma treatment. *Cancer Letters*, **393**:16-21.

Funding

This work was funded by the BBSRC, EPSRC, the RSE, the SEEK Group & ValiRx plc.

Collaborators

University of Leeds: R. Cain
External: S.J. Dilly (ValiRx plc), A.J. Clark, A. Marsh, D.A. Mitchell (Univ. of Warwick).

Titin control of exact myosin filament length in muscle

Larissa Tskhovrebova, Charlotte Scarff, Mehrnaz Montazeri and John Trinick

Introduction

The fundamental contractile unit of muscle is the sarcomere. This consists of two types of filament, thick and thin, which interdigitate and slide over each other to cause contraction. The thick and thin filaments are composed mainly of myosin and actin, respectively. Thick filaments are anchored in register by the M-line and the edges of the A-band mark their ends. The sharpness of the A-band edges indicate that thick filaments all have exactly the same length; they are therefore all likely to contain exactly the same number of myosin molecules. This number is thought to be 294, since 49 registers of myosin can be counted, each with 3 molecules and the filament is bipolar; thus 2 x 3 x 49 = 294. Thin filaments are anchored in the Z-line and extend across the I-band into the A-band.

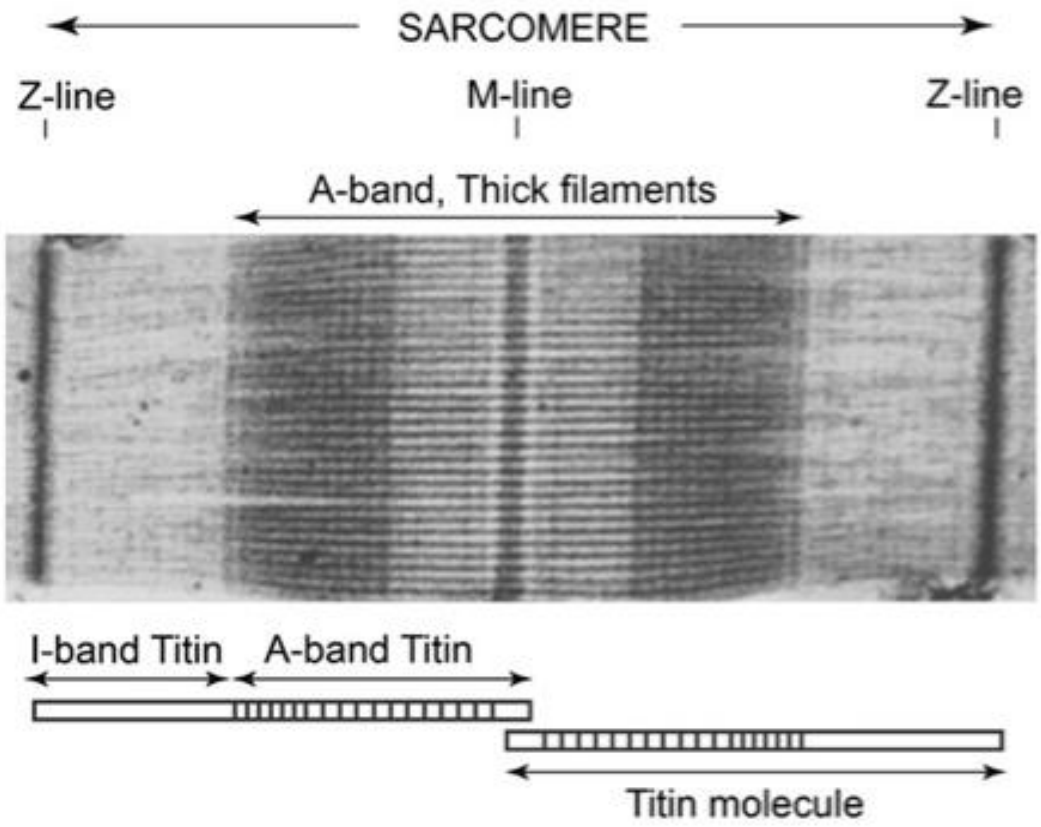

Figure 1: Electron micrograph of muscle sarcomere. The extent of the titin molecule is shown to the same scale.

How thick filaments are controlled to have exactly 294 myosins has been a long standing puzzle, since the filament is many times longer than the myosin molecule. Several mechanisms were proposed but none was proven. One model put proposed by the Trinick group involves titin, which is the largest known protein (polypeptide ~3.5 MDa) and the third most abundant muscle protein after myosin and actin. Titin is a long molecule, ~1 micron, and spans from the Z- to M-line in the sarcomere. Using monoclonal antibody labelling we showed that in the A-band titin is likely to be associated with the thick filament, attached to its surface and probably bound to myosin. This led to our proposal that titin could determine the length of the myosin filament, by acting as a template or 'protein-ruler'. We published this hypothesis in 1989 and it currently has ~200 citations.

Results

In 2015 workers at the University of Arizona in Tucson led by H Granzier attemped to use a modified mouse model to test the ruler hypothesis. They did this by deleting a part of titin ~30 nm long and spanning the edge of the A-band. No change in the length of the A-band was found, which led them to conclude that the ruler model was disproved, “settling a long standing hypothesis”, which was published in PNAS. However, in a rebuttal, also published in PNAS, we challenged this claim, pointing out that myosin is a long molecule, ~156 nm, and that its main binding site for titin is in its C-terminal tail. This is distant from the end of the thick filament and therefore not covered by the region of titin deleted in the mouse model. We therefore argued that a rigorous test of the ruler model had not been done. Contrary to their previous conclusions, in autumn 2017 the Granzier group published in Nature Communications work that deleted ~86 nm of the titin molecule from approximately halfway between the M-line and the edge of the A-band. This resulted in shortening of the A-band by approximately the deleted distance, providing support for the ruler model. The title of their paper is, “The giant protein titin regulates the length of the striated muscle thick filament”. Analogous to the titin ruler model, we also proposed that another giant protein, nebulin ~1 MDa, specifies exact actin filament length.

Publications

Tskhovrebova L and Trinick J. (2017) Titin and nebulin in thick and thin filament length regulation. *Sub-Cellular Biochemistry* **82**:285-318.

Funding

Supported by the British Heart Foundation and the Leverhulme Trust.

Collaborators

External: D. Winkelmann (Rutgers University).

Protein translocation dynamics revealed by single molecule fluorescence

Tomas Fessl, Peter Oatley, Jim Horne, Steve Baldwin, Sheena Radford and Roman Tuma

Introduction

Protein translocation across cell membranes is a ubiquitous process required for protein secretion and membrane protein insertion. This is mediated, for the majority of proteins, by the highly conserved Sec machinery. The bacterial translocon – $SecY_{MK}EG$ – resides in the plasma membrane, where translocation is driven through rounds of ATP hydrolysis by the cytoplasmic SecA ATPase, and the proton motive force (PMF). The protein channel is formed through the centre of SecY, between two pseudo-symmetrical halves, each containing five transmembrane helices, which separate and let the polypeptide pass across the membrane during secretion. At rest, the channel is kept closed by a short, helical plug and a ring of six hydrophobic residues. Activation is achieved by the ribosome nascent chain complex or by the association of the pre-protein, signal sequence (SS) within the pre-protein, and the translocating ATPase SecA. Several conformational changes accompany the activation and subsequent translocation, however, the order of events, energy requirements and kinetics of these steps have yet to be convoluted.

Results

We employ single molecule Förster resonance energy transfer (FRET) analyses to dissect the mechanism of protein translocation in unprecedented detail. This approach, which utilises an array of single molecule FRET experiments sensitive to different timescales (Figure 1), allowed us to delineate several stages of translocation: (1) SS-dependent but ATP-independent unlocking of the translocon; (2) ATP-dependent plug opening; (3) a pre-processive translocation stage; (4) ATP-dependent processive translocation and (5) ATP-independent, fast channel closing. This has enabled us to estimate an intrinsic, processive translocation rate of ~40 amino acids per second. The broad distribution of translocation rates is consistent with the stochastic Brownian ratchet model (Figure 2).

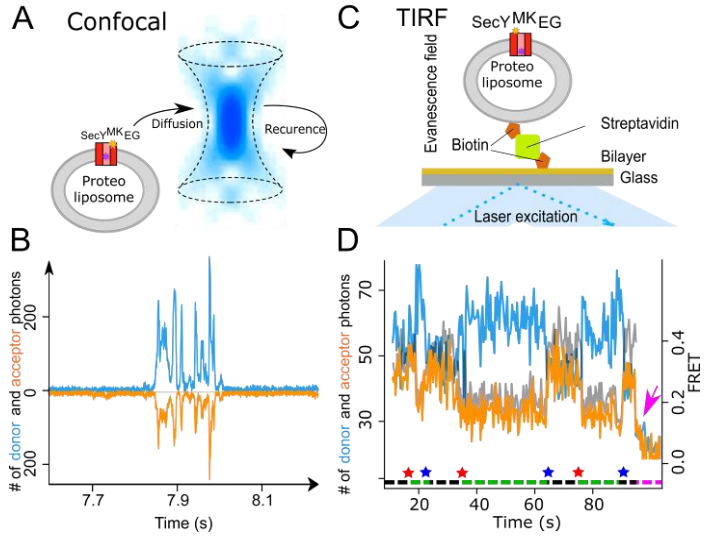

Figure 1: Monitoring plug opening by single molecule FRET. (A) Schematic depiction of confocal detection of freely diffusing proteoliposomes containing SecYMKEG (red) embedded in the bilayer (grey) with a recurrence path (arrow). (B) Fluorescence busts (blue-donor, orange - acceptor) resulting from confocal detection with recurrence enabling millisecond dynamics to be probed. (C) Schematic depiction of proteoliposome immobilized via a biotinylated lipid to a streptavidin (green) coated cover slip for total internal reflection fluorescence (TIRF). (D) TIRF fluorescence trace for translocation of 100 aa substrate, enabling direct observation of dwell times on seconds time scale.

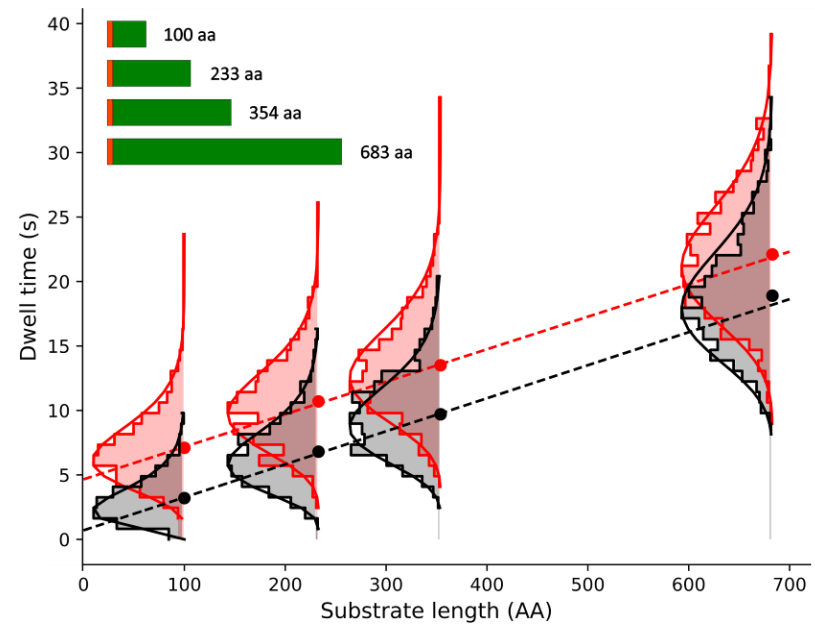

Figure 2: Dependence of open state (E_{FRET}~0.2) dwell times on the length of pOA constructs (inset, N-terminal SS depicted as orange bar). Ordinary least squares (OLS) linear regression (dashed lines) on all photobleaching corrected dwell times gave slopes corresponding to translocation rates of 39.6±6.0 aa/s (± standard error) in the absence of SecB (red) and 39.0±6.2 aa/s in the presence of SecB (black). Overlaid are dwell time histograms with gamma function fits (solid lines).

The results allow us unparalleled access to the kinetics of the complex reaction and provide a framework for understanding the molecular mechanism of protein secretion.

Funding
This work was funded by the BBSRC.

Collaborators
External: Daniel Watkins, William J. Allen, Robin A. Corey, Ian Collinson (University of Bristol).

The role of structured RNA in early virus replication events

Andrew Tuplin

Overview

Inhibition of HCV translation by disrupting the structure and interactions of the viral CRE and 3' X-tail.

A phylogenetically conserved RNA structure within the NS5B coding region of hepatitis C virus functions as a cis-replicating element (CRE). Integrity of this CRE, designated SL9266, is critical for genome replication. SL9266 forms the core of an extended pseudoknot, designated SL9266/PK, involving long distance RNA-RNA interactions between unpaired loops of SL9266 and distal regions of the genome. Previous studies demonstrated that SL9266/PK is dynamic, with 'open' and 'closed' conformations predicted to have distinct functions during virus replication. Using a combination of site-directed mutagenesis and locked nucleic acids (LNA) complementary to defined domains of SL9266 and its interacting regions, we have explored the influence of this structure on genome translation and replication. We demonstrate that LNAs which block formation of the closed conformation inhibit genome translation. Inhibition was at least partly independent of the initiation mechanism, whether driven by homologous or heterologous internal ribosome entry sites or from a capped message. Provision of SL9266/PK in trans relieved translational inhibition, and mutational analysis implied a mechanism in which the closed conformation recruits a cellular factor that would otherwise suppress translation. We propose that SL9266/PK functions as a temporal switch, modulating the mutually incompatible processes of translation and replication (Figure 1).

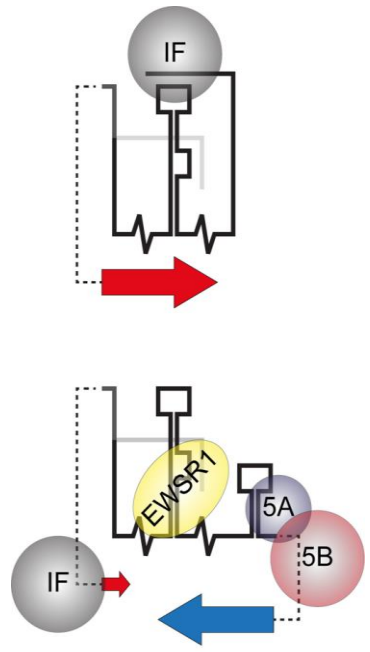

Figure 1: A cartoon interpretation of SL9266/PK conformational rearrangement as part of a translation/replication switch; illustrating the mechanism and role of negative feedback interactions in the proposed model. The upper cartoon illustrates up-regulation of HCV IRES initiated translation (large red arrow) due to the SL9266/PK closed conformation sequestering a cellular IRES inhibition factor (IF). The lower cartoon illustrates the open conformation, initiated by virally encoded non-structural proteins (5A and 5B) binding the 3'NCR and blocking 'kissing loop' formation. The open structure favours interaction between cellular protein EWSR1 and SL9266, up-regulating RNA replication (large blue arrow). As demonstrated in the current study the resulting open conformation actively inhibits HCV translation (small red arrow), which we speculate is due to EWRS1 displacing - and thus making available - translation inhibition factor IF.

Funding

MRC New Investigator Research Grant. Principle Investigator. *Mechanistic analysis of RNA-replication elements involved in early stages of chikungunya virus replication:* £635,212 FEC

Collaborators

University of Leeds: Prof. M. Harris, Dr. A. Zhuravleva, Prof Nic Stonehouse and Dr J. Mankouri

External: Dr. Alain Kohl (MRC Centre for Virus Research, UK), Dr Andrew Davidson (University of Bristol, UK) and Prof Andres Merits (University of Tartu, Estonia).

Multivalent protein-carbohydrate interactions

Clare Mahon, Martin Fascione, Chadamas Sakonsinsiri, Emma Poole
Yuan Guo, Dejian Zhou and Bruce Turnbull

Introduction

Protein-carbohydrate interactions at cell surfaces mediate many important processes in biology from fertilisation to adhesion of viruses, bacteria and their toxins. Individually, protein-sugar interactions are usually very weak, but both affinity and binding selectivity can be enhanced through a phenomenon called multivalency: multiple binding sites on the protein interact simultaneously with multiple copies of the sugar ligand to achieve a high avidity and enhance binding selectivity. The multivalency phenomenon can be reproduced using synthetic molecules that incorporate multiple copies of the carbohydrate ligands.

Some of our recently published research includes developing fluorescent probes based on glycosylated quantum dots for use in understanding the structures of multivalent complexes. Using such tools we have been able to probe the differences in binding selectivity for two very closely related human cell surface lectins (DC-SIGN and DC-SIGNR) which mediate virus invasion. We have been able to show that the different presentation of the binding sites determines whether or not the proteins can form stable interactions with virus-sized glycosylated quantum dots.

We have also developed methods to exploit multivalent protein-carbohydrate interactions for applications in materials science. We have found that single chain polymer nanoparticles bearing many pendant carbohydrate groups can be used to create stable polymer films on functionalised surfaces (Figure 1). The polymer nanoparticles contain hydrazone linkages that can be reversibly formed and broken under mild conditions. We have found that they can reorganise to form extended cross-linked films in a process that is dependent on formation of specific protein-carbohydrate interactions. These methods could be exploited in industrial biotechnology to “shrink-wrap” bacteria for immobilisation in bioreactors or to stabilise virus-based vaccines to give them longer shelf-lives without need for refrigeration process that increase the cost of biopharmaceuticals.

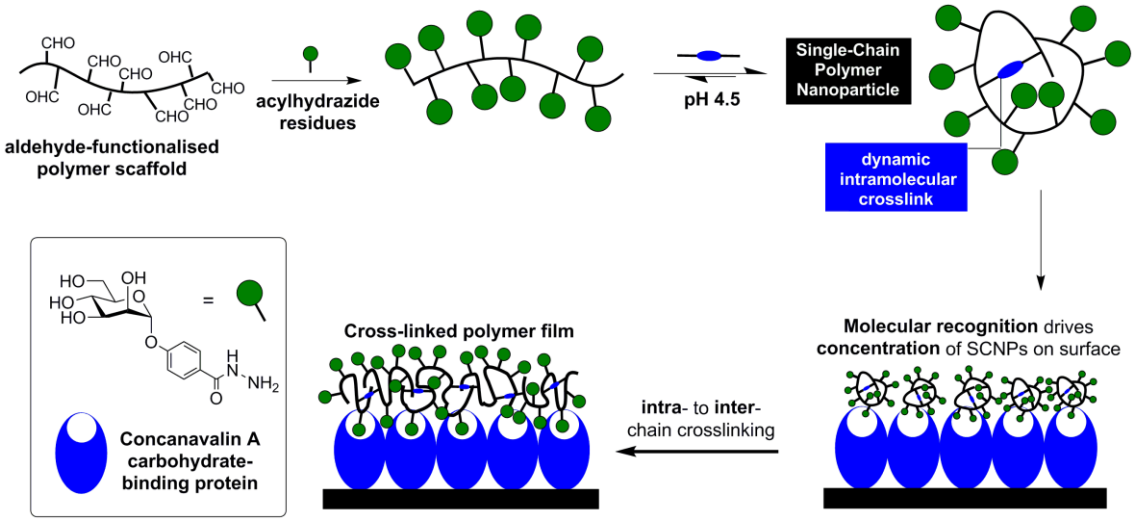

Figure 1: Derivatisation of aldehyde-functionalised polymer backbone with mannosyl sugar (green circle) hydrazides for formation of cross-linked polymer films on lectin-functionalised surfaces. Figure is adapted from Mahon *et al.,* (2017) *Angew. Chem. Int. Ed.* **42**, 13093-13098.

Publications

Guo Y., Nehlmeier I., Poole E., Sakonsinsiri C., Hondow N., Brown A., Li Q., Li S., Whitworth J., Li Z., Anchi Y., Brydson R., Turnbull W. B., Pöhlmann S., Zhou D. (2017) Dissecting multivalent lectin-carbohydrate recognition using polyvalent multifunctional glycan-quantum dots. *J. Am. Chem. Soc* **139**:11833-11844.

Mahon C.S., McGurk C.J., Watson S.M.D., Fascione M.A., Sakonsinsiri C., Turnbull W.B., Fulton D.A. (2017) Molecular-recognition mediated transformation of single-chain polymer nanoparticles into crosslinked polymer films. *Angew Chem Int Ed Engl* **56**:12913-12918

Funding

This work was funded by the EPSRC, BBSRC and Wellcome Trust.

Collaborators

External: D. Fulton (Newcastle University), S. Pöhlmann (German Primate Centre, Gottingen)

Protein-surface recognition using designed molecules

Hester Beard, Emma Cawood, Som Dutt, Zsofia Hegedus, Katherine Horner, Fruzsina Hobor, Thomas James, Kris Parashiv, Philip Rowell, Emma Stirk, Sonja Srdanovic, Thomas Edwards, Arnout Kalverda, Lars Kuhn, Adam Nelson, Darren Tomlinson, Stuart Warriner and Andrew Wilson

Introduction

This Report summarises our ongoing efforts to develop ligands that recognise protein surface (PPIs).

Highly functionalized ruthenium (II) *tris*-chelates

We used ruthenium (II) *tris*-chelates to project recognition groups over a large surface area to make multivalent contacts with protein-surfaces. For cytochrome c binding was electrostatically driven, with enhanced affinity achieved through enthalpic contributions thought to arise from the ability of the surface mimetics to make a greater number of noncovalent interactions with surface exposed basic residues than natural proteins. We also employed these reagents to develop array-based sensors for proteins.

Reversibly constrained peptides

The development of constrained peptides to fulfill a functional role is an emerging strategy in chemical biology. We developed a versatile, rapid and reversible approach to constrain peptides in a bioactive helical conformation using BID and RNase S peptides as models. This new "true stapling" methodology provides ready access to stabilized α-helical peptides with enhanced biophysical properties. The introduced constraint may be further functionalized to facilitate biophysical and cellular analyses. Peptides bearing Cys or *h*Cys amino acids in i → i + 4 positions could be cross-linked with dibromomaleimide to generate cyclic peptides with rapid and complete conversion and then fully regenerated by addition of an excess of thiol.

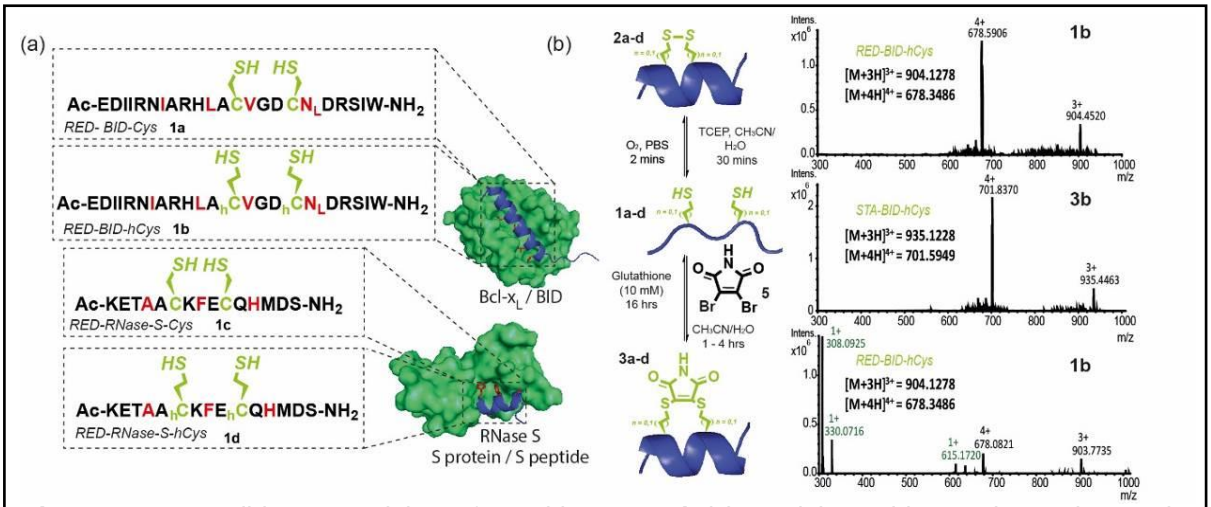

Figure 1: Reversible constraining of peptides **1-3a-d** (a) model peptides and protein-protein interactions used in this research (Bcl-x_L (green) / BID (blue) PDB ID: 4QVE; RNase S Protein (green) / S-Peptide (blue) PDB ID: 1CJQ; hotspot residues (red)); (b) conditions for conversion from the oxidised state (OX) through the intermediate reduced state (RED) to the constrained peptide (STA) and vice-versa (LHS); HRMS analyses of reaction mixture for reversible interconversion between **1b** and **3b** (RHS).

Identification of α-helix mimetic binding proteins

Considerable progress has been made in the "bottom-up" design of tertiary foldamers (i.e. non-natural protein like structures with function). A related approach would be to exploit the potential of combinatorial biology to identify natural biomacromolecule sequences that recognise synthetic foldamers. In identifying compatible natural and non-natural components

driven by complementary molecular recognition, such an approach could be used to identify potential biological targets of a given foldamer. Our group recently developed a series of proteomimetic aromatic oligoamide foldamers designed to mimic the α-helix: Proteomimetics are scaffolds that replicate the spatial and angular projection of essential recognition groups that represent 'hot-spot' residues at a PPI interfaces. Using the non-antibody-based Affimer scaffold in tandem with phage display screening and trimeric *N*-alkylated aromatic oligoamide foldamers, we identified selective peptide-foldamer interactions

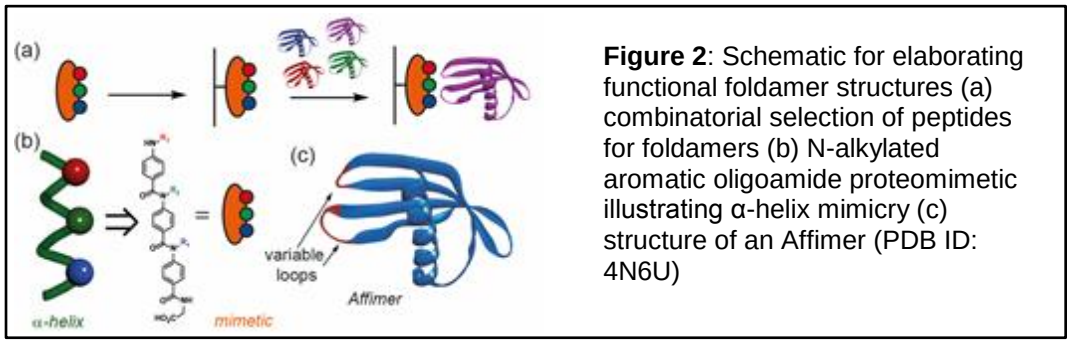

Figure 2: Schematic for elaborating functional foldamer structures (a) combinatorial selection of peptides for foldamers (b) N-alkylated aromatic oligoamide proteomimetic illustrating α-helix mimicry (c) structure of an Affimer (PDB ID: 4N6U)

Publications

Hewitt S.H. & Wilson A.J. (2017) Protein Sensing and Discrimination Using High Functionalised Ruthenium (II) tris(Bipyridyl) Protein Surface Mimetics in an Array Format. *Chem. Commun* **53**:12278-12281.

Grison C.M., Burslem G.M., Miles J.A ., Pilsl L.K.A., Yeo D.J., Imani Z., Warriner S.L., Webb M.E. & Wilson A.J. (2017) Double Quick, Double Click Reversible Peptide "Stapling". *Chem. Sci* **8**:5166-5171.

Burslem G.M., Kyle H.F., Nelson A., Edwards T.A. & Wilson A.J. (2017) Hypoxia inducible factor (HIF) as a model for studying inhibition of protein–protein interactions. *Chem. Sci* **8**: 4188-4202.

Arrata I., Barnard A., Tomlinson D.C., & Wilson A. J. (2017) Interfacing Native and Non Native Peptides: Using Affimers to Recognise α-Helix Mimicking Foldamers, *Chem. Commun* **53**:2834-2837.

Hewitt S.H., Filby M.H., Hayes E., Kuhn L.T., Kalverda A.P., Webb M.E. & A.J. Wilson (2017) Protein surface mimetics: understanding how ruthenium tris(bipyridines) interact with proteins. *ChemBioChem* **18**:223-231.

Funding

We acknowledge The University of Leeds, EPSRC, ERC, EU-H2020 and The Leverhulme Trust for financial support of this research.

Collaborators

External: Dek Woolfson, Richard Sessions and Gail Bartlett (University of Bristol), Christian Ottmann (Eindhoven)

Chemical probes reveal the mechanism of an inter-kingdom signal

Megan Wright

Introduction

Human and bacterial cells co-exist in a complex web of symbiotic and pathogenic relationships. Cell behaviour in multi-cellular and multi-organism communities is governed in large part by the secretion of signals and their detection by sensor or receptor proteins. In recent years, intriguing evidence has accumulated to suggest that bacteria specifically recognise host signalling molecules, such as neuroendocrine hormones and immune system signals. However, for the most part receptors remain unidentified and the molecular mechanisms of signal transduction have yet to be elucidated.

The dynorphins are important human opioid peptide hormones with many physiological roles, including the mediation of stress and pain responses. Previous research has shown that under conditions of host stress, levels of the human opioid hormone dynorphin are elevated, triggering virulence in the opportunistic pathogen *P. aeruginosa*. We hypothesised that dynorphin was being sensed by the bacterium, perhaps via interaction with a protein receptor. In this project we aimed to apply unbiased chemical biology approaches to define the mechanism of action of this putative interkingdom signal.

Results

We first explored the importance of peptide charge and sequence: only the canonical Dynorphin-A and a truncated peptide (DYN) were able to induce *P. aeruginosa* (*Pa*) production of the virulent pigment pyocyanin, confirming that recognition was sequence-dependent. We next developed novel chemical probes to identify binding partners of the peptide in live cells. Probes were equipped with three widely used photocrosslinking groups (benzophenone, aryl azide or diazirine) to maximize the chances of trapping specific interactions between the peptide and binding partners upon UV-irradiation of cells. Probes were also functionalised with a bio-orthogonal (alkyne) tag for downstream analysis. The tag is small and inert in biological systems, but can subsequently be detected by attachment of fluorophores or affinity labels via click chemistry (Figure 1).

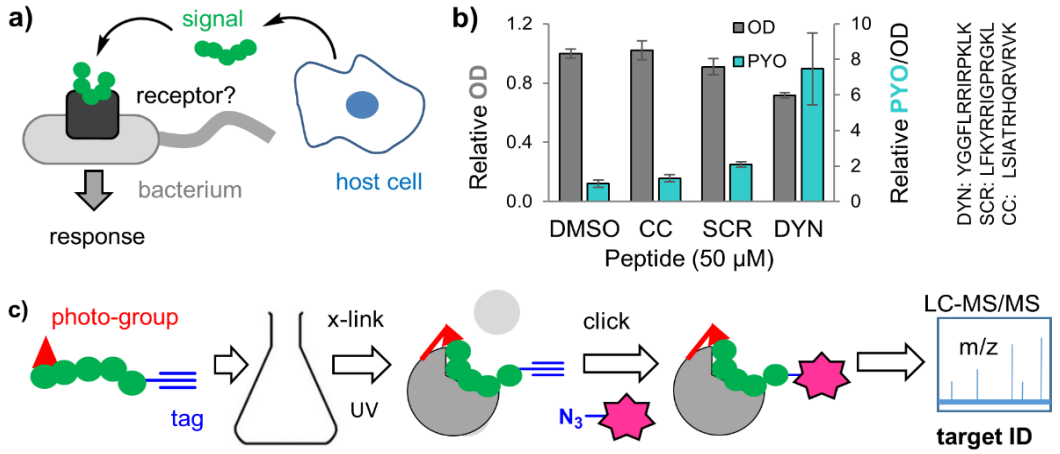

Figure 1: (A) Dynorphin is a human peptide hormone released by host cells during stress. It triggers a virulence response in *Pa* via an unknown pathway. (B) Peptide sequence-specific induction of virulence in *Pa*; PYO = pyocyanin. (C) Photoaffinity-click workflow to identify binding partners of peptide-inspired probes.

Following incubation of cells with the probes and click ligation of a fluorophore, gel-based analysis (Figure 2) revealed binding of the peptides to the bacterial lipopolysaccharide (LPS). We also observed mild probe toxicity towards *P. aeruginosa*. Together these observations are

consistent with perturbation of bacterial membranes by high concentrations of these cationic peptides, but did not explain the sequence-dependent induction of virulence. We therefore attached biotin via click chemistry, enriched binders and identified them via LC-MS/MS. Interestingly, while benzophenone and aryl azide probes failed to reveal selective labelling, proteome profiling with a diazirine-equipped probe showed binding to ParS, the sensor protein of the ParR/S two component system.

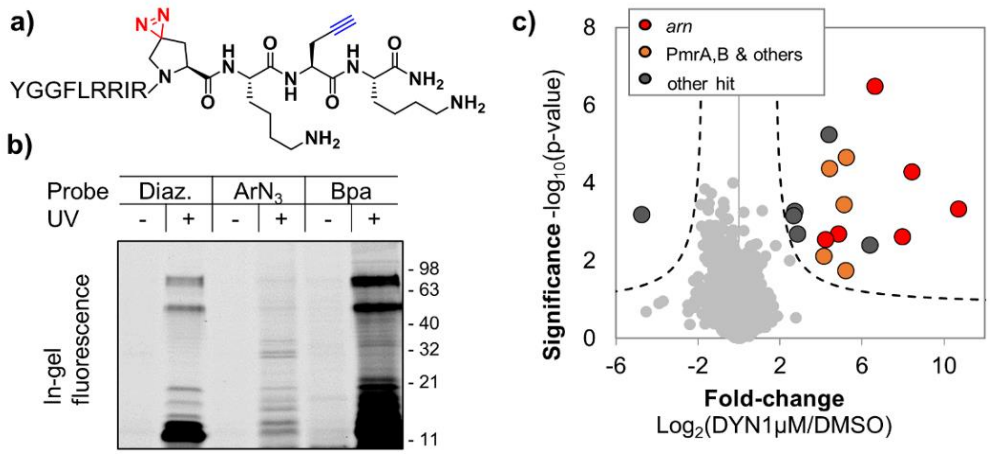

Figure 2: (A) Diazirine probe. (B) In-gel fluorescence analysis of the binding of different probes (Diaz. = diazirine; ArN_3 = aryl azide; Bpa = benzophenone) to *Pa* biomolecules. (C) Global proteome analysis of *Pa* treated with DYN; label-free quantification reveals specific upregulation of proteins involved in an antimicrobial peptide-like response.

To further explore the phenotype of dynorphin treatment, we performed full proteome analyses of treated bacteria, revealing a striking and specific upregulation of pathways involved in defence against antimicrobial (cationic) peptides. Importantly, a *parS* mutant showed no such response and was significantly more susceptible to peptide-induced toxicity, functionally linking the ParS-dynorphin interaction with this phenotype.

In summary, we used a chemical proteomic approach to show that binding of a human opioid to the bacterial sensor protein ParS triggers a bacterial defence response. Our data suggest that dynorphin may function as a reporter reflecting the onset of human defence mechanisms, including the secretion of antimicrobial peptides. This work also demonstrates the power of an unbiased chemical approach for unravelling the complex mode of action of a molecule in live cells. Current work focuses on further developing the chemical proteomic methodology to pinpoint probe binding sites in live cells, and on the biochemical basis of the DYN-ParS interaction. More broadly, we aim to apply interdisciplinary approaches to understand the mechanistic basis of host-microbe communication.

Publications

Wright M.H., Fetzer C.F., & Sieber S.A. (2017) Chemical Probes Unravel an Antimicrobial Defense Response Triggered by Binding of the Human Opioid Dynorphin to a Bacterial Sensor Kinase. *J. Am. Chem. Soc* **139**:6152-6159.

Funding

I thank the European Commission for a Marie Curie Fellowship (TU Munich) and the University of Leeds for start-up funding.

Collaborators

External: C. Fetzer and S. A. Sieber (TU Munich).

Assembly, activation and function of BRCC36 deubiquitylating complexes

Miriam Walden, Safi Kani Masandi, Upasana Sykora and Elton Zeqiraj

Introduction

Ubiquitylation of proteins serves as a post-translational signal to regulate virtually all cellular processes through the precise spatial and temporal control of protein stability, activity and/or localisation. Enzymes involved in the ubiquitin system are frequently dysregulated in cancer, neurodegeneration, autoimmunity and other human diseases. Ubiquitylation is a versatile post-translational modification aptly suited for a cellular communication system similar to other post-translational modifications (e.g. phosphorylation).

Ubiquitin (Ub) processing enzymes (E1, E2 and E3) write the Ub signalling code by adding Ub to substrates. A single Ub can be conjugated to lysine residues on the surface of substrate proteins (known as mono-ubiquitylation), or conjugated further to lysine residues on the surface of Ub itself, leading to poly-Ub chains with different topologies and unique signalling properties. Ub and poly-Ub chains can be "read out" by ubiquitin binding domains (UBDs), which allow signal decoding and transmission. Ubiquitylation is a reversible process and Ub is removed by deubiquitylating (DUB) enzymes. DUB actions produce monomeric Ub, recycle Ub from chains and reverse signalling events resulting from ubiquitylation.

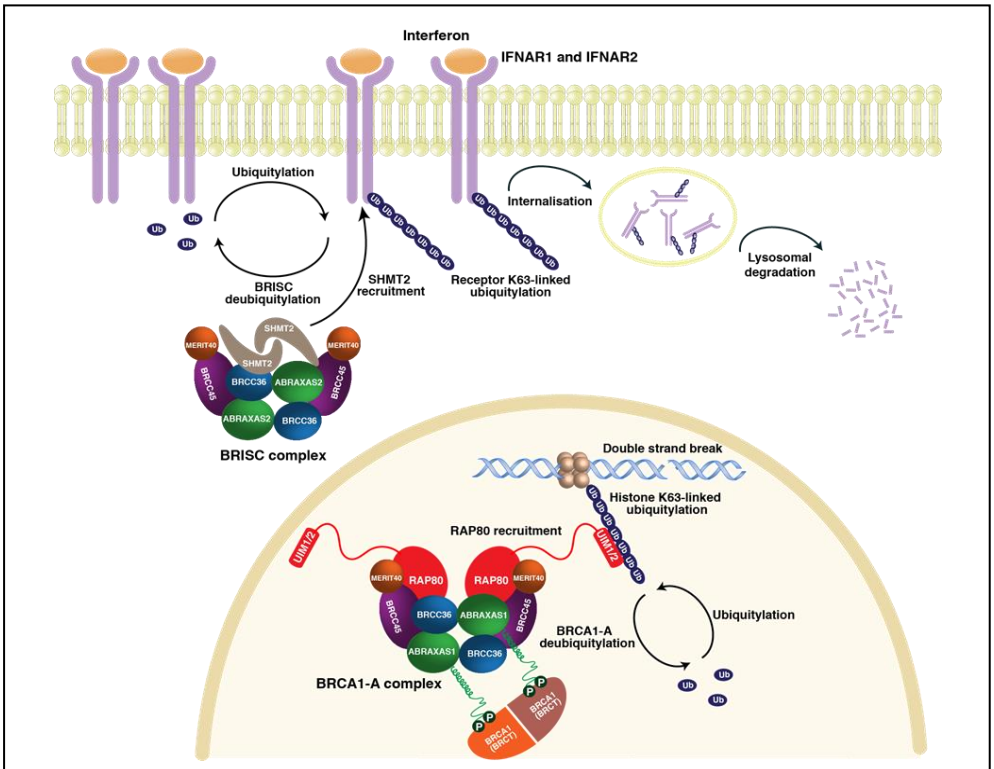

Figure 1: BRCC36 functions in two protein complexes. Illustration of the BRCC36 deubiquitylase (DUB) functions. Cytoplasmic BRCC36 regulates interferon receptor signalling as part of the BRISC complex. Nuclear BRCC36 takes part in DNA damage repair as the active DUB in the BRCA1-A complex. Pseudo-DUBs ABRAXAS1 and ABRAXAS2 are the main determinants for BRCC36 complex formation and subcellular localisation.

The active DUB BRCC36 is found in two macromolecular complexes (**Fig. 1**), depending on which inactive MPN⁻ pseudo-DUB it interacts with (ABRAXAS1 or ABRAXAS2). The BRCC36-ABRAXAS1 complex translocates to the nucleus and is part of a larger DUB complex called the BRCA1-A complex. This complex localises to sites of DNA damage (e.g. a double strand break) through RAP80 anchoring to K63-linked poly-Ub chains (**Fig. 1**). The BRCA1-A

complex plays at least two roles in DNA damage repair: (1) binding and cleaving K63-linked poly-Ub chains and (2) recruitment of BRCA1 to sites of DNA damage. In the cytoplasm, BRCC36 interacts with ABRAXAS2 and is part of a larger complex called BRISC-SHMT2 (**Fig. 1**). This cytoplasmic DUB complex interacts with and deubiquitylates interferon receptors 1 and 2 (IFANR1/2) and prevents the receptors from being prematurely endocytosed and entering the lysosomal degradation pathway. Thus, the BRISC-SHMT2 complex regulates interferon-dependent immune response by stabilising the interferon receptors and ensuring their availability at the membrane. BRISC deficiency in mice due to genetic deletion of the BRISC specific pseudo-DUB ABRAXAS2 resulted in resistance to bacterial lipopolysaccharide. Interestingly, the mice did not display any adverse phenotypes or deficiency in the DNA damage response, raising the possibility that BRISC inhibitors may have clinical utility against diseases stemming from elevated inflammatory cytokine signals.

Results

BRCC36 resides in the BRISC-SHMT2 and BRCA1-A complexes and regulates different aspects of cell biology **(Fig. 1)**. How do the different subunit compositions affect BRCC36 catalytic function, substrate recognition and regulation? How is each holoenzyme structurally organized? Is it possible to develop tool compounds that discriminate between complexes to selectively influence different arms of BRCC36 biology?

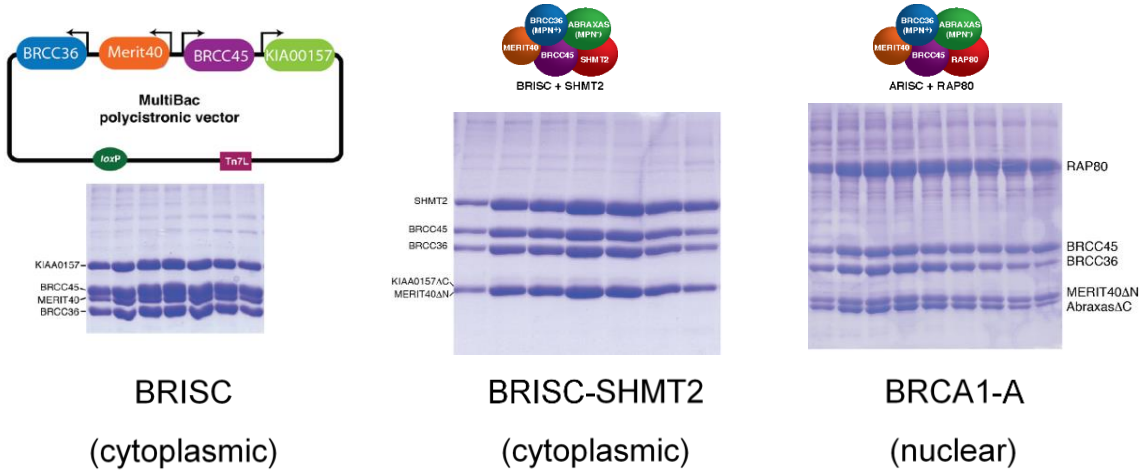

Figure 2: Large scale production of BRCC36-containing DUB complexes. Schematic of a polycistronic vector for co-expression of the BRISC complex in insect cells and a Coomassie-stained gel of a co-purified BRISC complex (left panel). Coomassie-stained gels of the indicated 5-subunit complexes (middle and right panels).

To probe these questions at a biochemical and structural level, we have developed preparative expression systems for each multi-protein complex using the MultiBac insect cell/baculovirus system (**Fig. 2**). We are currently performing cryo-EM studies of these preparations to better understand complex assembly and BRCC36 mechanism of action.

Funding

This work was funded by the Wellcome Trust and the Royal Society.

Collaborators

University of Leeds: Emma Hesketh, Neil Ranson, James Ault, Franc Sobott and Iain Mansfield.
External: Roger Greenberg (Unviversity of Pennsylvania).

Dissecting multivalent lectin–glycan recognition using polyvalent glycan-quantum dots based multimodal readout strategy

Yuan Guo, Emma Poole, Chadamas Sakonsinsiri, W. Bruce Turnbull and Dejian Zhou

Introduction

Multivalent lectin-glycan interactions initiate the first contact between pathogens and target cells that ultimately lead to infection. While monovalent lectin-glycan interactions are typically weak and biologically inactive, by displaying arrays of glycans on their surface, pathogens can bind to cell surface multimeric lectins multivalently to enhance affinity and gain cell entry. Glycoconjugates can block such interaction and prevent infection, whose inhibition potency depends critically on matching the spatial/orientation of multivalent binding partners. However, a lack of structural information has largely hampered the research progress, due to challenges in solving the structure of such flexible, complex and multimeric lectins. We have found that fluorescent quantum dot displayed with a dense array of mannose containing ligand (QD-Man) are powerful probes for multivalent lectin-glycan interactions. Using a sensitive FRET readout, we have revealed that QD-Man only binds to the dendritic cell receptor, DC-SIGN, but not to its close relative, DC-SIGNR, despite they have almost identical monovalent binding motif and tetrameric architecture. We have proposed that the different orientation of their sugar-binding-domains (CRDs) is responsible for such difference: the CRDs all face upwardly in DC-SIGN and so readily form strong multivalent binding, but point sideways in DC-SIGNR, making them unable to bind multivalently to one QD. However, QD-Man failed to distinguish between DC-SIGNR and monovalent CRD binding, hence the exact binding modes for DC-SIGN/R remained unclear.

Results

We hypothesised that QDs displayed with arrays of higher affinity sugars (e.g. man-α-1,2-man, QD-DiMan) may allow us to dissect DC-SIGN/R-glycan multivalent binding by exploiting the QD's all unique properties. The QD's strong fluorescence can be harnessed for binding affinity quantification *via* FRET; its high contrast in TEM imaging can be used to directly study binding induced particle arrangement, thereby probing the exact binding mode, and its nanoscale size can be exploited to probe binding modes by monitoring binding induced

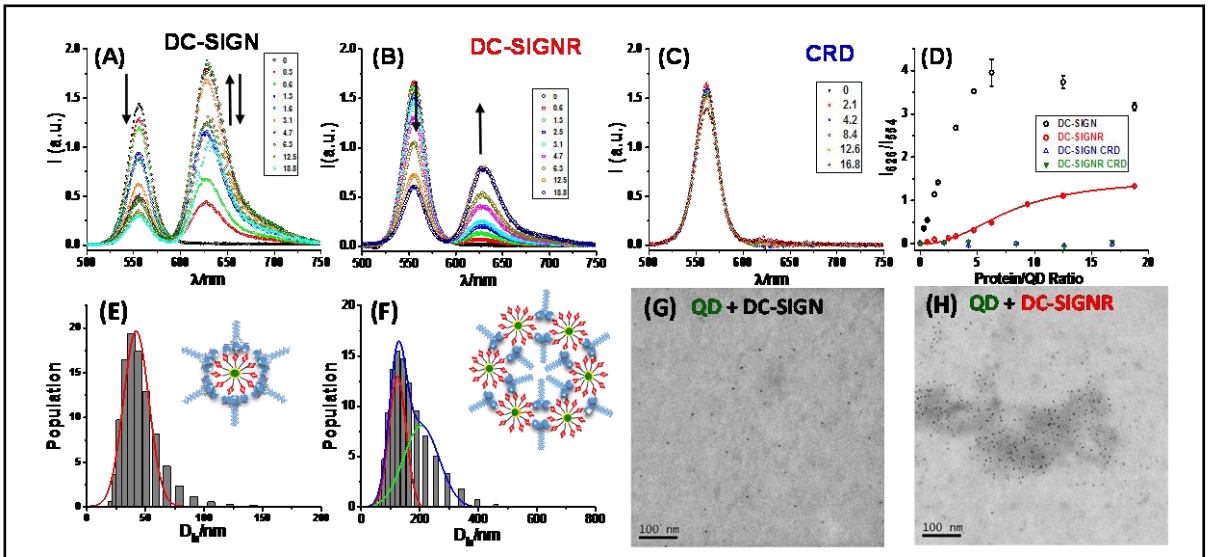

Figure 1: Fluorescence spectra of QD-DiMan (20 nM) after binding to different molar equivalent of Atto-594 labelled DC-SIGN (A), DC-SIGNR (B) and CRD (C), and the apparent FRET ratio *v.s.* protein:QD molar ratio relationship (D). Hydrodynamic size (D_h) histogram of QD-DiMan after binding to 12 molar equivalents of DC-SIGN (E) or DC-SIGNR (F) and the resulting TEM images of cryo-prepared QD-DiMan samples after binding to DC-SIGN (G) and DC-SIGNR (H). The schematic QD-DC-SIGN/R binding modes are given in (E) and (F) insets.

hydrodynamic size (D_h) changes. We prepared QDs densely capped with dihydrolipoic acid-oligo(ethylene glycol)-DiMan based ligands (denoted as QD-DiMan) and compared its DC-SIGN/R binding properties with QD-Man. Binding of DC-SIGN (dye-labelled) to QD-DiMan resulted in significantly quenched QD fluorescence and greatly enhanced dye FRET signal (Fig. 1A). Binding of DC-SIGNR yielded a weaker, but clearly detectable FRET signal which was stronger than that of monovalent CRD binding and non-specific adsorption background (Fig. 1B & 1C). The results were very different from those of QD-Man, where DC-SIGNR and CRD binding signals were equally weak and comparable to background. The differences were clearer from the apparent FRET ratio *vs.* protein:QD ratio plot (Fig. 1D), where the CRD binding signal was still comparable to background, but DC-SIGNR signal was signficantly higher and lay in between CRD and DC-SIGN. This result suggested that DC-SIGN should posess a higher binding multivalency to one QD than DC-SIGNR, *i.e.* DC-SIGN may bind tetravalently to one QD while DC-SIGNR may bind bis-divalently to two different QDs. By simultaneously varying the QD and protein concentrations while keeping their molar ratio fixed, and fitting the resulting FRET ratio-protein concentration relationship using the Hill's equation, we determined an apparent K_d of 0.61±0.07 and 62±8 nM for DC-SIGN and DC-SIGNR, respectively, confirming that QD-DiMan binding with DC-SIGN was >100 fold tighter than that with DC-SIGNR. Moreover, we further found that QD-DiMan pontently inhibited pseudo-Ebola infection of DC-SIGN expressing cells with a IC_{50} of 0.7±0.2 nM, matching well to its DC-SIGN binding K_d measured by FRET, suggesting that our QD-FRET K_d measurement could be used to predict the inhibition potency of glyconanoparticles against virus infections at the cellular level.

The exact binding modes of DC-SIGN/R were revealed by dynamic light scattering and TEM imaging. Binding of DC-SIGNR with QD-DiMan produced significantly larger assemblies than that of DC-SIGN, a strong indication of QD clustering *via* QD-protein inter-crosslinking (Fig. 1E & 1F). This conclusion was verified by direct S/TEM imaging of cryo-preserved QD-protein assembly samples where binding of DC-SIGN produced only isolated, individual QDs, consistent with its tetravalent binding mode with one QD. In contrast, binding of DC-SIGNR produced much larger and clustered QDs, consistent with QD-DC-SIGNR inter-crosslinking. Thus by deloping a novel multimodal readout strategy comprising of FRET, hydrodynamic size measurement and TEM imaging, we have successfully dissected the different binding modes for DC-SIGN/R.

Publications

Guo Y., Nehlmeier I., Poole E., Sakonsinsiri C., Hondow N., Brown A., Li Q., Li S., Whitworth J., Li Z., Yu A., Brydson R., Turnbull W.B., Pöhlmann S. & Zhou, D. (2017) Dissecting Multivalent Lectin–Carbohydrate Recognition Using Polyvalent Multifunctional Glycan-Quantum Dots. *J. Am. Chem. Soc* **139:**11833-11844.

Wang W., Guo Y., Tiede C., Chen S., Kopytynski M., Kong Y., Kulak A., Tomlinson D., Chen R., McPherson M. & Zhou D. (2017) Ultraefficient Cap-Exchange Protocol To Compact Biofunctional Quantum Dots for Sensitive Ratiometric Biosensing and Cell Imaging. *ACS Appl. Mater. Interfaces* **9:**15232-15244.

Funding

This work was supported by the Wellcome Trust (Grant No: 097354/Z/11/Z), BBSRC (Grant No: BB/M005666/1) and the University of Leeds.

Collaborators

University of Leeds: Dr N. Hondow and Prof. R. Brydson, School of Chemical and Process Engineering

External: Prof. S. Pöhlmann (German Primate Centre, Germany), Prof. A. Yu, Renmin (University of China, China), Prof. Z. Li and Prof. Q. Li (Peking University Health Sciences Centre, China).

Post-translational allosteric fine-tuning of the molecular chaperone BiP

Lukasz Wieteska, Samuel Dawes, Nicholas Hurst and Anastasia Zhuravleva

Introduction

The endoplasmic reticulum (ER) is an essential organelle in eukaryotic cells responsible for folding and maturation of the majority of secreted and membrane proteins. BiP, the only ER Hsp70 chaperone, binds to the majority of unfolded and misfolded proteins in this organelle to promote their folding and prevent aggregation. Similar to other Hsp70s, BiP chaperone activity relies on nucleotide- and substrate-controllable intra- and inter-domain rearrangements of its nucleotide-binding domain (NBD) and substrate-binding domain (SBD). Growing evidence has suggested that Hsp70 chaperones are extremely flexible in solution and co-exist as an ensemble of functional conformations. Redistributions in this conformational ensemble are believed to be responsible for evolutional and post-translational fine-tuning of the Hsp70 functional cycle. In this study, we deployed methyl nuclear magnetic resonance (NMR) and isothermal titration calorimetry (ITC) to characterize the allosteric cycle for the ER member of the Hsp70 family BiP and elucidate how the BiP function is regulated post-translationally.

Results

Conformational heterogeneity of the molecular chaperone BiP

To obtain molecular and thermodynamics details about the BiP conformational cycle, we used methyl nuclear magnetic resonance (NMR) and isothermal titration calorimetry (ITC). We have designed several BiP constructs and adopted the “divide-and-conquer’ strategy to dissect and characterize individual functional steps of the BiP chaperone cycle. Our results revealed several unique features of the BiP conformational landscape. We found that, similar to the bacterial Hsp70 (DnaK), the BiP can adopt several functionally and structurally distinct conformations, whilst ATP binding and hydrolysis tightly control the BiP conformational ensemble. We used methyl NMR to characterize these nucleotide-dependent conformational transitions and quantitatively monitor the population of each conformation. Our results revealed that in the presence of ADP, the NBD and SBD behave independently and the interdomain linker exposed to solvent (U, domain-undocked conformation). ATP binding triggers domain docking: The interdomain linker binds to the NBD; NBD interacts with two SBD subdomains, βSBD and αLid; whilst communication between the βSBD and αLid is mostly abolished. While this domain-docking conformation is structurally identical to one observed for DnaK; for BiP, it is only partially (ca. 50%) populated and co-exists in solution with the domain-undocked conformation (Fig. 1A).

In turn, local perturbations of the BiP SBD (either via physiologically important post-translational AMPylation of Thr518 or ‘soft’ single-site amino acid substitutions) enable allosteric fine-tuning of the BiP conformational ensemble in the presence of ATP (Fig. 1B). Moreover, AMPylation overpowers the effect of nucleotide binding, shifting the conformational equilibrium toward the domain-docked conformation even in the absence of ATP (Fig. 1B). An evident correlation between the free energy of nucleotide binding and domain docking (Fig. 1C) validates that populations of the domain-docked and -undocked conformations observed in NMR spectra indeed quantitatively represent thermodynamically relevant conformational distributions in the BiP functional ensemble (Fig. 1D). Intriguingly, local SBD perturbations in the BiP SBD can also complement each other. This possibility to combine effects of different SBD perturbations apparently provide an elegant tactic for gradual real-time fine-tuning of BiP function *in vivo* by covalent post-translational modifications and interactions with co-chaperones and other members of the ER protein quality control system.

From the basic BIP allosteric cycle to a realistic model of the protein quality control network

To understand how BIP functions *in vivo*, its interactions with co-chaperones, other components of the ER protein quality control system, and protein substrates need to be taken in account. We are using methyl NMR and other biophysical techniques to further explore how

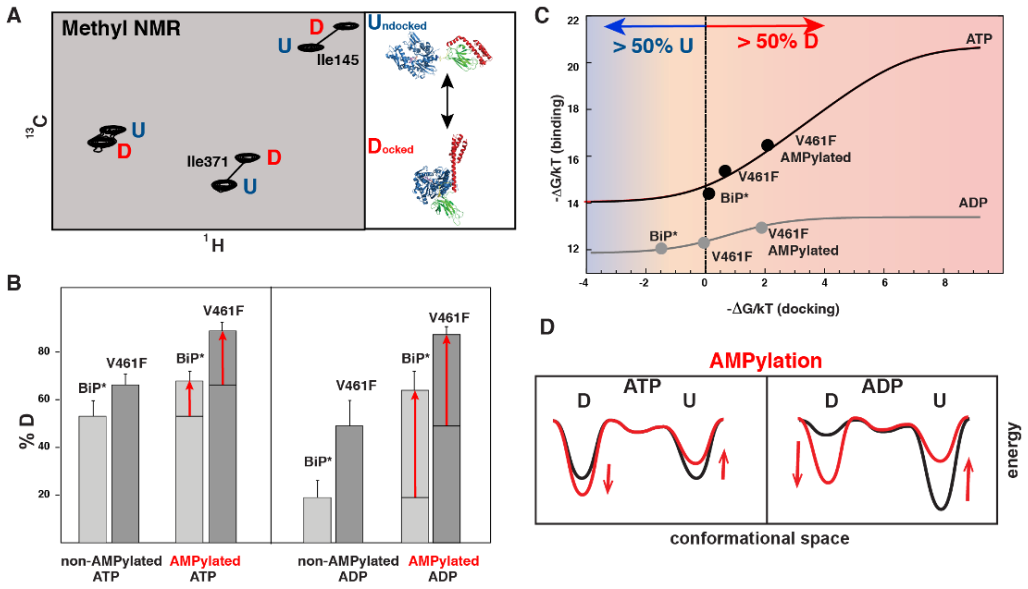

Figure 1: Post-translational regulation of the BiP conformational ensemble: (A) NMR fingerprints of two main functional conformations of BiP: Blowup of the representative region of methyl-TROSY spectra of ATP-bound ATPase deficient BiPT229G (BiP*), showing three non-overlapping domain-docked (D) and -undocked (U) peak doublets, used to calculate distributions in the BiP conformations ensemble. (B) Allosteric regulation of the BiP by AMPylation: Populations of the domain-docked conformation for AMPylated and non-AMPylated BiP* and its V461F variant in the presence of ATP and ADP, calculated using U and D methyl peak intensities (from A). (C) The thermodynamic linkage between NMR observed domain docking (perturbations in conformational ensemble) and ITC observed nucleotide binding (perturbations in BiP function): Plot of the experimental free energy of ATP (black dots) and ADP (grey dots) binding against the experimental free energy of domain docking for BiP* and its non-AMPylated and AMPylated V461F variant. (D) The mechanism of post-translational regulation of the BiP chaperone cycle: The BiP conformational landscape comprises three functionally and structurally distinct conformations: domain-docked (D), intermediate domain-undocked linker-bound (I), and domain-undocked linker-unbound (U), local perturbations of the BiP SBD (upon AMPylation or single-point mutations in the allosteric hotspots) fine-tune BiP function through redistribution in the BiP conformational ensemble (red arrows).

BiP communication with its co-chaperones and the ER stress sensor IRE1 affect the BiP functional cycle. And *vise versa*, we aim to understand how perturbations in the BiP conformational ensemble affect BiP interactions with its protein partners from the ER protein quality control system.

Publications

Wieteska L., Shahidi S., Zhuravleva A. (2017) Allosteric fine-tuning of the conformational equilibrium poises the chaperone BiP for post-translational regulation. *eLife* **6**:e29430

Funding

BBSRC, EPSRC, BBSRC DTP, White Rose University Consortium

Collaborators

External: David Ron (University of Cambridge, UK)

ASTBURY SEMINARS 2017

12th January
Structure and function of rotary ATP synthase and its role as new drug target against tuberculosis
Prof Thomas Meier, Imperial College London

2nd February
Synthetic Biology meets Structural Biology: New Perspectives and Opportunities
Prof Imre Berger, University of Bristol

2nd March
Understanding how regulation is achieved at different scales of complexity in cellular systems
Dr Madan Babu, MRC-LMB, Cambridge

6h April
Watching Proteins Dance, Viruses Assemble and Mitochondria Move: Using Fluorescence to Illuminate the Processes of Life
Prof Don Lamb, Ludwig Maximilians Universistät, Munich

4th May
Histone chaperones key players of chromatin assembly: from structure function studies to the design of inhibitors
Dr Francoise Ochsenbein, Institut de Biologie Intégrative de la Cellule, Gif-sur-Yvette

1st June
Design and synthesis of small molecule therapeutics for the treatment of cancer
Prof Julian Blagg, Institute for Cancer Research

7th July
Astbury Annual Lecture 2017
T Synthetic Protein Chemistry: from the test tube to the cell
Prof Tom Muir, Princeton University

5th October
New phase plate methods for cryoEM of small proteins
Dr Radostin Danev, Max Plank Institute for Biochemistry

9th November
Correlative Imaging: From Cells to Stars
Dr Lucy Collinson, The Francis Crick Institute

7th December
Synthetic Biology via programmable directed evolution
Dr Mark Isalan, Imperial College London

Abdul-Sada H., Muller M., Mehta R., Toth R., Arthur J.S.C., Whitehouse A. & Macdonald A. (2017) The pp4r1 sub-unit of protein phosphatase pp4 is essential for inhibition of NF-κB by merkel polyomavirus small tumour antigen. *Oncotarget* **8**:25418-25432.

Abidin F.N.Z. & Westhead D.R. (2017) Flexible model-based clustering of mixed binary and continuous data: Application to genetic regulation and cancer. *Nucleic Acids Res* **45**:e53

Adal E., Sadeghpour A., Connell S., Rappolt M., Ibanoglu E. & Sarkar A. (2017) Heteroprotein complex formation of bovine lactoferrin and pea protein isolate: A multiscale structural analysis. *Biomacromolecules* **18**:625-635.

Adeyemi O.O., Nicol C., Stonehouse N.J. & Rowlands D.J. (2017) Increasing type 1 poliovirus capsid stability by thermal selection. *J Virol* **91**:e01586-16.

Alotaibi K.M., Shiels L., Lacaze L., Peshkur T.A., Anderson P., Machala L., Critchley K., Patwardhan S.V. & Gibson L.T. (2017) Iron supported on bioinspired green silica for water remediation. *Chem Sci* **8**:567-576.

Antanaviciute A., Baquero-Perez B., Watson C.M., Harrison S.M., Lascelles C., Crinnion L., Markham A.F., Bonthron D.T., Whitehouse A. & Carr I.M. (2017) M6aviewer: Software for the detection, analysis, and visualization of N-6-methyladenosine peaks from m(6)A-seq/ME-RIP sequencing data. *RNA* **23**:1493-1501.

Arnott Z.L.P., Nozaki S., Monteiro D.C.F., Morgan H.E., Pearson A.R., Niki H. & Webb M.E. (2017) The mechanism of regulation of pantothenate biosynthesis by the PanD-PanZ·AcCoa complex reveals an additional mode of action for the antimetabolite n-pentyl pantothenamide (n5-pan). *Biochemistry* **56**:4931-4939.

Arrata I., Barnard A., Tomlinson D.C. & Wilson A.J. (2017) Interfacing native and non-native peptides: Using affimers to recognise alpha-helix mimicking foldamers. *Chem Commun* **53**:2834-2837.

Aufderhorst-Roberts A., Chandra U. & Connell S.D. (2017) Three-phase coexistence in lipid membranes. *Biophys J* **112**:313-324.

Bao P., Cartron M.L., Sheikh K.H., Johnson B.R.G., Hunter C.N. & Evans S.D. (2017) Controlling transmembrane protein concentration and orientation in supported lipid bilayers. *Chem Commun* **53**:4250-4253.

Batson S., De Chiara C., Majce V., Lloyd A.J., Gobec S., Rea D., Fulop V., Thoroughgood C.W., Simmons K.J., Dowson C.G., *et al.* (2017) Inhibition of d-Ala:D-Ala ligase through a phosphorylated form of the antibiotic d-cycloserine. *Nat Commun* **8**:1939.

Bayliss R., Burgess S.G., Leen E. & Richards M.W. (2017) A moving target: Structure and disorder in pursuit of myc inhibitors. *Biochem Soc Trans* **45**:709-717.

Bayliss R., Burgess S.G. & Mcintyre P.J. (2017) Switching Aurora-A kinase on and off at an allosteric site. *FEBS J* **284**:2947-2954.

Beales P.A. (2017) Biophysics a toehold in cell surface dynamics. *Nature Nanotechnol* **12**:404-406.

Beales P.A., Khan S., Muench S.P. & Jeuken L.J.C. (2017) Durable vesicles for reconstitution of membrane proteins in biotechnology. *Biochem Soc Trans* **45**:15-26.

Bedford, R., Tiede, C., Hughes, R., Curd, A., McPherson, M. J., Peckham, M., and Tomlinson, D. C. (2017) Alternative reagents to antibodies in imaging applications. *Biophys Rev* **9**:299-308.

Berrout J., Kyriakopoulou E., Moparthi L., Hogea A.S., Berrout L., Ivan C., Lorger M., Boyle J., Peers C., Muench S.*, et al.* (2017) TRPA1-FGFR2 binding event is a regulatory oncogenic driver modulated by miRNA-142-3p. *Nature Commun* **8**:947.

Boschmans J., Lemiere F. & Sobott F. (2017) Analyzing complex mixtures of drug-like molecules: Ion mobility as an adjunct to existing liquid chromatography-(tandem) mass spectrometry methods. *J Chromatogr A* **1490**:80-88.

Bridge K., Revill C., Macrae F., Bailey M., Yuldasheva N., Wheatcroft S., Butlin R., Foster R., Scott D.J., Gils A.*, et al.* (2017) Inhibition of plasmin-mediated tafi activation may affect development but not progression of abdominal aortic aneurysms. *PLoS One* **12**:e0177117.

Buchel G., Carstensen A., Mak K.Y., Roeschert I., Leen E., Sumara O., Hofstetter J., Herold S., Kalb J., Baluapuri A.*, et al.* (2017) Association with Aurora-A controls n-myc-dependent promoter escape and pause release of RNA polymerase ii during the cell cycle. *Cell Rep* **21**:3483-3497.

Burslem G.M., Kyle H.F., Nelson A., Edwards T.A. & Wilson A.J. (2017) Hypoxia inducible factor (hif) as a model for studying inhibition of protein-protein interactions. *Chem Sci* **8**:4188-4202.

Cahill S.T., Cain R., Wang D.Y., Lohans C.T., Wareham D.W., Oswin H.P., Mohammed J., Spencer J., Fishwick C.W.G., Mcdonough M.A.*, et al.* (2017) Cyclic boronates inhibit all classes of beta-lactamases. *Antimicrob Agents Chemother* **61**:e02260-16.

Calabrese A.N., Jackson S.M., Jones L.N., Beckstein O., Heinkel F., Gsponer J., Sharples D., Sans M., Kokkinidou M., Pearson A.R.*, et al.* (2017) Topological dissection of the membrane transport protein mhp1 derived from cysteine accessibility and mass spectrometry. *Anal Chem* **89**:8844-8852.

Calvopina K., Hinchliffe P., Brem J., Heesom K.J., Johnson S., Cain R., Lohans C.T., Fishwick C.W.G., Schofield C.J., Spencer J.*, et al.* (2017) Structural/mechanistic insights into the efficacy of nonclassical β-lactamase inhibitors against extensively drug resistant *Stenotrophomonas maltophilia* clinical isolates. *Mol Microbiol* **106**:492-504.

Campos G.R.F., Bittar C., Jardim A.C.G., Shimizu J.F., Batista M.N., Paganini E.R., De Assis L.R., Bartlett C., Harris M., Bolzani V.D.*, et al.* (2017) Hepatitis C virus *in vitro* replication is efficiently inhibited by acridone Fac4. *J Gen Virol* **98**:1693-1701.

Caseley E.A., Muench S.P. & Jiang L.H. (2017) Conformational changes during human P2X7 receptor activation examined by structural modelling and cysteine-based cross-linking studies. *Purinergic Signal* **13**:135-141.

Ceasar S.A., Baker A. & Ignacimuthu S. (2017) Functional characterization of the PHT1 family transporters of foxtail millet with development of a novel agrobacterium-mediated transformation procedure. *Sci Rep* **7**:14064.

Chammas O., Bonass W.A. & Thomson N.H. (2017) Effect of heparin and heparan sulphate on open promoter complex formation for a simple tandem gene model using *ex situ* atomic force microscopy. *Methods* **120**:91-102.

Chankhunthod N., Aslam Z., Critchley K., Evans S.D., Brydson R. (2017) Kinetically controlled fabrication of gold nanorods and investigation of their thermal stability via *in-situ* TEM heating. *J Phys Conf Ser* **902**:012007.

Chavali P.L., Stojic L., Meredith L.W., Joseph N., Nahorski M.S., Sanford T.J., Sweeney T.R., Krishna B.A., Hosmillo M., Firth A.E.*, et al.* (2017) Neurodevelopmental protein Musashi-1 interacts with the Zika genome and promotes viral replication. *Science* **357**:83-88.

Chow S.Y. & Nelson A. (2017) Embarking on a chemical space odyssey. *J Med Chem* **60**:3591-3593.

Costa L., Li-Destri G., Pontoni D., Konovalov O. & Thomson N.H. (2017) Liquid-liquid interfacial imaging using atomic force microscopy. *Adv Mater Interfaces* **4**: 1700203.

Cottom J., Abellan P., Hage F.S., Ramasse Q.M., Critchley K., Brydson R. (2017) Fabrication and characterisation of an adaptable plasmonic nanorod array for solar energy conversion. *J Phys Conf Ser* **902**:012025.

Cross L.L., Paudyal R., Kamisugi Y., Berry A., Cuming A.C., Baker A. & Warriner S.L. (2017) Towards designer organelles by subverting the peroxisomal import pathway. *Nature Commun* **8**:454.

Da Silva M.A., Lenton S., Hughes M., Brockwell D.J. & Dougan L. (2017) Assessing the potential of folded globular polyproteins as hydrogel building blocks. *Biomacromolecules* **18**:636-646.

Degardin M., Thakar D., Claron M., Richter R.P., Coche-Guerente L. & Boturyn D. (2017) Development of a selective cell capture and release assay: Impact of clustered RGD ligands. *J Mater Chem B* **5**:4745-4753.

Devine P.W.A., Fisher H.C., Calabrese A.N., Whelan F., Higazi D.R., Potts J.R., Lowe D.C., Radford S.E. & Ashcroft A.E. (2017) Investigating the structural compaction of biomolecules upon transition to the gas-phase using ESI-TWIMS-MS. *J Am Soc Mass Spectrom* **28**:1855-1862.

Deyaert E., Wauters L., Guaitoli G., Konijnenberg A., Leemans M., Terheyden S., Petrovic A., Gallardo R., Nederveen-Schippers L.M., Athanasopoulos P.S.*, et al.* (2017) A homologue of the Parkinson's disease-associated protein lrrk2 undergoes a monomer-dimer transition during GTP turnover. *Nature Commun* **8**:1008.

Diggle C.P., Martinez-Garay I., Molnar Z., Brinkworth M.H., White E., Fowler E., Hughes R., Hayward B.E., Carr I.M., Watson C.M.*, et al.* (2017) A tubulin alpha 8 mouse knockout model indicates a likely role in spermatogenesis but not in brain development. *Plos One* **12**:e0174264.

Dilly S.J., Clark A.J., Marsh A., Mitchell D.A., Cain R., Fishwick C.W.G. & Taylor P.C. (2017) A chemical genomics approach to drug reprofiling in oncology: Antipsychotic drug risperidone as a potential adenocarcinoma treatment. *Cancer Lett* **393**:16-21.

Dobson J., Kumar A., Willis L.F., Tuma R., Higazi D.R., Turner R., Lowe D.C., Ashcroft A.E., Radford S.E., Kapur N.*, et al.* (2017) Inducing protein aggregation by extensional flow. *Proc Natl Acad Sci USA* **114**:4673-4678.

Dow M., Marchetti F., Abrahams K.A., Vaz L., Besra G.S., Warriner S. & Nelson A. (2017) Modular synthesis of diverse natural product-like macrocycles: Discovery of hits with antimycobacterial activity. *Chemistry* **23**:7207-7211.

Dubacheva G.V., Araya-Callis C., Volbeda A.G., Fairhead M., Codee J., Howarth M. & Richter R.P. (2017) Controlling multivalent binding through surface chemistry: Model study on streptavidin. *J Am Chem Soc* **139**:4157-4167.

Dyer D.P., Migliorini E., Salanga C.L., Thakar D., Handel T.M. & Richter R.P. (2017) Differential structural remodelling of heparan sulfate by chemokines: The role of chemokine oligomerization. *Open Biol* **7**:160286.

Elkrewi E., Randall C.P., Ooi N., Cottell J.L. & O'Neill A.J. (2017) Cryptic silver resistance is prevalent and readily activated in certain gram-negative pathogens. *J Antimicrob Chemother* **72**:3043-3046.

Fisher G.L.M., Pastrana C.L., Higman V.A., Koh A., Taylor J.A., Butterer A., Craggs T., Sobott F., Murray H., Crump M.P.*, et al.* (2017) The structural basis for dynamic DNA binding and bridging interactions which condense the bacterial centromere. *Elife* **6**:e28086.

Foley D.J., Craven P.G.E., Collins P.M., Doveston R.G., Aimon A., Talon R., Churcher I., Von Delft F., Marsden S.P. & Nelson A. (2017) Synthesis and demonstration of the biological relevance of sp(3)-rich scaffolds distantly related to natural product frameworks. *Chemistry* **23**:15227-15232.

Fontana J., Atanasiu D., Saw W.T., Gallagher J.R., Cox R.G., Whitbeck J.C., Brown L.M., Eisenberg R.J. & Cohen G.H. (2017) The fusion loops of the initial prefusion conformation of herpes simplex virus 1 fusion protein point toward the membrane. *Mbio* **8**:e01268-17.

Goonawardane N., Gebhardt A., Bartlett C., Pichlmair A. & Harris M. (2017) Phosphorylation of serine 225 in hepatitis C virus NS5a regulates protein-protein interactions. *J Virol* **91**:e00805-17.

Gordon J.A., Fishwick C.W.G. & Mcphillie M.J. (2017) New opportunities in the structure-based design of anti-protozoan agents. *Curr Top Med Chem* **17**:79-90.

Gowdy J., Batchelor M., Neelov I. & Paci E. (2017) Nonexponential kinetics of loop formation in proteins and peptides: A signature of rugged free energy landscapes? *J Phys Chem B* **121**:9518-9525.

Grison C.M., Burslem G.M., Miles J.A., Pilsl L.K.A., Yeo D.J., Imani Z., Warriner S.L., Webb M.E. & Wilson A.J. (2017) Double quick, double click reversible peptide "stapling". *Chem Sci* **8**:5166-5171.

Groppelli E., Levy H.C., Sun E., Strauss M., Nicol C., Gold S., Zhuang X.W., Tuthill T.J., Hogle J.M. & Rowlands D.J. (2017) Picornavirus RNA is protected from cleavage by ribonuclease during virion uncoating and transfer across cellular and model membranes. *PloS Pathog* **13**:e1006197.

Guo Y., Nehlmeier I., Poole E., Sakonsinsiri C., Hondow N., Brown A., Li Q., Li S., Whitworth J., Li Z.J.*, et al.* (2017) Dissecting multivalent lectin-carbohydrate recognition using polyvalent multifunctional glycan-quantum dots. *J Am Chem Soc* **139**:11833-11844.

Hassan K.A., Fagerlund A., Elbourne L.D.H., Voros A., Kroeger J.K., Simm R., Tourasse N.J., Finke S., Henderson P.J.F., Okstad O.A.*, et al.* (2017) The putative drug efflux systems of the *Bacillus cereus* group. *PLoS One* **12**:e0176188.

Heath G.R., Li M.Q., Rong H.L., Radu V., Frielingsdorf S., Lenz O., Butt J.N. & Jeuken L.J.C. (2017) Multilayered lipid membrane stacks for biocatalysis using membrane enzymes. *Adv Funct Mater* **27**:1606265.

Heirbaut M., Lermyte F., Martin E.M., Beelen S., Sobott F., Strelkov S.V. & Weeks S.D. (2017) Specific sequences in the N-terminal domain of human small heat-shock protein HSPB6 dictate preferential hetero-oligomerization with the orthologue HSPB1. *J Biol Chem* **292**:9944-9957.

Herod M.R., Gold S., Lasecka-Dykes L., Wright C., Ward J.C., Mclean T.C., Forrest S., Jackson T., Tuthill T.J., Rowlands D.J.*, et al.* (2017) Genetic economy in picornaviruses: Foot-and-mouth disease virus replication exploits alternative precursor cleavage pathways. *PLoS Pathog* **13**:e1006666.

Hesketh E.L., Meshcheriakova Y., Thompson R.F., Lomonossoff G.P. & Ranson N.A. (2017) The structures of a naturally empty cowpea mosaic virus particle and its genome-containing counterpart by cryo-electron microscopy. *Sci Rep* **7**:539.

Hewitt S.H., Filby M.H., Hayes E., Kuhn L.T., Kalverda A.P., Webb M.E. & Wilson A.J. (2017) Protein surface mimetics: Understanding how ruthenium tris(bipyridines) interact with proteins. *Chembiochem* **18**:223-231.

Hewitt S.H. & Wilson A.J. (2017) Protein sensing and discrimination using highly functionalised ruthenium(ii) tris(bipyridyl) protein surface mimetics in an array format. *Chem Commun* **53**:12278-12281.

Hickman S.J., Cooper R.E.M., Bellucci L., Paci E. & Brockwell D.J. (2017) Gating of Ton B-dependent transporters by substrate-specific forced remodelling. *Nature Commun* **8**:14804.

Holmes K., Lefevre P., Sadreev I., Munir T., Rawstron A., Westhead D. & Hillmen P. (2017) Ibrutinib mediates changes in chromatin structure in chronic lymphocytic leukaemia (CLL): Epigenetic studies from the bloodwise tap IciCLLe trial. *Leuk Lymphoma* **58**:19-20.

Hover S., Foster B., Barr J.N. & Mankouri J. (2017) Viral dependence on cellular ion channels - an emerging anti-viral target? *J Gen Virol* **98**:345-351.

Hughes D.J., Tiede C., Penswick N., Tang A.a.S., Trinh C.H., Mandal U., Zajac K.Z., Gaule T., Howell G., Edwards T.A.*, et al.* (2017) Generation of specific inhibitors of SUMO-1-and SUMO-2/3-mediated protein-protein interactions using affimer (adhiron) technology. *Sci Signal* **10**:eaaj2005.

Hunter J., Rice S., Lowe R., Pask C.M., Warriner S. & Sridharan V. (2017) Iridium catalyzed alkylation of 2 '-hydroxyacetophenone with alcohols under thermal or microwave conditions. *Tetrahedron Lett* **58**:4400-4402.

Hwang E.T., Orchard K.L., Hojo D., Beton J., Lockwood C.W.J., Adschiri T., Butt J.N., Reisner E. & Jeuken L.J.C. (2017) Exploring step-by-step assembly of nanoparticle: Cytochrome biohybrid photoanodes. *Chemelectrochem* **4**:1959-1968.

Jackson M.P. & Hewitt E.W. (2017) Why are functional amyloids non-toxic in humans? *Biomolecules* **7**:71.

Johnson A., Madsen J., Chapman P., Alswieleh A., Al-Jaf O., Bao P., *et al.* (2017) Micrometre and nanometre scale patterning of binary polymer brushes, supported lipid bilayers and proteins. *Chem Sci* **8**:4517-4526.

Johnson A., Bao P., Hurley C.R., Cartron M., *et al*. (2017) Simple, direct routes to polymer brush traps and nanostructures for studies of diffusional transport in supported lipid bilayers. *Langmuir* **33**:3672-3679.

Jurenas D., Chatterjee S., Konijnenberg A., Sobott F., Droogmans L., Garcia-Pino A. & Van Melderen L. (2017) AtaT blocks translation initiation by N-acetylation of the initiator tRNA(fMet). *Nature Chem Biol* **13**:640-646.

Kay P., Hughes S.R., Ault J.R., Ashcroft A.E. & Brown L.E. (2017) Widespread, routine occurrence of pharmaceuticals in sewage effluent, combined sewer overflows and receiving waters. *Environ Pollut* **220**:1447-1455.

Kazaks A., Lu I.N., Farinelle S., Ramirez A., Crescente V., Blaha B., Ogonah O., Mukhopadhyay T., De Obanos M.P., Krimer A.*, et al.* (2017) Production and purification of chimeric HBc virus-like particles carrying influenza virus LAH domain as vaccine candidates. *BMC Biotechnol* **17**:79.

Kearney K., Tomlinson D., Smith K. & Ajjan R. (2017) Hypofibrinolysis in diabetes: A therapeutic target for the reduction of cardiovascular risk. *Cardiovasc Diabetol* **16**:34.

Kelly L., Badhan A., Roberts G.C., Mbisa J.L. & Harris M. (2017) Manipulation of both virus- and cell-specific factors is required for robust transient replication of a hepatitis C virus genotype 3a sub-genomic replicon. *J Gen Virol* **98**:2495-2506.

Klein M., Krivov S.V., Ferrer A.J., Luo L.J., Samuel A.D.T. & Karplus M. (2017) Exploratory search during directed navigation in *C. elegans* and *Drosophila* larva. *Elife* **6**:e30503.

Kolodziejczyk R., Mikula K.M., Kotila T., Postis V.L.G., Jokiranta T.S., Goldman A. & Meri T. (2017) Crystal structure of a tripartite complex between C3dg, c-terminal domains of factor H and OspE of *Borrelia burgdorferi*. *PLoS One* **12**:0188127.

Koutsoumpeli E., Tiede C., Murray J., Tang A., Bon R.S., Tomlinson D.C. & Johnson S. (2017) Antibody mimetics for the detection of small organic compounds using a quartz crystal microbalance. *Anal Chem* **89**:3051-3058.

Laftsoglou T. & Jeuken L.J.C. (2017) Supramolecular electrode assemblies for bioelectrochemistry. *Chem Commun* **53**:3801-3809.

Lee V.E. & O'neill A.J. (2017) Batumin does not exert its antistaphylococcal effect through inhibition of aminoacyl-tRNA synthetase enzymes. *Int J Antimicrob Agents* **49**:121-122.

Lenton S., Rhys N.H., Towey J.J., Soper A.K. & Dougan L. (2017) Highly compressed water structure observed in a perchlorate aqueous solution. *Nature Commun* **8**:919.

Lermyte F. & Sobott F. (2017) A broader view on ion heating in traveling-wave devices using fragmentation of CsI clusters and extent of H• Migration as molecular thermometers. *Analyst* **142**:3388-3399.

Li J.Y., Lyu W.P., Rossetti G., Konijnenberg A., Natalello A., Ippoliti E., Orozco M., Sobott F., Grandori R. & Carloni P. (2017) Proton dynamics in protein mass spectrometry. *J Phys Chem Lett* **8**:1105-1112.

Li M.Q., Khan S., Rong H.L., Tuma R., Hatzakis N.S. & Jeuken L.J.C. (2017) Effects of membrane curvature and pH on proton pumping activity of single cytochrome bo_3 enzymes. *Biochim Biophys Acta* **1858**:763-770.

Li S.B., Zeng M.L., Gaule T., McPherson M.J. & Meldrum F.C. (2017) Passive picoinjection enables controlled crystallization in a droplet microfluidic device. *Small* **13**:1702154.

Mahon C.S., Mcgurk C.J., Watson S.M.D., Fascione M.A., Sakonsinsiri C., Turnbull W.B. & Fulton D.A. (2017) Molecular recognition-mediated transformation of single-chain polymer nanoparticles into crosslinked polymer films. *Angew Chem Int Ed Engl* **56**:12913-12918.

Marsian J., Fox H., Bahar M.W., Kotecha A., Fry E.E., Stuart D.I., Macadam A.J., Rowlands D.J. & Lomonossoff G.P. (2017) Plant-made polio type 3 stabilized VLPs-a candidate synthetic polio vaccine. *Nature Commun* **8**:245.

Martir D.R., Escudero D., Jacquemin D., Cordes D.B., Slawin A.M.Z., Fruchtl H.A., Warriner S.L. & Zysman-Colman E. (2017) Homochiral emissive Λ8- and Δ8-[Ir8Pd4]16+ supramolecular cages. *Chemistry* **23**:14358-14366.

Mayol-Llinas J., Farnaby W. & Nelson A. (2017) Modular synthesis of thirty lead-like scaffolds suitable for CNS drug discovery. *Chem Commun* **53**:12345-12348.

Mayol-Llinas J., Nelson A., Farnaby W. & Ayscough A. (2017) Assessing molecular scaffolds for CNS drug discovery. *Drug Discov Today* **22**:965-969.

Mcconkey G.A., Bedingfield P.T.P., Burrell D.R., Chambers N.C., Cunningham F., Prior T.J., Fishwick C.W.G. & Boa A.N. (2017) Interconvertible geometric isomers of *Plasmodium falciparum* dihydroorotate dehydrogenase inhibitors exhibit multiple binding modes. *Bioorg Med Chem Lett* **27**:3878-3882.

Mcintyre P.J., Collins P.M., Vrzal L., Birchall K., Arnold L.H., Mpamhanga C., Coombs P.J., Burgess S.G., Richards M.W., Winter A.*, et al.* (2017) Characterization of three druggable hot-spots in the Aurora-A/TPX2 interaction using biochemical, biophysical, and fragment-based approaches. *ACS Chem Biol* **12**:2906-2914.

Mensch C., Konijnenberg A., Van Elzen R., Lambeir A.M., Sobott F. & Johannessen C. (2017) Raman optical activity of human α-synuclein in intrinsically disordered, micelle-bound α-helical, molten globule and oligomeric β-sheet state. *J Raman Spectrosc* **48**:910-918.

Meshcheriakova Y., Durrant A., Hesketh E.L., Ranson N.A. & Lomonossoff G.P. (2017) Combining high-resolution cryo-electron microscopy and mutagenesis to develop cowpea mosaic virus for bionanotechnology. *Biochem Soc Trans* **45**:1263-1269.

Muench S.P. (2017) Everyone needs good neighbours - the intricate relationship between the acetylcholine-receptor channel and its membrane environment. *IUCrJ* **4**:306-307.

Muraki K., Ohnishi K., Takezawa A., Suzuki H., Hatano N., Muraki Y., Hamzah N., Foster R., Waldmann H., Nussbaumer P.*, et al.* (2017) Na^+ entry through heteromeric TRPC4/C1 channels mediates (-) Englerin A-induced cytotoxicity in synovial sarcoma cells. *Sci Rep* **7**:16988.

Nass N.M., Farooque S., Hind C., Wand M.E., Randall C.P., Sutton J.M., Seipke R.F., Rayner C.M. & O'Neill A.J. (2017) Revisiting unexploited antibiotics in search of new antibacterial drug candidates: The case of γ-actinorhodin. *Sci Rep* **7**:17419.

Newcomb W.W., Fontana J., Winkler D.C., Cheng N.Q., Heymann J.B. & Steven A.C. (2017) The primary enveloped virion of herpes simplex virus 1: Its role in nuclear egress. *Mbio* **8**:e00825-17.

Ni T., Kalli A.C., Naughton F.B., Yates L.A., Naneh O., Kozorog M., Anderluh G., Sansom M.S.P. & Gilbert R.J.C. (2017) Structure and lipid-binding properties of the kindlin-3 pleckstrin homology domain. *Biochem J* **474**:539-556.

Noy A., Maxwell A. & Harris S.A. (2017) Interference between triplex and protein binding to distal sites on supercoiled DNA. *Biophys J* **112**:523-531.

Ooi N. & O'Neill A.J. (2017) Revisiting unexploited antibiotics in search of new antibacterial drug candidates: The case of MSD-819 (6-chloro-2-quinoxalinecarboxylic acid 1,4-dioxide). *J Antibiot* **70**:317-319.

Ozsvari B., Bonuccelli G., Sanchez-Alvarez R., Foster R., Sotgia F. & Lisanti M.P. (2017) Targeting flavin-containing enzymes eliminates cancer stem cells (CSCs), by inhibiting mitochondrial respiration: Vitamin B2 (riboflavin) in cancer therapy. *Aging* **9**:2610-2628.

Ozsvari B., Fiorillo M., Bonuccelli G., Cappello A.R., Frattaruolo L., Sotgia F., Trowbridge R., Foster R. & Lisanti M.P. (2017) Mitoriboscins: Mitochondrial-based therapeutics targeting cancer stem cells (CSCs), bacteria and pathogenic yeast. *Oncotarget* **8**:67457-67472.

Ozsvari B., Sotgia F., Simmons K., Trowbridge R., Foster R. & Lisanti M.P. (2017) Mitoketoscins: Novel mitochondrial inhibitors for targeting ketone metabolism in cancer stem cells (CSCs). *Oncotarget* **8**:78340-78350.

Patel N., White S.J., Thompson R.F., Bingham R., Weiss E.U., Maskell D.P., Zlotnick A., Dykeman E.C., Tuma R., Twarock R.*, et al.* (2017) HBV RNA pre-genome encodes specific motifs that mediate interactions with the viral core protein that promote nucleocapsid assembly. *Nature Microbiol* **2**:17098.

Patel N., Wroblewski E., Leonov G., Phillips S.E.V., Tuma R., Twarock R. & Stockley P.G. (2017) Rewriting nature's assembly manual for a ssRNA virus. *Proc Natl Acad Sci USA* **114**:12255-12260.

Qin Z.W., Munnoch J.T., Devine R., Holmes N.A., Seipke R.F., Wilkinson K.A., Wilkinson B. & Hutchings M.I. (2017) Formicamycins, antibacterial polyketides produced by *Streptomyces formicae* isolated from african *Tetraponera* plant-ants. *Chem Sci* **8**:3218-3227.

Rawson S., Mcphillie M.J., Johnson R.M., Fishwick C.W.G. & Muench S.P. (2017) The potential use of single-particle electron microscopy as a tool for structure-based inhibitor design. *Acta Crystallogr D Struct Biol* **73**:534-540.

Remenyi R., Roberts G.C., Zothner C., Merits A. & Harris M. (2017) Snap-tagged chikungunya virus replicons improve visualisation of non-structural protein 3 by fluorescence microscopy. *Sci Rep* **7**:5682.

Renzoni A., Von Dach E., Landelle C., Diene S.M., Manzano C., Gonzales R., Abdelhady W., Randall C.P., Bonetti E.J., Baud D.*, et al.* (2017) Impact of exposure of methicillin-resistant *Staphylococcus aureus* to polyhexanide *in vitro* and *in vivo*. *Antimicrob Agents Chemother* **61**:e00272-17.

Reuillard B., Ly K.H., Hildebrandt P., Jeuken L.J.C., Butt J.N. & Reisner E. (2017) High performance reduction of H_2O_2 with an electron transport decaheme cytochrome on a porous ITO electrode. *J Am Chem Soc* **139**:3324-3327.

Roberts G.C., Zothner C., Remenyi R., Merits A., Stonehouse N.J. & Harris M. (2017) Evaluation of a range of mammalian and mosquito cell lines for use in chikungunya virus research. *Sci Rep* **7**:14641.

Robinson C. & Connell S.D. (2017) Crystal initiation structures in developing enamel: Possible implications for caries dissolution of enamel crystals. *Front Physiol* **8**:405.

Rode B., Shi J., Endesh N., Drinkhill M.J., Webster P.J., Lotteau S.J., Bailey M.A., Yuldasheva N.Y., Ludlow M.J., Cubbon R.M.*, et al.* (2017) Piezo1 channels sense whole body physical activity to reset cardiovascular homeostasis and enhance performance. *Nature Commun* **8**:350.

Roedig P., Ginn H.M., Pakendorf T., Sutton G., Harlos K., Walter T.S., Meyer J., Fischer P., Duman R., Vartiainen I.*, et al.* (2017) High-speed fixed-target serial virus crystallography. *Nature Methods* **14**:805-810.

Rowe S.F., Le Gall G., Ainsworth E.V., Davies J.A., Lockwood C.W.J., Shi L., Elliston A., Roberts I.N., Waldron K.W., Richardson D.J.*, et al.* (2017) Light-driven H_2 evolution and C=C or C=O bond hydrogenation by *Shewanella oneidensis*: A versatile strategy for photocatalysis by nonphotosynthetic microorganisms. *ACS Catal* **7**:7558-7566.

Rubaiy H.N., Ludlow M.J., Bon R.S. & Beech D.J. (2017) Pico145-powerful new tool for TRPC1/4/5 channels. *Channels* **11**:362-364.

Rubaiy H.N., Ludlow M.J., Henrot M., Gaunt H.J., Miteva K., Cheung S.Y., Tanahashi Y., Hamzah N., Musialowski K.E., Blythe N.M.*, et al.* (2017) Picomolar, selective, and subtype-specific small-molecule inhibition of TRPC1/4/5 channels. *J Biol Chem* **292**:8158-8173.

Rusu M., Hu Z.H., Taylor K.A. & Trinick J. (2017) Structure of isolated z-disks from honeybee flight muscle. *J Muscle Res Cell Motil* **38**:241-250.

Saarenpaa T., Kogan K., Sidorova Y., Mahato A.K., Tascon I., Kaljunen H., Yu L.Y., Kaiiijarvi J., Jurvansuu J., Saarma M.*, et al.* (2017) Zebrafish gdnf and its co-receptor gfr□1 activate the human RET receptor and promote the survival of dopaminergic neurons *in vitro*. *PLoS One* **12**: 0176166.

Saarma M. & Goldman A. (2017) Obesity receptors identified for a weight regulator. *Nature* **550**:195-197.

Sabir S.R., Yeoh S., Jackson G. & Bayliss R. (2017) EML4-ALK variants: Biological and molecular properties, and the implications for patients. *Cancers* **9**:E118

Sampson J., O'Regan L., Dyer M.J.S., Bayliss R. & Fry A.M. (2017) Hsp72 and Nek6 cooperate to cluster amplified centrosomes in cancer cells. *Cancer Res* **77**:4785-4796.

Schiffrin B., Brockwell D.J. & Radford S.E. (2017) Outer membrane protein folding from an energy landscape perspective. *BMC Biol* **15**:123.

Schiffrin B., Calabrese A.N., Higgins A.J., Humes J.R., Ashcroft A.E., Kalli A.C., Brockwell D.J. & Radford S.E. (2017) Effects of periplasmic chaperones and membrane thickness on BamA-catalyzed outer-membrane protein folding. *J Mol Biol* **429**:3776-3792.

Schnieders R., Richter C., Warhaut S., De Jesus V., Keyhani S., Duchardt-Ferner E., Keller H., Wohnert J., Kuhn L.T., Breeze A.L.*, et al.* (2017) Evaluation of ^{15}N-detected H-N correlation experiments on increasingly large RNAs. *J Biomol NMR* **69**:31-44.

Schumann S., Jackson B.R., Yule I., Whitehead S.K., Revill C., Foster R. & Whitehouse A. (2017) Targeting the ATP-dependent formation of herpesvirus ribonucleoprotein particle assembly as an antiviral approach. *Nature Microbiol* **2**:16201.

Schumann S. & Whitehouse A. (2017) Targeting the human TREX complex to prevent herpesvirus replication: What is new? *Future Virol* **12**:81-83.

Shah N.R., Wilkinson C., Harborne S.P.D., Turku A., Li K.M., Sun Y.J., Harris S. & Goldman A. (2017) Insights into the mechanism of membrane pyrophosphatases by combining experiment and computer simulation. *Struct Dyn* **4**:032105.

Shakeel S., Dykeman E.C., White S.J., Ora A., Cockburn J.J.B., Butcher S.J., Stockley P.G. & Twarock R. (2017) Genomic RNA folding mediates assembly of human parechovirus. *Nature Commun* **8**:5.

Shimizu J.F., Lima C.S., Pereira C.M., Bittar C., Batista M.N., Nazare A.C., Polaquini C.R., Zothner C., Harris M., Rahal P.*, et al.* (2017) Flavonoids from *Pterogyne nitens* inhibit hepatitis C virus entry. *Sci Rep* **7**:16127.

Shimizu J.F., Pereira C.M., Bittar C., Batista M.N., Campos G.R.F., Da Silva S., Cintra A.C.O., Zothner C., Harris M., Sampaio S.V.*, et al.* (2017) Multiple effects of toxins isolated from *Crotalus durissus terrificus* on the hepatitis C virus life cycle. *PLoS One* **12**:e0187857.

Smith G.A., Fearnley G.W., Abdul-Zani I., Wheatcroft S.B., Tomlinson D.C., Harrison M.A. & Ponnambalam S. (2017) Ubiquitination of basal vegfr2 regulates signal transduction and endothelial function. *Biol Open* **6**:1404-1415.

Som N.F., Heine D., Holmes N., Knowles F., Chandra G., Seipke R.F., Hoskisson P.A., Wilkinson B. & Hutchings M.I. (2017) The MtrAB two-component system controls antibiotic production in *Streptomyces coelicolor* A3(2). *Microbiology* **163**:1415-1419.

Som N.F., Heine D., Holmes N.A., Munnoch J.T., Chandra G., Seipke R.F., Hoskisson P.A., Wilkinson B. & Hutchings M.I. (2017) The conserved actinobacterial two-component system MtrAB coordinates chloramphenicol production with sporulation in *Streptomyces venezuelae* NRRL B-65442. *Front Microbiol* **8**:1145.

Stewart K.L., Hughes E., Yates E.A., Middleton D.A. & Radford S.E. (2017) Molecular origins of the compatibility between glycosaminoglycans and Aβ40 amyloid fibrils. *J Mol Biol* **429**:2449-2462.

Tang A.a.S., Tiede C., Hughes D.J., McPherson M. & Tomlinson D.C. (2017) Isolation of isoform-specific binding proteins (affimers) by phage display using negative selection. *Sci Signal* **10**:eaan0868.

Thorp-Greenwood F.L., Brennan A.D., Oldknow S., Henkelis J.J., Simmons K.J., Fishwick C.W.G. & Hardie M.J. (2017) Tris-n-alkylpyridinium-functionalised cyclotriguaiacylene hosts as axles in branched 4 pseudorotaxane formation. *Supramol Chem* **29**:430-440.

Tiede C., Bedford R., Heseltine S.J., Smith G., Wijetunga I., Ross R., Al Qallaf D., Roberts A.P.E., Balls A., Curd A*., et al.* (2017) Affimers proteins are versatile and renewable affinity reagents. *Elife* **6**: e24903.

Tskhovrebova, L and Trinick, J. (2017) Titin and nebulin in thick and thin filament length regulation. *Subcell Biochem* **82**:285-318.

Turner L.D., Summers A.J., Johnson L.O., Knowles M.A. & Fishwick C.W.G. (2017) Identification of an indazole-based pharmacophore for the inhibition of FGFR kinases using fragment-led *de novo* design. *ACS Med Chem Lett* **8**:1264-1268.

Van Oosten-Hawle P., Bolon D.N.A. & Lapointe P. (2017) The diverse roles of Hsp90 and where to find them. *Nature Struct Mol Biol* **24**:1-4.

Verlackt C.C.W., Van Boxem W., Dewaele D., Lemiere F., Sobott F., Benedikt J., Neyts E.C. & Bogaerts A. (2017) Mechanisms of peptide oxidation by hydroxyl radicals: Insight at the molecular scale. *J Phys Chem C* **121**:5787-5799.

Virzbickas K., Rimkute L., Harvie A.J. & Critchley K. (2017) Surfactant-dependent photoluminescence of CdTe/CdS nanocrystals. *J Exp Nanosci* **12**:94-103.

Wang W.L., Guo Y., Tiede C., Chen S.Y., Kopytynski M., Kong Y.F., Kulak A., Tomlinson D.R., Chen R.J., McPherson M*., et al.* (2017) Ultraefficient cap-exchange protocol to compact biofunctional quantum dots for sensitive ratiometric biosensing and cell imaging. *ACS Appl Mater Interfaces* **9**:15232-15244.

Wanjun, Q.I., Manfield, I.W., Muench, S.P. & Baker, A. (2017) AtSPX1 affects the AtPHR1 dimer-DNA binding equilibrium by binding monomeric AtPHR1 in solution. *Biochem J* **474**: 3675-3687.

Wasson C.W., Morgan E.L., Muller M., Ross R.L., Hartley M., Roberts S. & Macdonald A. (2017) Human papillomavirus type 18 E5 oncogene supports cell cycle progression and impairs epithelial differentiation by modulating growth factor receptor signalling during the virus life cycle. *Oncotarget* **8**:103581-103600.

Watkinson T.G., Calabrese A.N., Ault J.R., Radford S.E. & Ashcroft A.E. (2017) FPOP-LC-MS/MS suggests differences in interaction sites of amphipols and detergents with outer membrane proteins. *J Am Soc Mass Spectrom* **28**:50-55.

Webster P.J., Littlejohns A.T., Gaunt H.J., Young R.S., Rode B., Ritchie J.E., Stead L.F., Harrison S., Droop A., Martin H.L*., et al.* (2017) Upregulated WEE1 protects endothelial cells of colorectal cancer liver metastases. *Oncotarget* **8**:42288-42299.

Wieteska L., Shahidi S. & Zhuravleva A. (2017) Allosteric fine-tuning of the conformational equilibrium poises the chaperone BiP for post-translational regulation. *Elife* **6**:e29430.

Windle C.L., Berry A. & Nelson A. (2017) Aldolase-catalysed stereoselective synthesis of fluorinated small molecules. *Curr Opin Chem Biol* **37**:33-38.

Windle C.L., Simmons K.J., Ault J.R., Trinh C.H., Nelson A., Pearson A.R. & Berry A. (2017) Extending enzyme molecular recognition with an expanded amino acid alphabet. *Proc Natl Acad Sci USA* **114**:2610-2615.

Wolny M., Batchelor M., Bartlett G.J., Baker E.G., Kurzawa M., Knight P.J., Dougan L., Woolfson D.N., Paci E. & Peckham M. (2017) Characterization of long and stable *de novo* single α-helix domains provides novel insight into their stability. *Sci Rep* **7**:44341.

Woo C.G., Seo S., Kim S.W., Jang S.J., Park K.S., Song J.Y., Lee B., Richards M.W., Bayliss R., Lee D.H.*, et al.* (2017) Differential protein stability and clinical responses of EML4-ALK fusion variants to various ALK inhibitors in advanced ALK-rearranged non-small cell lung cancer. *Ann Oncol* **28**:791-797.

Wright J., Thomsen M., Kolodziejczyk R., Ridley J., Sinclair J., Carrington G., Singh B., Riesbeck K. & Goldman A. (2017) The crystal structure of pd1, a haemophilus surface fibril domain. *Acta Crystallogr F Struct Biol Commun* **73**:101-108.

Wright M.H., Fetzer C. & Sieber S.A. (2017) Chemical probes unravel an antimicrobial defense response triggered by binding of the human opioid dynorphin to a bacterial sensor kinase. *J Am Chem Soc* **139**:6152-6159.

Wright M.H., Tao Y., Drechsel J., Krysiak J., Chamni S., Weigert-Munoz A., Harvey N.L., Romo D. & Sieber S.A. (2017) Quantitative chemoproteomic profiling reveals multiple target interactions of spongiolactone derivatives in leukemia cells. *Chem Commun* **53**:12818-12821.

Xie C.M., Tiede C., Zhang X.Y., Wang C.R., Li Z.X., Xu X., McPherson M.J., Tomlinson D.C. & Xu W.W. (2017) Development of an affimer antibody combined immunological diagnosis kit for glypican-3. *Sci Rep* **7**:9608.

Yamamoto E., Akimoto T., Kalli A.C., Yasuoka K. & Sansom M.S.P. (2017) Dynamic interactions between a membrane binding protein and lipids induce fluctuating diffusivity. *Sci Adv* **3**: e1601871.

Yefremova Y., Melder F.T.I., Danquah B.D., Opuni K.F.M., Koy C., Ehrens A., Frommholz D., Illges H., Koelbel K., Sobott F.*, et al.* (2017) Apparent activation energies of protein-protein complex dissociation in the gas-phase determined by electrospray mass spectrometry. *Anal Bioanal Chem* **409**:6549-6558.

Young L.M., Ashcroft A.E. & Radford S.E. (2017) Small molecule probes of protein aggregation. *Curr Opin Chem Biol* **39**:90-99.

Young L.M., Tu L.H., Raleigh D.P., Ashcroft A.E. & Radford S.E. (2017) Understanding co-polymerization in amyloid formation by direct observation of mixed oligomers. *Chem Sci* **8**:5030-5040.

Zhuravleva A. & Korzhnev D.M. (2017) Protein folding by NMR. *Prog Nucl Magn Reson Spectrosc* **100**:52-77.

The Astbury Centre for
Structural Molecular Biology
University of Leeds
Leeds
LS2 9JT
Tel: 0113 343 3086
astbury@leeds.ac.uk
www.astbury.leeds.ac.uk

UNIVERSITY OF LEEDS
University of Leeds
Leeds, United Kingdom
LS2 9JT
Tel: 0113 243 1751
www.leeds.ac.uk